



**TURUN
YLIOPISTO**
UNIVERSITY
OF TURKU

N-METHOXYOXAZOLIDINE- LIGATION IN OLIGONUCLEOTIDES

Aapo Aho



**TURUN
YLIOPISTO**
UNIVERSITY
OF TURKU

***N*-METHOXYOXAZOLIDINE- LIGATION IN OLIGONUCLEOTIDES**

Aapo Aho

University of Turku

Faculty of Science
Department of Chemistry
Chemistry
Doctoral Programme in Exact Sciences (EXACTUS)

Supervised by

Professor, Pasi Virta
Department of Chemistry
University of Turku
Turku, Finland

Professor, Tuomas Lönnerberg
Department of Chemistry
University of Turku
Turku, Finland

Doctor, Heidi Korhonen
Department of Chemistry
University of Turku
Turku, Finland

Reviewed by

Professor, Sabine Müller
Institute of Biochemistry
University of Greifswald
Greifswald, Germany

Professor, Michael Smietana
Institute of Biomolecules Max Mousseron
University of Montpellier
Montpellier, France

Opponent

Doctor, Lajos Kovács
Department of Medicinal Chemistry
University of Szeged
Szeged, Hungary

The originality of this publication has been checked in accordance with the University of Turku quality assurance system using the Turnitin OriginalityCheck service.

ISBN 978-951-29-9794-7 (PRINT)
ISBN 978-951-29-9795-4 (PDF)
ISSN 0082-7002 (Print)
ISSN 2343-3175 (Online)
Painosalama, Turku, Finland 2024

UNIVERSITY OF TURKU

Faculty of Science

Department of Chemistry

Chemistry

AAPO AHO: *N*-methoxyoxazolidine ligation in oligonucleotides

Doctoral Dissertation, 112 pp.

Doctoral Programme in Exact Sciences (EXACTUS)

September 2024

ABSTRACT

Aqueous coupling reactions are used in modern medicinal chemistry and biotechnological applications. As an example, DNA-templated synthesis (DTS) is employed to generate massive chemical libraries up to trillions of compounds, which can be utilized for screening of new active pharmaceutical ingredients (APIs). Furthermore, high-affinity receptors and ligands can be discovered by performing the synthesis and screening in a single process called target-directed dynamic combinatorial chemistry (tdDCC), which is based on settling of a thermodynamic equilibrium directed by the targets of interests – the templates. Reversible template-induced assembly is also attractive for detection as chemical sensors. tdDCC with biological target requires reversible aqueous coupling reactions. These kinds of coupling reactions have also been used as linkers for conjugation of APIs with various cell-specific or membrane-penetrating molecular agents to increase the efficacy of the API by more efficient cellular uptake.

In this thesis, formation of *N*-methoxyoxazolidines is presented as a potential pH-responsive coupling chemistry suitable for tdDCC and conjugation of unprotected oligonucleotides. By studying a model reaction between 2'-deoxy-2'-*N*-methoxyuridine and aldehydes, it was found out that *N*-methoxyoxazolidines are obtained in high yields under aqueous conditions. The reaction is reversible, and its rate is dependent on the acidity of the reaction solution. In practice, the reaction is dynamic under slightly acidic conditions (pH 4–6) while the obtained products (*N*-methoxyoxazolidines) are stable at pH 7 or above. The *N*-methoxyoxazolidine formation was applied for the preparation of various oligonucleotide conjugates (including carbohydrates and peptides). The conjugates were shown to be cleavable in acidic conditions perceived to early endosomes. Based on these studies, *N*-methoxyoxazolidines could be used as dynamic cleavable linkers for therapeutic oligonucleotide conjugates. In addition, the applicability of the reaction for DNA- and small-molecule-templated syntheses were studied. This was demonstrated for the assembly of dynamic pH-responsive split-aptamers and G-quadruplexes, induced by a small molecule substrate and metal ions, respectively. Therefore, *N*-methoxyoxazolidine was proven to be a suitable tool for tdDCC.

KEYWORDS: oligonucleotide, conjugate, linker, acetal, *N*-methoxyoxazolidine, template, ligation, dynamic

TURUN YLIOPISTO

Matemaattis-luonnontieteellinen tiedekunta

Kemian laitos

Kemia

AAPO AHO: *N*-metoksioksatsolidiiniligaatio oligonukleotideilla

Väitöskirja, 112 s.

Eksaktien tieteiden tohtoriohjelma (EXACTUS)

Syyskuu 2024

TIIVISTELMÄ

Vedessä tapahtuvia kytkentäreaktioita hyödynnetään modernissa lääkekehityksen kemiassa ja bioteknologisissa sovelluksissa. Esimerkiksi DNA-templatoidun synteesin avulla valmistetaan laajoja molekyylikirjastoja, jotka sisältävät jopa triljoonia erilaisia yhdisteitä. Kirjastojen avulla voidaan tehokkaasti löytää uusia lääkeainekandidaatteja. Tällaisia kandidaatteja sekä muita kemiallisia reseptoreita sekä ligandeja voidaan valmistaa myös dynaamisella kombinatorisella kemialla. Dynaaminen kombinatorinen kemia hyödyntää tasapainoreaktioita, joiden tuotesuhdetta voidaan ohjata spesifisesti sitoutuvilla vastinrakenteilla eli templaateilla. Dynaamisen kombinatorisen kemian etuna on aktiivisten yhdisteiden samanaikainen synteesi ja seulonta. Biologisesti aktiivisten aineiden seulonta dynaamisella kombinatorisella kemialla vaatii vedessä tapahtuvia reversiibeilitä kytkentäreaktioita. Tällaisia kytkentäreaktioita hyödynnetään myös lääkeainekonjugaattien valmistukseen, jossa vaikuttavaan lääkeaineeseen kiinnitetään apuryhmä, jonka tehtävänä on edesauttaa lääkeaineen kuljetusta tiettyyn kohteeseen elimistössä, tehostaen näin lääkeaineen vaikutusta.

Tässä väitöskirjassa tutkittiin *N*-metoksioksatsolidiinin käyttöä oligonukleotidien ligaatioissa. Tutkimalla 2'-deoksi-2'-*N*-metoksiuridiinin ja aldehydien välistä reaktiota, havaittiin, että *N*-metoksioksatsolidiinit muodostuivat tehokkaasti vesiliuoksessa. Tämä kondensaatioreaktio oli reversiibeli ja sen nopeus riippui liuoksen happamuudesta. Käytännössä reaktio oli dynaaminen lievästi happamissa olosuhteissa (pH 4–6), mutta tuotteet olivat pysyviä pH 7:ssä ja sen yläpuolella. *N*-metoksioksatsolidiinia hyödynnettiin terapeuttisesti relevanttien oligonukleotidikonjugaattien valmistukseen, jotka purkaantuivat endosomeille tyypillisissä happamissa olosuhteissa. Tällä perusteella *N*-metoksioksatsolidiineja voitaisiin käyttää kytkentärakenteena lääkeaineiden kuljetukseen kohdesoluihin. Toisena sovellusalueena tutkittiin *N*-metoksioksatsolidiinin käyttöä DNA- ja pienmolekyylitemplatoidussa synteesissä. Osoitettiin, että sekä komplementaarista DNA-juostetta tai pienmolekyyliä voitiin käyttää indusoimaan oligonukleotidien välistä *N*-metoksioksatsolidiiniligaatiota. *N*-metoksioksatsolidiiniligaatio osoittautui siis toimivaksi työkaluksi dynaamisen kombinatorisen kemian tutkimukseen oligonukleotidella.

ASIASANAT: Oligonukleotidi, konjugaatti, kytkentä, asetaali, *N*-metoksioksatsolidiini, templaatti, ligaatio, dynaaminen.

Table of Contents

Abbreviations	8
List of Original Publications	10
1 Introduction.....	11
1.1 Acetal formation	12
1.1.1 O- and S-acetals	12
1.1.2 Aminals (<i>N,N</i> -acetals)	13
1.1.3 <i>N,O</i> - and <i>N,S</i> -acetals	16
1.2 Imines, hydrazones, and oximes	17
1.3 Combinatorial chemistry.....	22
1.4 DNA-templated synthesis.....	27
1.5 pH-responsive cleavable linkers in therapeutic oligonucleotides	31
2 Aims of the Thesis.....	33
3 Results and Discussion	34
3.1 Kinetic and thermodynamic assessment of <i>N</i> - methoxyoxazolidine formation by small-molecular models	34
3.2 Acid-labile conjugation of therapeutic oligonucleotides.....	37
3.2.1 Synthesis of oligonucleotides bearing 3'-terminal 2'- deoxy-2'- <i>N</i> -methoxyuridine (U ^{NOMe} -ONs).....	37
3.2.2 Synthesis of peptides, a PNA, and a GalNAc cluster bearing aldehyde handles	38
3.2.3 Preparation of <i>N</i> -methoxyoxazolidine conjugates.....	41
3.2.3.1 Bis-conjugation via <i>N</i> -methoxyoxazolidine and SPAAC	44
3.2.4 Hydrolysis of <i>N</i> -methoxyoxazolidine conjugates.....	46
3.3 Target-directed dynamic combinatorial chemistry of oligonucleotides	48
3.3.1 Synthesis of oligonucleotides modified by 5'- terminal aldehyde.....	49
3.3.2 <i>N</i> -methoxyoxazolidine formation on DNA hairpin template	52
3.3.3 Quinine-templated aptamer assembly	57
3.3.4 Potassium-induced G-quadruplex assembly	61
4 Summary	65

5	Materials and Methods	67
5.1	General	67
5.2	Thermodynamic and kinetic experiments	67
5.2.1	<i>N</i> -methoxyoxazolidine formation between 1 and small-molecular aldehydes	67
5.2.2	Hydrolysis of conjugates C1–C5	68
5.2.3	Target-directed dynamic combinatorial chemistry	68
5.2.3.1	Self-assembly of a DNA-hairpin	68
5.2.3.2	Quinine- and potassium-templated aptamer and G-quadruplex assembly	69
	Acknowledgements	70
	List of References.....	72
	Original Publications	77

Abbreviations

Ac	Acetyl protecting group
AcOH	Acetic acid
AEEA	Aminoethoxyethoxyacetic acid
ALS	Amyotrophic lateral sclerosis
API	Active pharmaceutical ingredient
Boc	tert-butyloxycarbonyl protecting group
BOP	Benzotriazol-1-yloxytris(dimethylamino)phosphonium hexafluorophosphate
CBA	Cocaine-binding aptamer
CNS	Central nervous system
CPP	Cell-penetrating peptide
CuAAC	Cu(I)-catalyzed alkyne–azide cycloaddition
DCC	Dynamic combinatorial chemistry
DCL	Dynamic combinatorial library
DEL	DNA-encoded library
DIPEA	Diisopropylethylamine
DMAP	Dimethylaminopyridine
DMF	Dimethylformamide
DMSO	Dimethylsulfoxide
DNA	Deoxyribonucleic acid
DNAzyme	Deoxyribozyme, catalytic DNA
DTS	DNA-templated synthesis
EDG	Electron-donating group
EDT	Ethane-1,2-dithiol
ESI–TOF	Electrospray ionisation time-of-flight
EWG	Electron-withdrawing group
Fmoc	Fluorenylmethoxycarbonyl protecting group
GalNAc	N-Acetylgalactosamine
HRMS	High-resolution mass spectrometry
LCAA-CPG	Long chain alkylamine controlled pore glass
PAGE	Polyacrylamide gel electrophoresis

PCR	Polymerase chain reaction
PNA	Peptide nucleic acid
RNA	Ribonucleic acid
RP HPLC	Reversed phase high performance liquid chromatography
RT	Room temperature
siRNA	Small-interfering RNA
SPAAC	Strain-promoted azide–alkyne cycloaddition
TBDMSCl	tert-butyldimethylsilylchloride
tdDCC	Target-directed dynamic combinatorial chemistry
TEAA	Triethylammoniumacetate
TFA	Trifluoroacetic acid
THF	Tetrahydrofuran
TON	Therapeutic oligonucleotide
tRNA	Transfer RNA
UNOMe-ON	Oligonucleotide with 3'-terminal 2'-deoxy-2'-N-methoxyuridine

List of Original Publications

This dissertation is based on the following original publications, which are referred to in the text by their Roman numerals:

- I Aho, A.; Sulkanen, M.; Korhonen, H.; Virta, P. Conjugation of Oligonucleotides to Peptide Aldehydes via a pH-Responsive N-Methoxyoxazolidine Linker. *Org. Lett.* **2020**, *22*, 671.
- II Aho, A.; Äärelä, A.; Korhonen, H.; Virta, P. Expanding the Scope of the Cleavable N-(Methoxy)Oxazolidine Linker for the Synthesis of Oligonucleotide Conjugates. *Molecules* **2021**, *26*, 490.
- III Aho, A.; Österlund, T.; Rahkila, J.; Virta, P. DNA-Templated Formation and N,O-Transacetalization of N-Methoxyoxazolidines. *Eur. J. Org. Chem.* **2022**, e202200583
- IV Aho, A.; Virta, P. Assembly of split aptamers by a dynamic pH-responsive covalent ligation. *Chem. Comm.* **2023**, *59*, 5689.

The original publications have been reproduced with the permission of the copyright holders.

1 Introduction

Aqueous coupling reactions are used in modern medicinal chemistry and biotechnological applications. As an example, DNA-templated synthesis (DTS)^{1,2} is used to generate massive chemical libraries³ up to trillions of compounds, which can be used for screening of new active pharmaceutical ingredients (APIs)⁴. Taking a step further, target-directed dynamic combinatorial chemistry (tdDCC)⁵⁻¹¹ is a method for discovering high-affinity binders, such as artificial receptors and ligands, by performing the synthesis and screening in a single process. This is based on settling of a thermodynamic equilibrium between reversible chemical reactions, which is directed by the targets of interest. For tdDCC, it is desired that the reaction proceeds in near-physiological conditions but can be halted in a traceless manner (e.g. temperature, light, pH, or reduction/oxidation), facilitating the analysis of the compound library. Furthermore, reversible bioorthogonal reactions are of special interest for controlled release of APIs¹²⁻¹⁴, molecular devices such as biosensors¹⁵, and self-healing materials¹⁵⁻¹⁷.

This thesis is based on acetals. *O*-acetals are one of the most common protection groups used for aldehydes, ketones and hydroxyl groups. They are reversibly formed under acidic conditions, but stable in basic conditions towards all kinds of nucleophiles. Generally, anhydrous conditions are required for their synthesis. *S*- and *N*-acetals are also commonly used structures. While *S*-acetals may be regarded as a more stable version of *O*-acetals, *N*-acetals are chemically more diverse due to different electron configuration of nitrogen and its tendency to form three covalent bonds. By definition, two of those bonds are reserved for the acetal alkyl groups, but the third *N*-substituent can be used to adjust the acetal reactivity.

The reactivity of *N*-substituted *N*-acetals may be compared to imines. While imines with *N*-alkyl-substitutions are often unstable in aqueous conditions, *N*-*N*- and *N*-*O*-substituted imines (hydrazones and oximes, respectively) are stable enough to be applied for bioconjugation under aqueous conditions. Peculiarly, these α -nucleophilic imines have been known since the 19th century¹⁸, but the putatively analogous reactivity patterns of *N*-acetals have not been explored in detail. In this thesis, the kinetics and thermodynamics for the dynamic formation of five-membered cyclic *N,O*-acetals, *N*-methoxyoxazolidines, are studied. Furthermore, the

synthetic feasibility and applicability of the *N*-methoxyoxazolidines in oligonucleotide ligation are examined from the perspective of drug-delivery, DTS, and tDCC.

1.1 Acetal formation

1.1.1 O- and S-acetals

Carbonyl compounds and alcohols form *O*-acetals, which can be acyclic, cyclic, and acyclic/cyclic (**Figure 1**). Five- and six-membered cyclic acetals are often utilized as synthetic intermediates.¹⁹ Acyclic/cyclic acetals are abundantly found in nature as glycosides.²⁰ In general, efficient conversion of carbonyl compounds into *O*-acetals require excess of alcohol due to low equilibrium constant of the acetalization. Aliphatic aldehydes form thermodynamically more stable acetals than aromatic or conjugated ones, and ketones are increasingly more difficult substrates.²¹

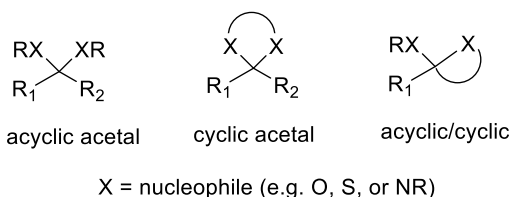
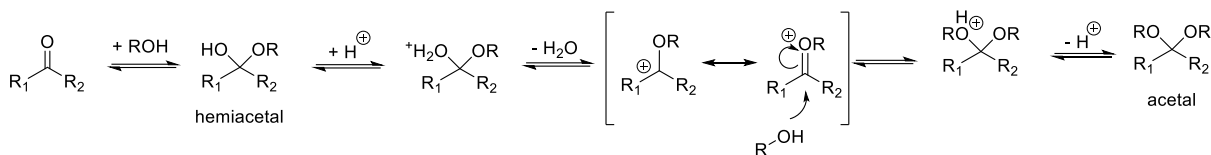


Figure 1. The variety of acetal forms.

Acetalization proceeds via acid-catalyzed S_N1 pathway (**Scheme 1**) including addition and substitution steps. In this mechanism, the hemiacetal is formed and followed by the rate-limiting dehydration to form a carbocation. Before dehydration, the leaving water must be protonated into oxonium intermediate. Low pK_a of the oxonium intermediate makes the protonation favorable only under acidic conditions.²² Therefore, the rate of acetalization is dependent on the acidity of the solution. Structurally speaking, the stability of the carbocation dictates the rate of acetalization. Thus, EDG and EWG (electron-donating and electron-withdrawing groups, respectively) next to the carbocation (R_1 and R_2 groups in **Scheme 1**) makes the reaction proceeding faster and slower, respectively.²³ Acetals are highly stable towards all kinds of nucleophiles and reductants/oxidants in neutral to basic conditions (with certain exceptions^{24,25}), but faithfully cleaved by acidic hydrolysis.¹⁹ This makes them exceptionally good protection groups for carbonyl and hydroxyl groups. They have also been studied as linkers in acid-triggered release of APIs in acidic compartments of cells.²⁶



Scheme 1. Acid-catalyzed acetal formation mechanism.

Thiols react with carbonyl compounds to form *S*-hemiacetals and *S*-acetals. Mixtures of alcohols and thiols can form hybrid *O,S*-acetals. *S*-acetals are hydrolytically more stable compared to *O*-acetals.²⁷ For deprotection, metal-coordination, oxidation or alkylation is usually needed.²⁸ Comparison of the kinetic stabilities of common *O*-, *S*-, and *O,S*-acetals towards acid-catalyzed hydrolysis are shown in (**Figure 2**).

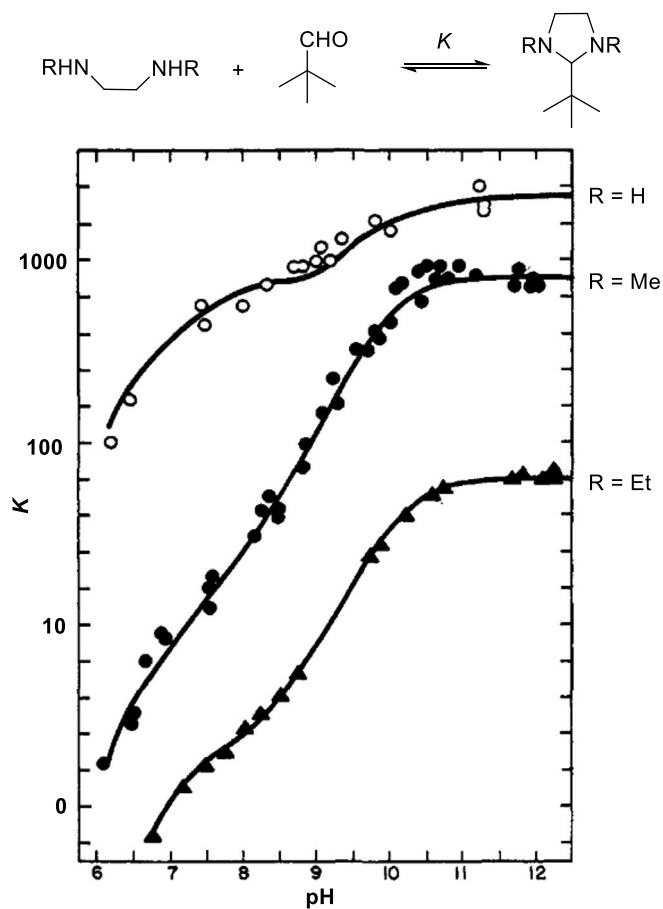
acetal	k_h ($M^{-1} s^{-1}$)	acetal	k_h ($M^{-1} s^{-1}$)
	1.3E-3		1.6E2
	6E-3		1.3
	3E-7		3.5E-4

Figure 2. Rate constants (k_h) at 25-30 °C for the acid-catalyzed hydrolysis of cyclic O/S-acetals.¹⁹

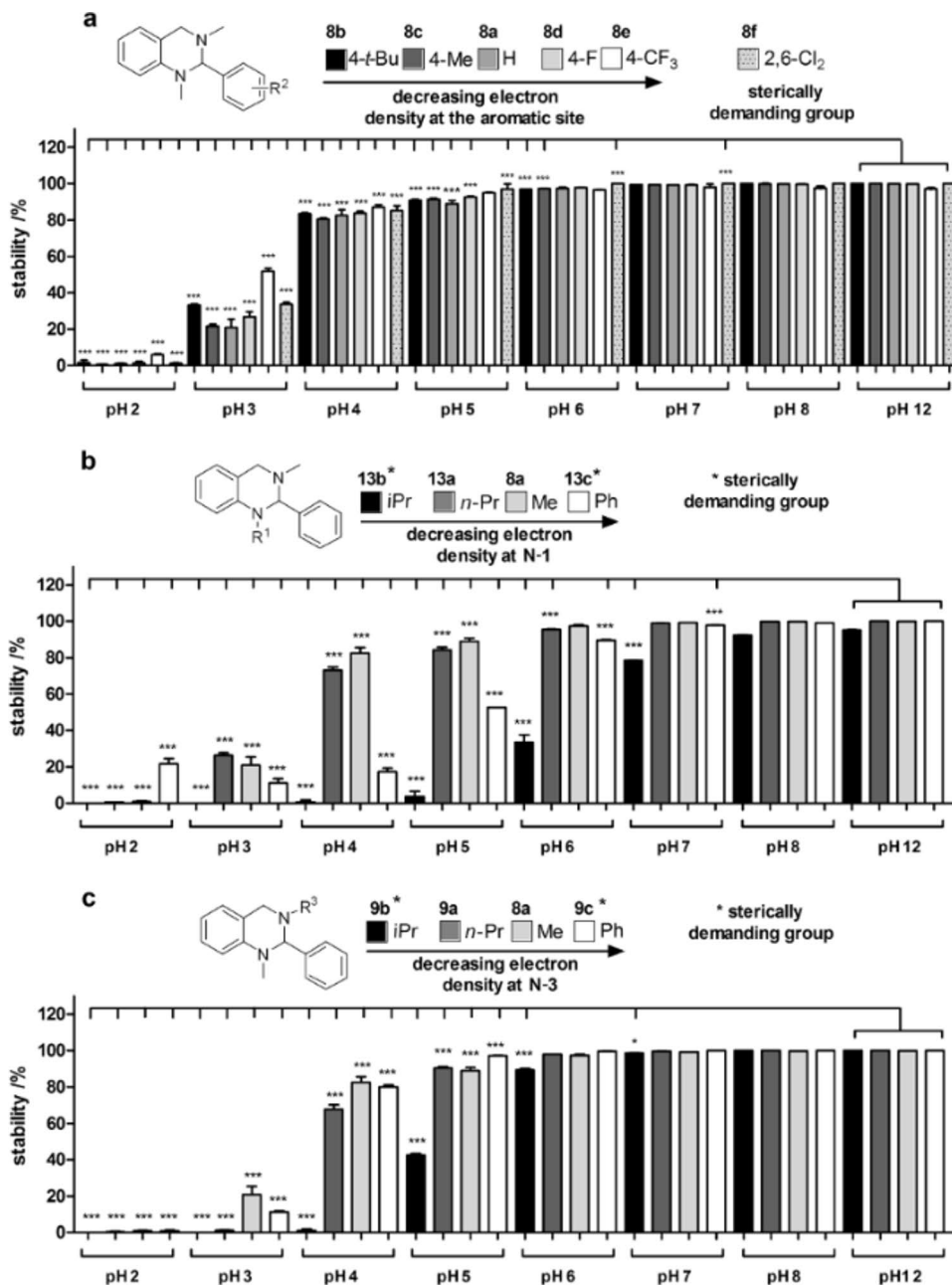
1.1.2 Aminals (*N,N*-acetals)

Aminals (*N,N*-acetals) are intriguing due to nitrogen's tendency to share three covalent bonds. This allows modification of the acetal properties by the extra substituent at the nitrogen compared to the *O*- or *S*-acetals. Five- and six-membered cyclic aminals (1,3-imidazolidines and 1,3-diazinanes, respectively) are often found in synthetic products and intermediates.²⁹ The equilibrium constant is dependent on the *N*-substituents and pH of the reaction solution. For example, in aqueous solution, isobutyrylaldehyde forms imidazolidines with ethylenediamine, *N,N'*-dimethylethylenediamine and *N,N'*-diethyleneamine with K of 100–3000 M^{-1} , 2–800 M^{-1} , and 0.6–63 M^{-1} (respectively) between pH 6–12 (**Scheme 2**).³⁰ This data set implies, that high pH-favors the aminal formation, which has been supported by computational studies.²⁹ Hydrolysis rate of diazinanes and imidazolidines is dependent on the acidity of the solution, being more facile in acidic conditions.^{29,31–33} Conformational energy of the ring system affects the stability. Sterically

demanding *N*-substitutions on benzaldehyde-derived diazinanes hydrolyze more quickly, whereas EWG/EDG on the benzaldehyde has less impact (**Scheme 3**).²⁹



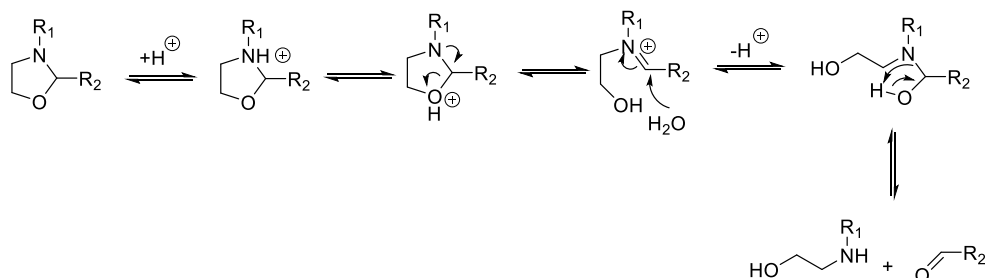
Scheme 2. Thermodynamic stability and its pH-sensitivity of three different aliphatic imidazolidines. Reaction conditions: isobutyrylaldehyde (0.61 M), diethylenediamine (titrated up to 0.13 M), 35 °C until steady equilibrium. Monitoring: UV spectroscopy at 285 nm. Adapted with permission from reference³⁰. Copyright 1973 American Chemical Society.



Scheme 3. Electronic and steric effects for the hydrolytic stability of benzaldehyde-derived diazinanes. Reaction conditions: 100 $\mu\text{g L}^{-1}$ (ca. 0.35–45 mM) of diazine in 30/70 MeCN/H₂O (v:v), 1 h at RT. Adapted with permission from reference²⁹. Copyright 2016 Beilstein Institute for the Advancement of Chemical Sciences.

1.1.3 *N,O*- and *N,S*-acetals

N,O-acetals are abundantly found in nature in cyclic and acyclic/cyclic form. Notable examples of the latter ones are *N*-glycosides such as nucleosides and glycoproteins. Cyclic *N,O*-acetals have been studied using their most stable variants: the five- and six-membered rings, (1,3)-oxazolidines and (1,3)-diazinanes, respectively. Acid-catalyzed hydrolysis of oxazolidines proceeds via protonation of the nitrogen, followed by breaking of the C–O bond and formation of imine intermediate (**Scheme 4**).³⁴ Up to 100-fold rate-differences have been observed depending on the pH of the reaction solution. Typically, the pH-rate profiles are bell-curved with maximum rate around pKa of the *N,O*-acetal, but sigmoidal hydrolytic profiles are also known for specific structures, such as those bearing intramolecular acid/base-catalysts (**Figure 3**).^{34–39} Generally, cyclic *N,O*-acetals hydrolyze quickly under common aqueous conditions (pH 1–12, 37 °C), but they can be stabilized by protecting the ring nitrogen by Boc^{40,41}, Fmoc⁴², or Ac^{43–46}. The aforementioned protecting groups can be used to turn the *N,O*-acetal into acid- (Boc) or base-labile (Fmoc). Especially the latter one may be found handy, because mildly base-labile aldehyde/ketone protection groups are scarce.⁴²



Scheme 4. Oxazolidine hydrolysis mechanisms.³⁴

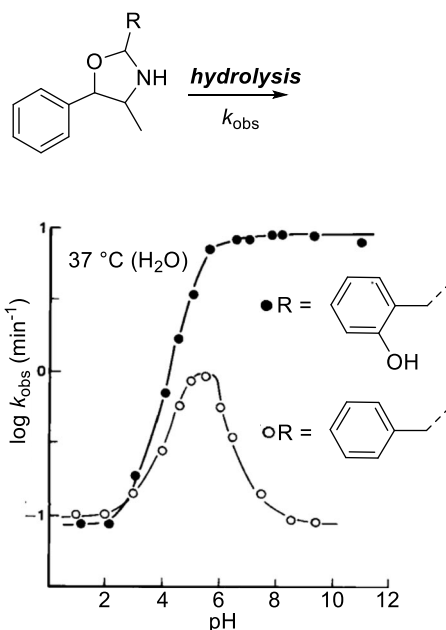


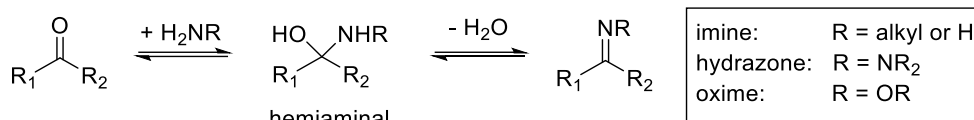
Figure 3. The kinetic pH-profiles for hydrolysis of two different oxazolidines. Adapted with permission from reference³⁹. Copyright 1982 Elsevier.

Hybrid *N,S*-acetals are found from nature as (1,3)-thiazolidines (e.g. penicillin).⁴⁷ Thiazolidines are readily formed by condensing 1,2-aminothiols with aldehydes. For example, an 5'-aldehyde-bearing oligonucleotide (10 μM) was conjugated to a peptide with *N*-terminal cysteine (1 mM) in aqueous solution (pH 7.4) with complete conversion after 30 min.⁴⁸ Aliphatic aldehydes reacted faster and reached higher conversion than aromatic ones.⁴⁸ The hydrolysis rate of thiazolidines is generally lower than of oxazolidines but is also pH-dependent.^{49,50} For their easy formation and modest hydrolysis rate, thiazolidines have been studied as acid-cleavable linkers in antibody–drug-conjugates⁵¹ and in aqueous dynamic combinatorial libraries (DCL)⁵⁰.

1.2 Imines, hydrazones, and oximes

Imines are C–N-double-bonded condensation products of carbonyl compounds and amines (**Scheme 5**). The imine formation is affected both by steric and electronic effects (**Figure 4**). With aliphatic aldehydes, the equilibrium constant for imine formation in water is usually small ($< 100 \text{ M}^{-1}$) but varies up to 10^3 M^{-1} with more stable aromatic aldehydes. Contrariwise, aliphatic amines give more stable imines than aromatic amines. EWGs on the amine makes the imine formation slower and thermodynamically less favorable.^{52–54} In other words, amines with higher pKa form

imines faster and with higher yield. In contrast, EWGs on the carbonyl compound makes the imine thermodynamically more stable.^{52,55,56}



Scheme 5. Formation of imine, hydrazone, and oxime.

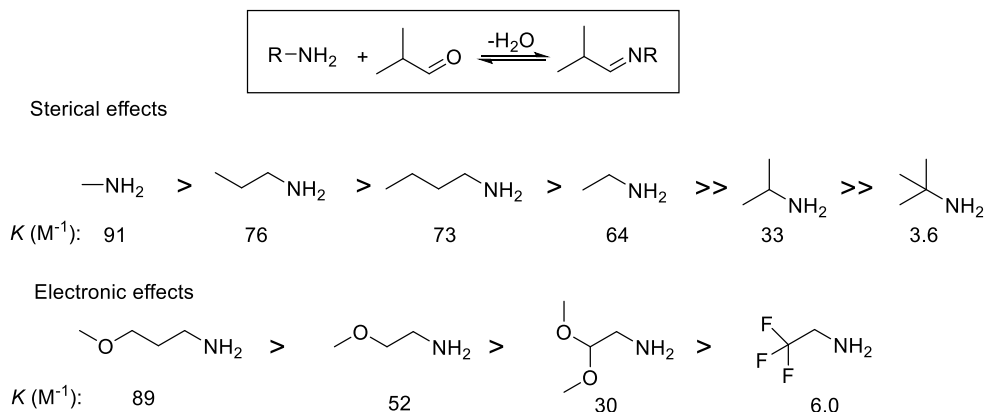


Figure 4. Equilibrium constants for a set of aliphatic imines. Reaction conditions: Isobutyrylaldehyde (0.02–0.16 M), amine (0.02–0.38 M), H₂O (pH ca. 10), 35 °C. Monitoring: UV-spectroscopy detected at 285 (aldehyde) or 230 (imine) nm.^{54,57}

The imine formation is pH-dependent. Thermodynamically, high pH favors imine formation, and rise of only three pH units can change the equilibrium yield from zero to nearly quantitative (**Figure 5**).⁵⁸ Kinetically, acidic conditions promote the protonation of the hydroxyl group which facilitates cleavage of water from the hemiaminal intermediate, but too low pH hinders nucleophilicity of the amine via protonation. The rate-determining step changes from dehydration to nucleophilic attack of amine when increasing the acidity, and optimal pH is dependent on the pK_a of the amine.⁵⁹ Typically this results in bell-curved kinetic pH profiles (**Figure 6**).^{57,60} With benzaldehyde-derived imines, the shape of the kinetic hydrolysis pH profiles can vary depending on the substituents: EWGs on the benzaldehyde can shift the maximum hydrolysis rate on the acidic side, while for EDGs or non-substituted benzaldehydic imines, the hydrolysis rate is inversely related to the acidity with a capped rate at the base-end (**Figure 7**).⁶¹ The thermodynamic and kinetic properties of imines are very broad depending on the specific structure and conditions.

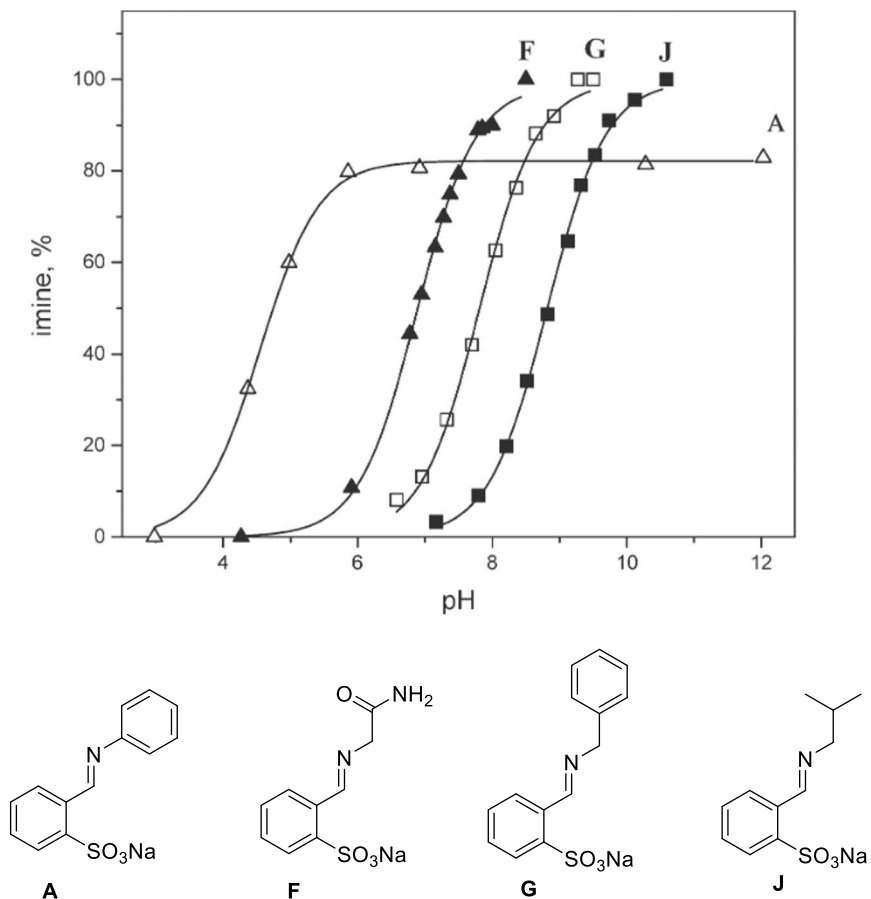


Figure 5. Typical pH-yield profiles for aromatic imines. Reaction conditions: amine (0.1 M) and aldehyde (0.01 M) were mixed in water at RT. Adapted with permission from reference⁵⁸. Copyright 2005 Wiley.

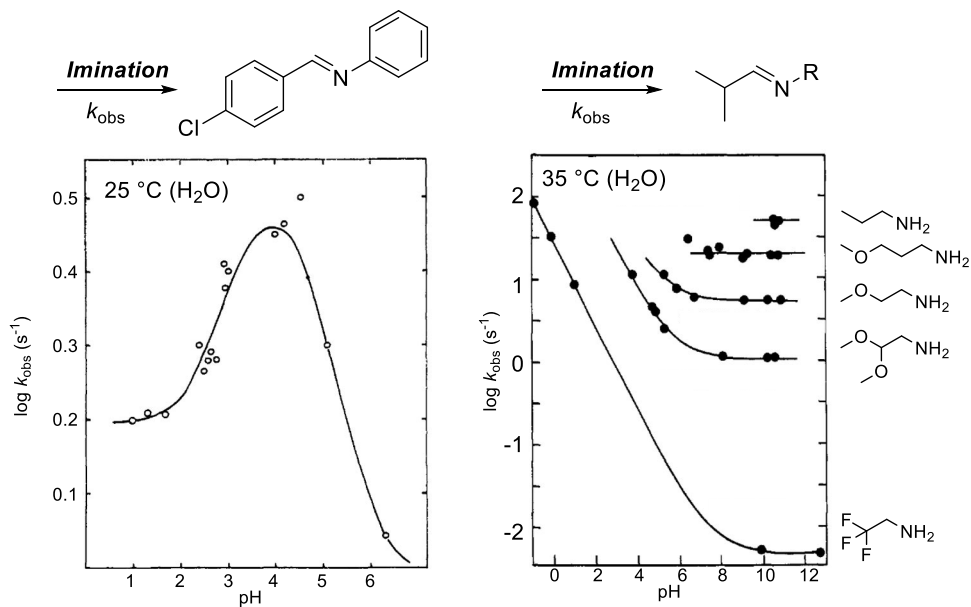


Figure 6. Kinetic pH-profiles for the formation of selected imines. Adapted with permission from references^{57,59}. Copyright 1972–1974 American Chemical Society.

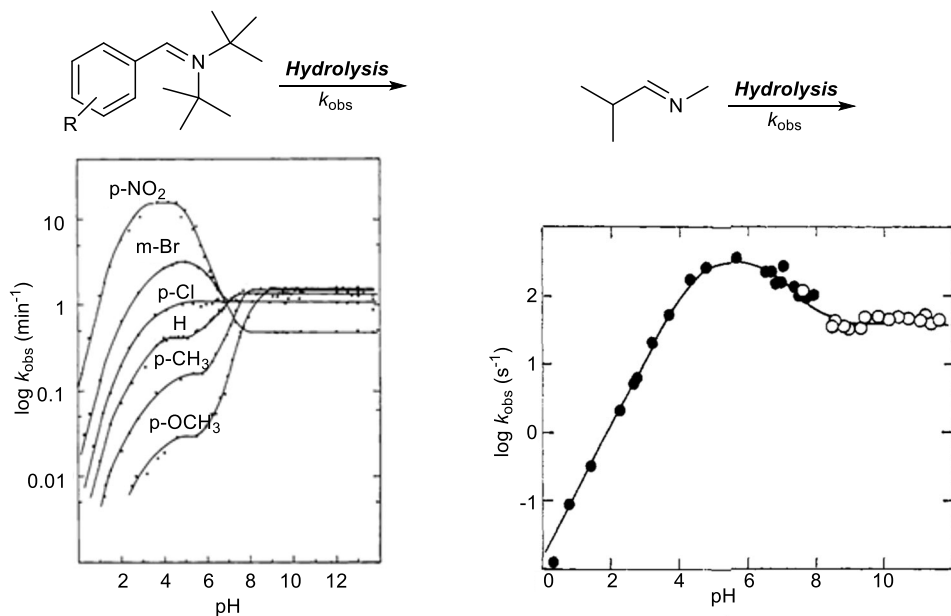
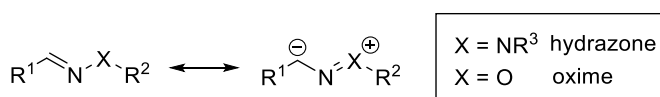


Figure 7. Kinetic pH-profiles for the hydrolysis of selected imines. Adapted with permission from references^{60,61}. Copyright 1963–1970 American Chemical Society.

Hydrazones and oximes are special cases of imines, in which hydrazines or *N*-alkoxy-amines (respectively) react with carbonyl compounds (cf. **Scheme 5**). Generally, the thermodynamic and kinetic stability trend found is oxime > hydrazone > imine.⁶² The stability of hydrazones and oximes, coined as the α -effect, is explained by the resonance structures: delocalization of the iminic double bond for carbonyl carbon renders it less electrophilic against hydrolysis (**Scheme 6**).⁶² This is in accordance with the fact that EDGs on the nitrogen generally stabilize imines.^{52–54} An alternative explanation stems from the repulsion of the electrons in the α -nucleophile, which is relieved in the imine form.⁶³ The different stabilities have been demonstrated in a study⁶⁴ in which formylpyridine (**Fp**) was exposed to various amines (**A**, **B**, **C**, **D**) simultaneously (**Scheme 7**). At the beginning of the reaction, imine **FpA** was the most abundant condensation product, after 2 h acylhydrazone **FpB**, after 23 h aryl hydrazone **FpC**, and finally after 317 h oxime **FpD** was the major product. This simple dynamic combinatorial experiment indicated that the relative thermodynamic stabilities for the products are oxime **FpD** > aryl hydrazone **FpC** > acyl hydrazone **FpB** > imine **FpA**, while the reaction rate was reverse in order. In another study, the hydrolysis rates of hydrazones and oximes were compared. It was shown, that *N*-Me hydrazone hydrolyzes 600-fold faster than similar *N*-OMe oxime (**Figure 8**). Due to the differences in hydrolytic stabilities, oximes and hydrazones are often used for irreversible and reversible bioconjugation, respectively.⁶⁵ The oxime and hydrazone formation and hydrolysis are pH-dependent and proceed optimally under acidic conditions. For this reason, hydrazones are commonly used as acid-labile linkers e.g. in drug delivery. For example, a hydrazone-linker used in an anti-cancer drug conjugate hydrolyzes at half-life ($t_{1/2}$) of 4.4 h and 183 h at pH 5.0 and pH 7.2, respectively.⁶⁶



Scheme 6. Resonance structures of hydrazones and oximes. The partial delocalization of the free electron pair for carbonyl carbon stabilizes the α -nucleophilic imines towards nucleophilic attack.⁶²

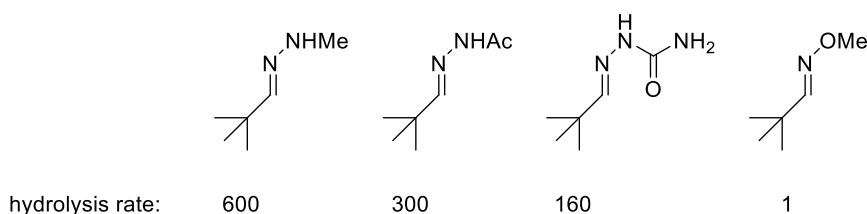
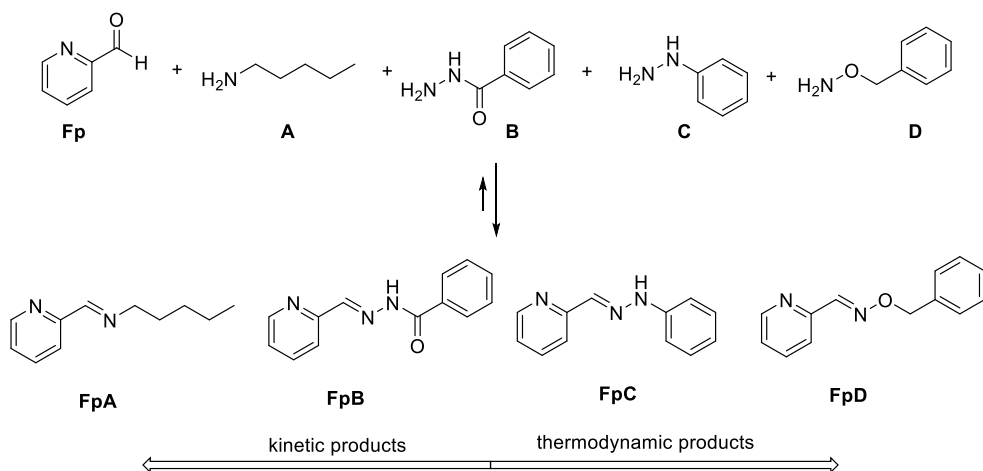
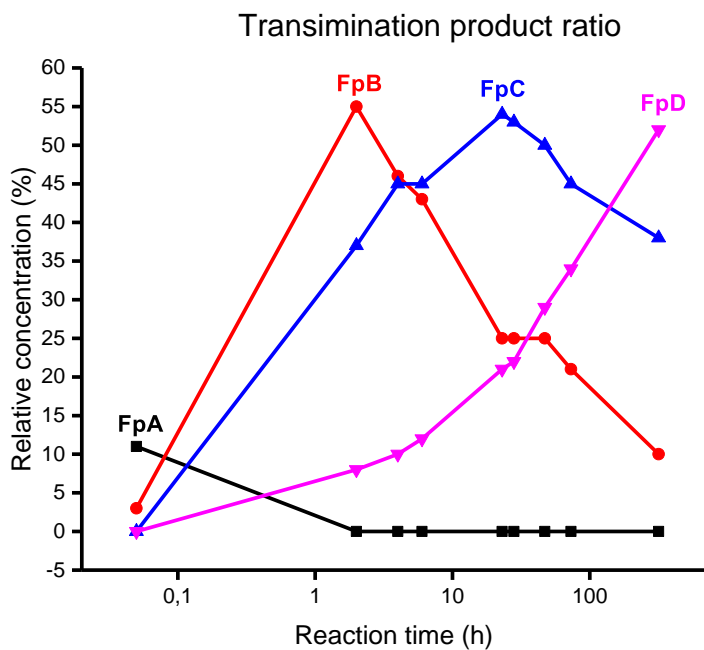


Figure 8. Relative hydrolysis rate of various hydrazones and oximes.⁶²

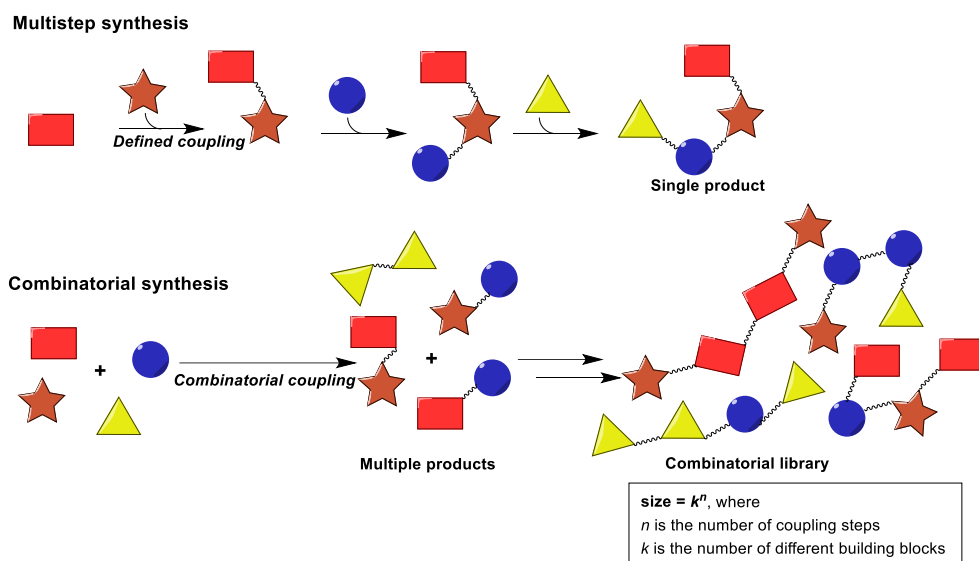


Scheme 7. Dynamic combinatorial transimination experiment. Reaction conditions: **Fp** + **A** + **B** + **C** + **D** (20 mM each), MeOD, 60 °C.⁶⁴

1.3 Combinatorial chemistry

Combinatorial chemistry is a concept of simultaneous synthesis of multiple products from a set of starting materials. In comparison, classic organic synthesis is based on

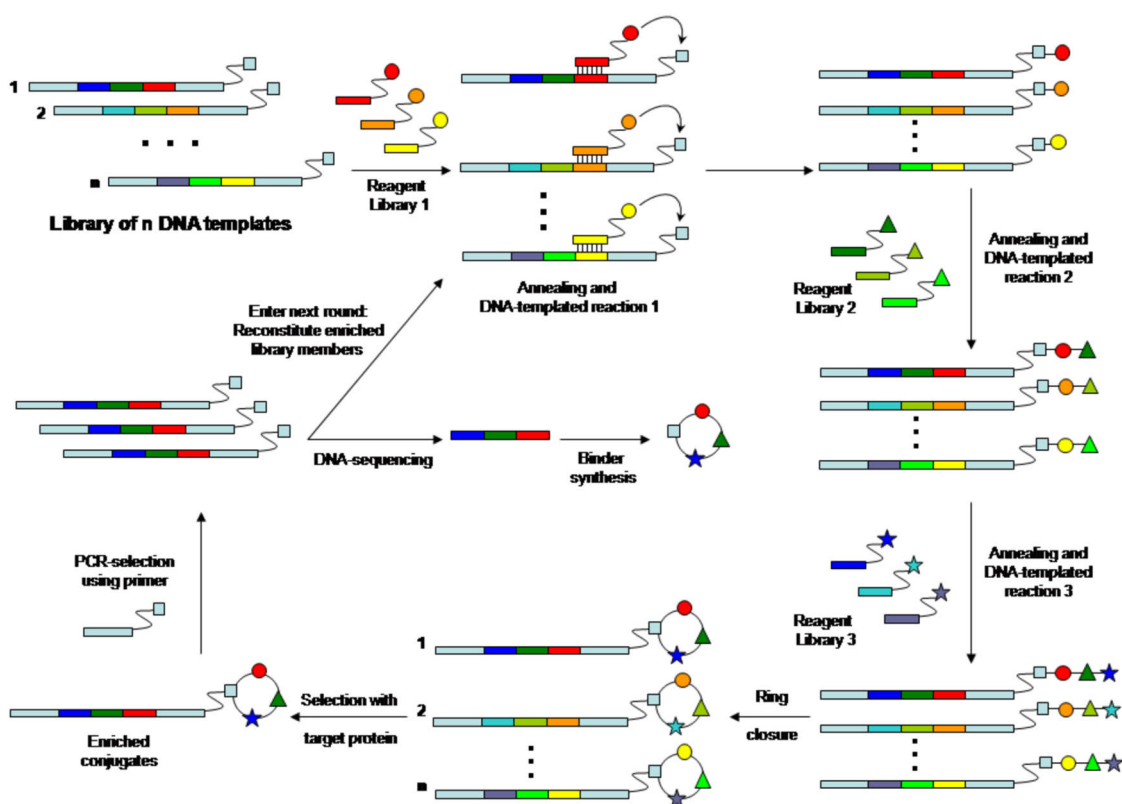
multiple steps and often yields a single desired product, whereas combinatorial synthesis means synthesis of multiple products in a single step. Furthermore, the combinatorial steps can be done in a sequence to produce an even wider range of products. For example, traditional peptide synthesis is based on coupling a defined amino acid in each coupling step, but a combinatorial approach would be to expose multiple amino acids for each coupling step (Scheme 8). The desired result from traditional synthesis is one sequence-defined peptide, while the combinatorial approach gives all the possible sequences. The mixture of combinatorial products is called combinatorial library, size of which is dependent on the number of different amino acids and coupling steps.



Scheme 8. Comparison of multistep synthesis and combinatorial synthesis.

Combinatorial chemistry is now a common approach in early phase drug development for discovering bioactive small molecules.⁶⁷ Affinity screening can be used to pick the desired molecules from the library (i.e. by attaching the target on a solid support), but characterization of those is difficult due to low concentration of each binder. To solve this problem, DNA-encoded libraries (DELs)⁶⁸ have been designed. In synthesis of DELs, a DNA-template guides a multistep combinatorial synthesis, and the final products can be deconvoluted based on the sequence of the template (Scheme 9). A small amount of material is no longer an issue, as PCR can be used to amplify the enriched templates after selection for new synthesis/selection round or for sequencing. DELs are utilized in the pharmaceutical industry, where software-controlled platforms are used to perform all the steps in the process,

including library design, synthesis, affinity screening, sequencing, and deconvoluting the hits.⁴ Adopting DELs in drug discovery is motivated by its low costs. It is estimated, that synthesizing and screening a library via traditional “one reaction per well” high-throughput methods and DELs costs 1100\$ and 0.0002\$ per compound, respectively.⁶⁸ The intrinsic limitation of DNA-templated synthesis (DTS) is that the reactions must be carried out in aqueous solution to enable DNA-hybridization, whereas organic reactions are typically carried out in non-aqueous conditions. Still, up to 40 trillion member DELs have been generated.³ For accessing more variety to the chemical space to improve the hit rate, it is important to develop DTS-compatible chemistry and building blocks.

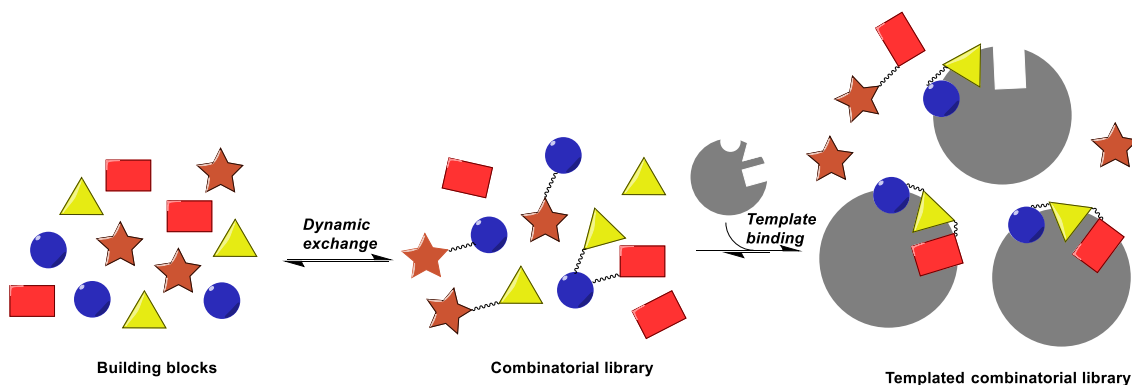


Scheme 9. Creation of a DNA-encoded chemical library by DNA-templated synthesis, screening for binder and deconvolution of its structure. Adapted with permission⁶⁹ from reference⁷⁰.

Dynamic combinatorial chemistry^{5,8,10,11,71–73} (DCC) is combinatorial chemistry based on reversible reactions. The concept includes supramolecular assembly of building blocks and their reversible covalent coupling. The obtained dynamic set of

building blocks and products is called a dynamic combinatorial library (DCL). The early definition of DCL is that all members are in thermodynamic equilibrium, but the definition has later been expanded into study of all reversible systems driven either by kinetics or thermodynamics.⁷¹ The main idea of DCC is that the quality and ratio of products can be altered by changing environmental conditions, such as pH, temperature, electronic field, and most often, a molecular template.⁷³

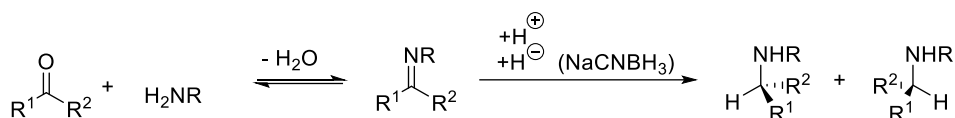
Using a molecular template in DCL generation, termed as target-directed DCC (tdDCC), was the original purpose of DCC for discovering new ligands for biomolecules and creating artificial receptors. The inspiring viewpoint on tdDCC is, that the synthesis and screening of the high-affinity binders can be done in a single process,⁸ with the potential to streamline early phase drug discovery. The most often employed strategy is comparative tdDCC, in which the DCLs formed in the presence and without a template are compared. The molecular species which have binding affinity to the template will be amplified at the expense of the non-binders (**Scheme 10**). Today, tdDCC has been used to discover synthetic receptors^{74–80} aptamers^{81,82}, ligands for proteins^{8,83–85} and nucleic acids^{7,86}, and catalysts^{87–89}.



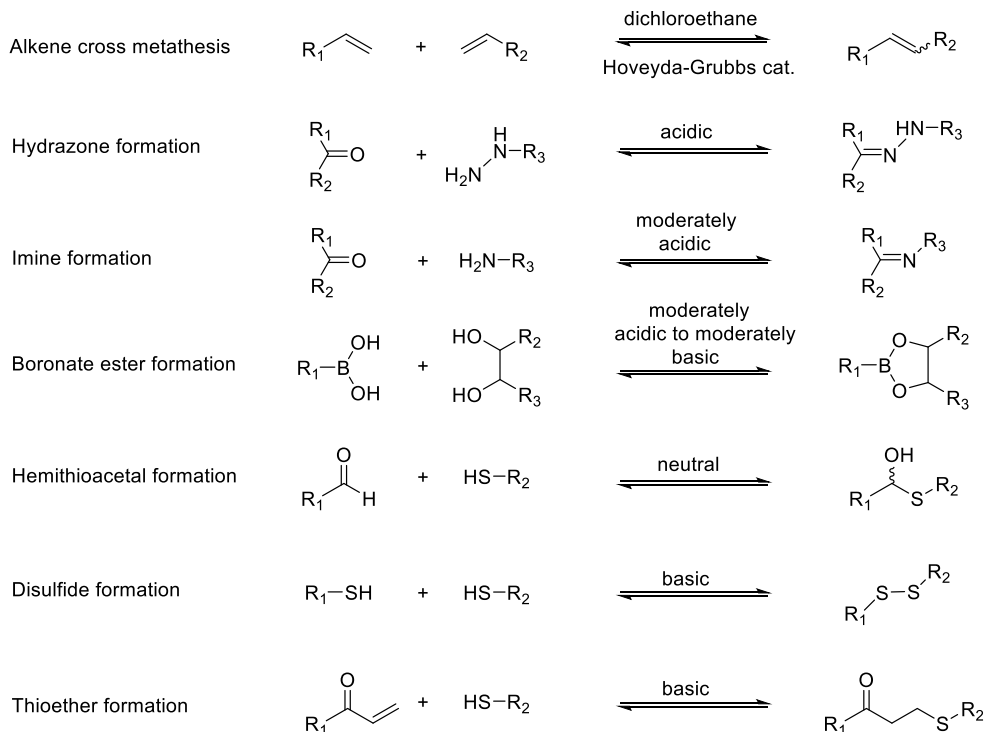
Scheme 10. Target-directed dynamic combinatorial chemistry: Templated DCL generation.

Reactions and structures used for biological targets in tdDCC include alkene cross metathesis,⁹⁰ hydrazones^{6,91–93}, imines^{94,95}, boronate esters^{96,97}, hemithioacetals⁹⁸, disulfides^{99,100}, and thioethers (**Scheme 12**). Biocompatible reactions should proceed in near-physiological conditions and be bioorthogonal, i.e., they cannot cross react with common biological functional groups. From analytical perspective, it is desirable that the reaction can be halted. For example, the dynamic trans-amination can be halted by addition of sodium cyanoborohydride, which results in stable amines (**Scheme 11**).⁹⁴ A rarer strategy converts imines into bis-amides via Ugi reaction (**Scheme 13**)¹⁰¹. A shortcoming of these strategies is that the resulting stable products may have different binding modes than their parent DCL members. Also,

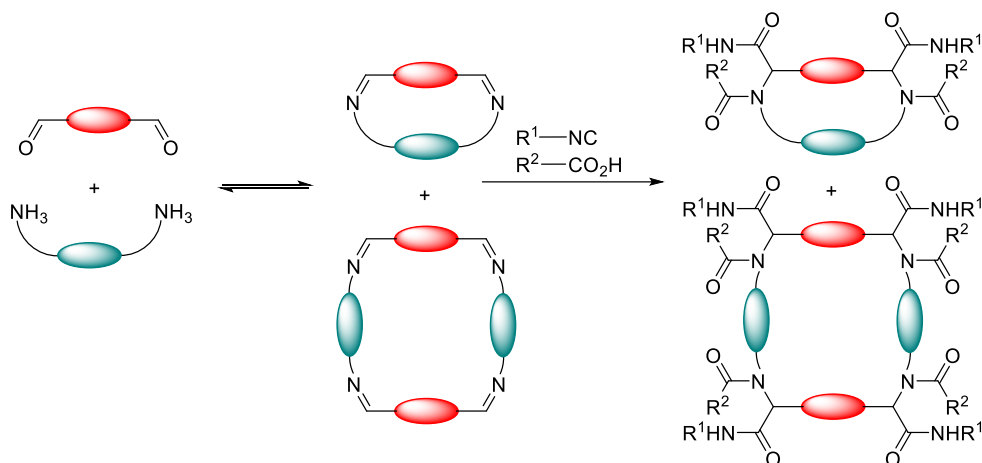
the best binders may be partially shielded from the irreversible transformation step, which may result in false deconvolution of the DCL members. Therefore, it is desirable that the reaction could be halted by simple change in reaction conditions. For example, hydrazones are labile or stable structures in slightly acidic or basic conditions, respectively. Disulfides are also commonly used in DCLs. Disulfide exchange can be started by mixing thiols under neutral to basic conditions (pH 7–9), and it is halted by oxidation under atmospheric oxygen.⁷² Disulfide exchanges can be reactivated or prolonged by addition of reducing catalysts such as dithiothreitol.¹⁰² Notable is, that neither of these reactions are fully bioorthogonal: hydrazones may react e.g. with carbohydrates¹⁰³ whereas disulfides may react with cysteine residues of proteins.



Scheme 11. Reductive amination: Irreversible hydride reduction of reversible imine intermediate. A racemic mixture of amines is obtained.



Scheme 12. Reactions used in target-directed DCC to find bioactive molecules. Adapted with permission from reference⁸³. Copyright 2019 Chemistry Europe.



Scheme 13. Transimination of macrocycles freed by Ugi reaction. Adapted with permission from reference ¹⁰¹. Copyright 2007 American Chemical Society.

1.4 DNA-templated synthesis

DNA-templated synthesis^{1,2} (DTS), or more broadly speaking, nucleic acid templated synthesis, is a common chemical reaction found in all living beings. The reading of the genetic information from DNA and RNA is based on templated synthesis. These processes include replication of DNA, translation, and transcription. DTS is based on Watson-Crick base pairs A-T and G-C, which are formed due to complementary hydrogen bonding (**Figure 9**). Due to the hydrogen bonding, two nucleic acid chains will hybridize, i.e., bind to each other in water solution, forming a structurally well-defined duplex if they have enough complementary bases. Similarly, self-complementary nucleic acids can hybridize intramolecularly to form hairpins and more complex secondary structures such as tRNA (**Figure 10**).

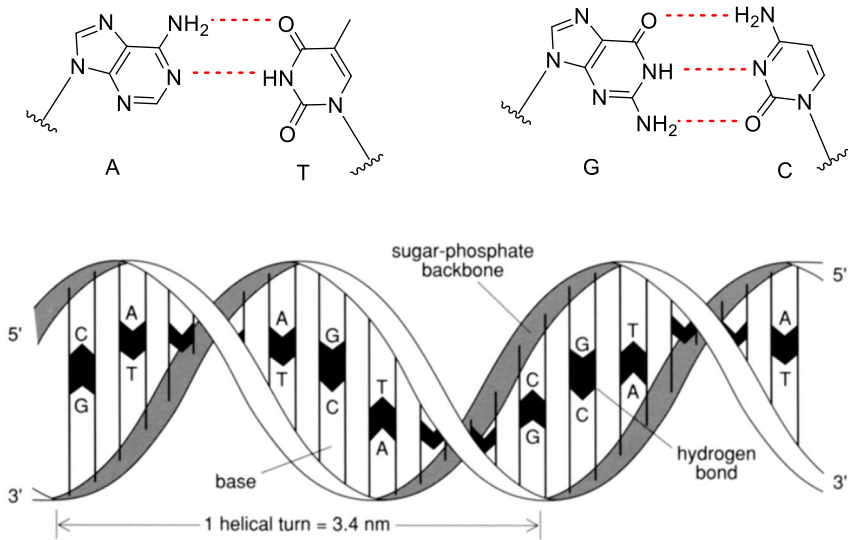


Figure 9. Watson-Crick basepairs A-T and G-C on the top and double helix of the DNA on the bottom. Adapted with permission from reference¹⁰⁴ Copyright 1990 Taylor & Francis.

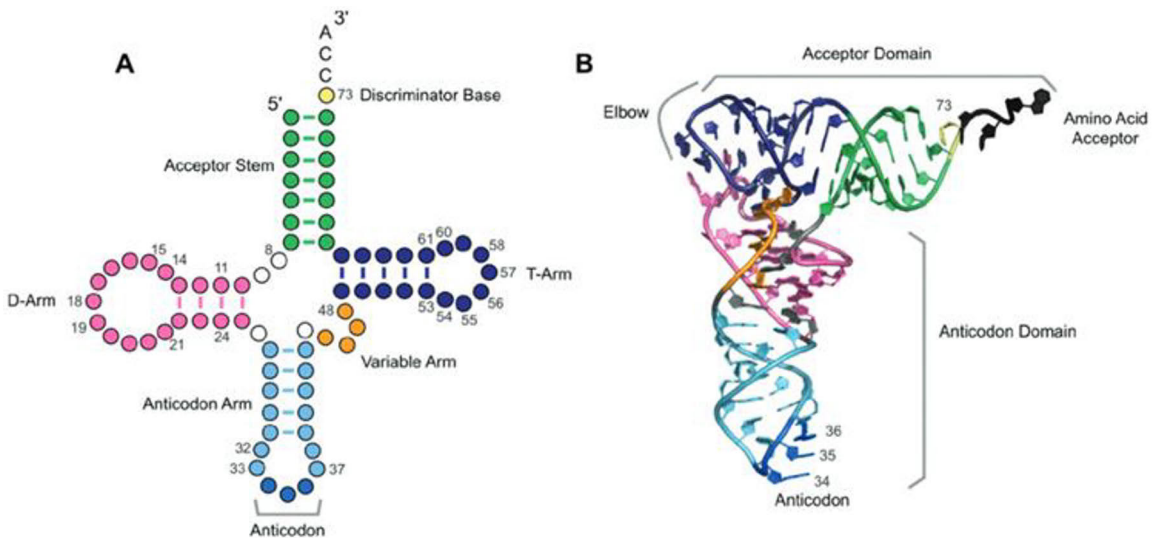


Figure 10. The secondary structure of tRNA (A) 2D-projection showing the three hairpin loops and four-way junction (B) 3D-structure. Adapted with permission from reference¹⁰⁵. Copyright 2021 Taylor & Francis.

Hybridization of DNA is driven by enthalpy and penalized by entropy loss.¹⁰⁶ At high temperatures, the entropic penalty is higher than the enthalpic gain.¹⁰⁷ Therefore, a certain temperature threshold will lead to dissociation of the complementary strands, i.e., melting of the secondary structure (or duplex). The

melting point (T_m) of a secondary structure is defined as the temperature where 50% of the structures are dissociated. It is affected by the amount of complementary base pairs (where G-C is more stable than A-T), salt concentration¹⁰⁸, pH¹⁰⁹, and detergents¹¹⁰. In practice, the dynamic association of even short complementary nucleic acids is efficient and rapid in neutral aqueous solution. For example, a micromolar concentration of DNA-duplexes of 15 nucleobases usually have T_m well-above room temperature.¹¹¹ The high equilibrium constant of the hybridization makes it an efficient tool to drive sluggish reactions forward under low concentration.

A prototypical model of DNA-templated synthesis consists of a template strand that forms simultaneous duplexes with two reactant strands (**Figure 11B**). The duplex formation brings the reactive ends of the reactant strands to proximity of each other. The effective concentration increment allows the templated ligation reaction to proceed faster and achieve higher yields than predicted by the nominal concentration of the reactive species. Another often utilized model is the hairpin, in which the template catalyses ligation (**Figure 11C**) with a single reactant strand. The hairpin model is more efficient template compared to a similar length duplex, because the overhang region of the hairpin template is partially preorganized into the double helical form. This results in less entropic penalty when the reactant hybridizes.¹¹²

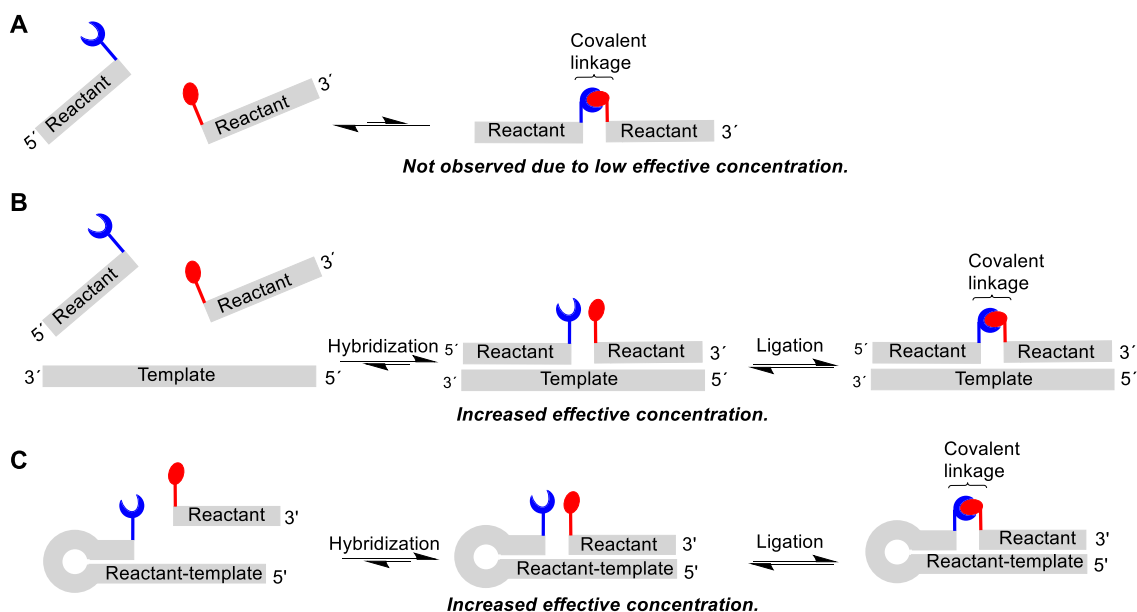


Figure 11. Comparison of a reversible ligation as a non-templated (A) or DNA-templated (B and C) reaction.

As discussed in the previous chapter, DTS is commonly used in pharmaceutical industry to generate DELs, consisting of trillions of small-molecules (cf. **Scheme 9**).⁶⁸ Based on similar principle, DNA-encoded polymers have been studied. A DEL consisting of 4.3×10^8 40-mer PNA-polymers have been synthesized from 5-mer building blocks.¹¹³ The DEL was exposed to iterative selection by protein affinity, followed by PCR amplification of the survived members, and then applied for a new round. Combining this with the fact that sidechains can be incorporated to the PNA building blocks without losing polymerization efficacy,¹¹⁴ it may be possible to produce, using evolutive cycles, target-specific synthetic polymers with additional properties compared to antibodies or aptamers.

Dynamic DNA-templated boronate ester ligation has been studied for self-assembly of artificial biopolymers.^{115,116} It is based on ligation between 3'-ribose nucleotide and modified 5'-boronic acid nucleotide (**Figure 12**). The ligation is controllable by the acidity of the solution. High pH favours the ligation, while acidic conditions favour the non-ligated starting material. The boronate ester ligation has been used for reversible oligomerization of bifunctional building blocks encoded by a DNA template.^{115,116} The boronate ester ligation has also been used in assembly of split DNAzyme.¹¹⁷ In this work, a RNA substrate templated the assembly of a 10–23 DNAzyme via boronate ester ligation. The assembly of 10–23 DNAzyme led to cleavage of the RNA substrate. While splitting of an unmodified 10–23 DNAzyme strongly inhibited its activity due to low stability of the functional structure, the boronic acid modification restored the activity. Later, the same chemistry was applied in restoring the activity of split ribozyme and light-up aptamer,¹¹⁸ proving the boronate ester ligation as a tool for synthesis of dynamic oligomers with template-induced functionality. These kinds of oligomers may find use in applications such as cellular monitoring.

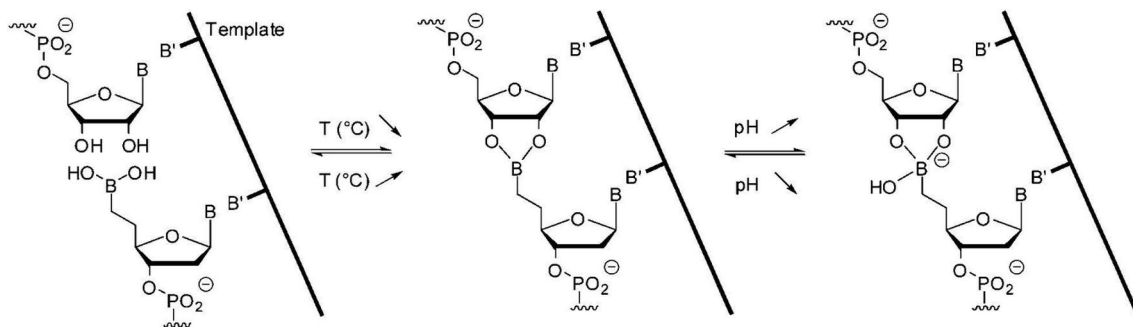
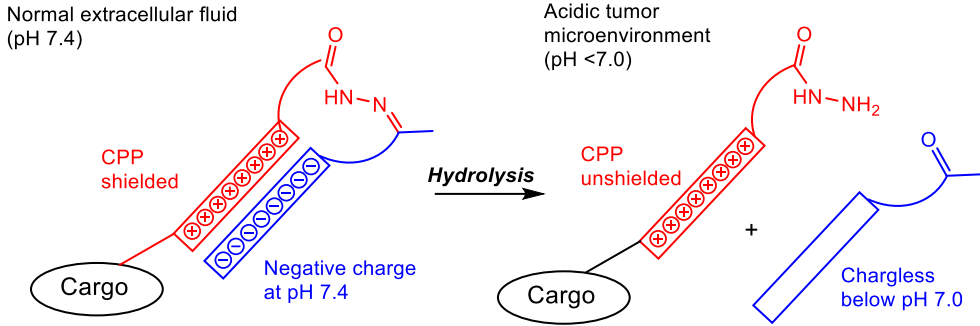


Figure 12. DNA-templated boronate ester ligation controlled by temperature and acidity of the solution. Adapted with permission from reference ¹¹⁵. Copyright 2015 Royal Society of Chemistry.

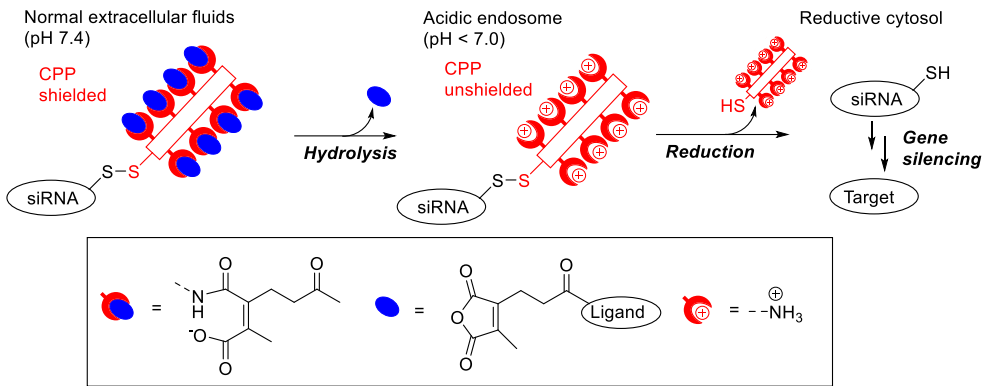
1.5 pH-responsive cleavable linkers in therapeutic oligonucleotides

Dynamic coupling reactions are utilized in delivery of APIs into target cells. Antibody–small molecule drug conjugates are examples of warheads attached to cell-specific targeting groups.^{12–14,119} Likewise, in the emerging field of oligonucleotide therapeutics (TONs), techniques are needed to deliver polyanionic oligonucleotides through the cell membranes into cytosol to reach the target site inside the cell.^{120,121} Cleavable linkers are utilized in TON-conjugates to shake off the delivery agents with the final goal of TONs interacting freely with the cytosolic target. Furthermore, cleavable linkers are used to mask membrane-penetrating agents to be activated only in endosomal compartments for less off-target delivery.
122–124

Cell penetrating peptides (CPPs) have been investigated for delivery of TONs using cleavable linkers.^{125,126} Acidic tumor microenvironment was targeted in the delivery of a siRNA–CPP conjugate, where the cationic CPP moiety was shielded by anionic peptide sequence in a hairpin structure (**Scheme 14**). The approach relied on the cleavage of the acid-labile hydrazone linker when exposed to acidic microenvironment and subsequent dissociation of the shielding peptide, exposing the cationic CPP to penetrate the conjugate into a tumor cell.¹²⁴ Most preferably, the delivery vehicle of TON would include both tissue-specific targeting ligands and endosomal escape domain. As an example, a siRNA was conjugated via disulfide to a CPP, while the CPPs were covered with cell-specific ligands, using acid-labile maleimide linker (**Scheme 15**). In the construct, CPPs are activated after receptor-mediated endocytosis and acidic cleavage of the ligands, leading to more efficient endosomal escape. After endosomal escape, the disulfide linkage between the CPP and the siRNA is cleaved due to reductive environment of the cytosol, allowing the siRNA to reach its target unhindered.^{122,123} While efficient delivery may be obtained by highly sophisticated targeting–transfection-agents, cost-effective synthesis of these is another challenge. Both the optimization of the delivery strategies and large-scale synthesis of oligonucleotides and their conjugates remains a challenge for the commercial success of TONs.



Scheme 14. Shielding of a cationic CPP by hydrazone-linked anionic peptide. The cationic CPP is inactive in neutral conditions while linked to the anionic peptide, but acidic environment causes the shielding peptide lose its charge and hydrolysis of the hydrazone linker.¹²⁴



Scheme 15. Sophisticated siRNA-delivery by conjugation via disulfide to a cationic polymer dynamically shielded by cell-targeting ligands.^{122,123}

2 Aims of the Thesis

N-methoxyoxazolidine was studied as a pH-sensitive dynamic linker for conjugation of oligonucleotides. The handles required for the reaction (i.e. aldehyde and *N*-methoxyaminoethanol moieties) can be introduced to oligonucleotides using automated synthesis. For this purpose, appropriate building blocks and a solid-supported material were prepared. The aim was to study (i) the reversibility, reaction kinetics, and pH-dependency of *N*-methoxyoxazolidine formation (ii) the applicability of the reaction for the preparation of pH-responsive oligonucleotide conjugates with various conjugate groups (small molecules, carbohydrates, and peptides) and (iii) in DNA-templated ligation. The *N*-methoxyoxazolidine ligation was then further demonstrated in dynamic assembly of (iv) split-aptamers and (v) G-quadruplexes in small-molecule and metal-ion templated ligations, respectively.

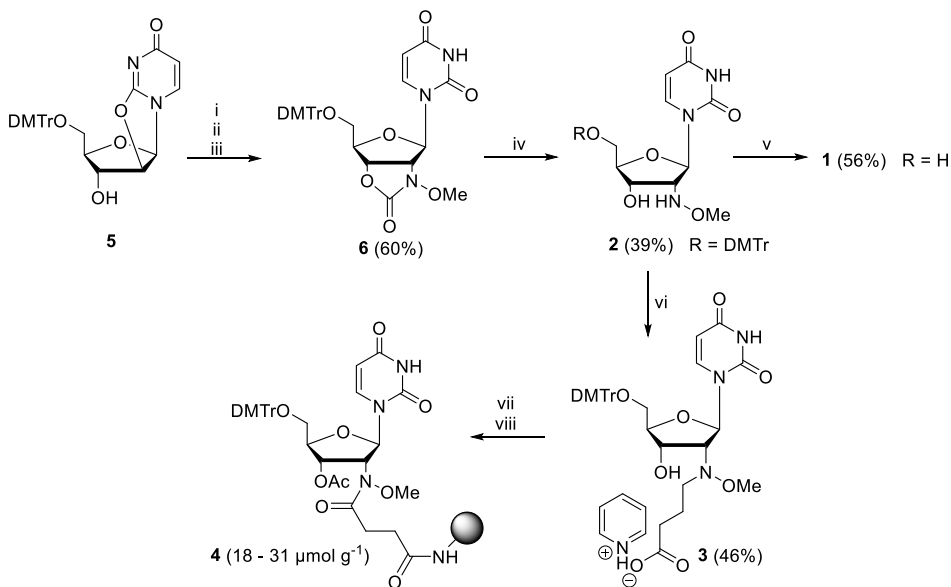
The aims of the thesis may be summarized as follows:

- i) Determine the reversibility, reaction kinetics and pH-dependency of *N*-methoxyoxazolidine formation.
- ii) Conjugate oligonucleotides to various conjugate groups (small molecules, peptides, PNA) via *N*-methoxyoxazolidine linker and study the pH-sensitive degradation of the conjugate.
- iii) Study the viability of the dynamic *N*-methoxyoxazolidine formation for DNA-templated ligation between two complementary DNA-strands.
- iv) Study the dynamic *N*-methoxyoxazolidine ligation between split aptamer DNA fragments. The effect of small-molecular substrate on the ligation yield is determined.
- v) Study the dynamic *N*-methoxyoxazolidine ligation between G-quadruplex-forming DNA fragments. The effect of metal-ion concentration in the ligation yield is determined.

3 Results and Discussion

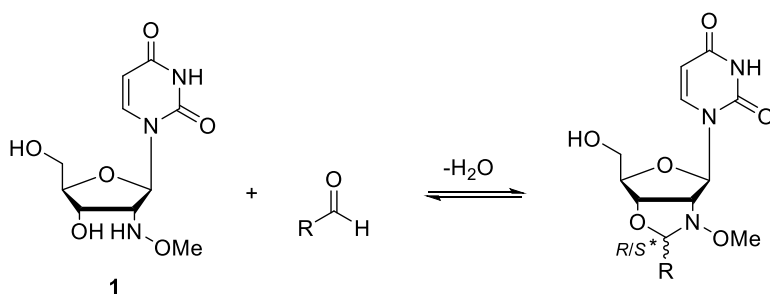
3.1 Kinetic and thermodynamic assessment of *N*-methoxyoxazolidine formation by small-molecular models

The dynamic formation *N*-methoxyoxazolidines was studied first using small-molecular models. For this, 2'-deoxy-2'-*N*-methoxyuridine (**1**) was synthesized as shown in **Scheme 16**. Notably, the key intermediate **2** (which was synthesized according to a previously published procedure¹²⁷) was also derived into *N*-succinylated nucleoside analog **3** that was attached to LCAA-CPG to obtain solid support **4**. The solid support **4** was used in automated synthesis of oligonucleotides bearing nucleoside **1** at the 3'-terminus (U^{NOMe}-ONs, cf. synthesis in chapter 3.2.1), which were studied for dynamic oligonucleotide conjugation (chapters 3.2 and 3.3).



Scheme 16. Synthesis of nucleoside **1** and solid support **4**. Conditions: i) CDI 1.5 equiv., pyridine, RT; ii) MeONH₂ 4.0 equiv., pyridine, RT; iii) DBU 0.2 equiv., THF, RT; iv) Cs₂CO₃ 3.0 equiv., MeOH, RT; v) HCl (aq.), MeOH, RT; vi) succinic anhydride 1.4 equiv., DMAP cat., pyridine; RT; vii) PyBOP 1.0 equiv., DIPEA 2.0 equiv., LCAA-CPG.

The *N*-methoxyoxazolidine formation was studied as a reaction between nucleoside analog **1** and small-molecular aldehydes (**Scheme 17**). While reactions with aromatic aldehydes (benzaldehyde and anisaldehyde), and ketones (acetone) were sluggish and not studied in detail, aliphatic aldehydes (acetaldehyde, butyraldehyde, *N*-Bz-glycinaldehyde, *N*-Bz- β -alaninealdehyde, and *N*-Bz-oxopropionaldehyde) were examined more closely due to their higher reactivity. The aliphatic aldehydes (5 mM) were mixed with nucleoside **1** (5 mM) under aqueous conditions at room temperature. The reactions were monitored using RP HPLC showing two products (**Figure 13A**), which were isolated and identified (by NMR and mass spectrometry) as *R/S*-isomers of the expected *N*-methoxyoxazolidines. The kinetic data was fitted to reversible bimolecular integrated rate law (**Figure 13B**) to obtain half-lives ($t_{1/2}$) and equilibrium constants for the reactions at pH 4, 5, and 6 (**Table 1**). Similarly, decay reactions were studied by redissolving the isolated *N*-methoxyoxazolidines in acidic water and monitoring their hydrolysis (**Table 1**). The equilibrium yields varied between 49% (butyraldehyde at pH 6) and 86% (*N*-Bz-Gly-H at pH 5), which converts to 379–9038 M⁻¹ equilibrium constants. Both the formation and hydrolysis rates were proportional to the acidity of the reaction solution with up to 58-fold shorter half-life at pH 4 compared to pH 6 (*N*-Bz- β -alaninealdehyde). No clear pH-dependency of the equilibrium constant was observed in the studied range. The rate of the reaction was dependent on the aldehyde structure in following order: acetaldehyde > butyraldehyde > 3-benzyloxypropionaldehyde > *N*-Bz- β -Ala-H > *N*-Bz-Gly-H. From this set it is concluded that EWGs on the aldehyde slow both the formation and hydrolysis of *N*-methoxyoxazolidines. This is coherent with the general trends of acetals and was recently found to be true also for *N*-methoxy-1,3-oxazinanes (6-ring variant of *N*-methoxyoxazolidines).¹²⁸



Scheme 17. The dynamic formation of *N*-methoxyoxazolidine between nucleoside **1** and aldehydes.

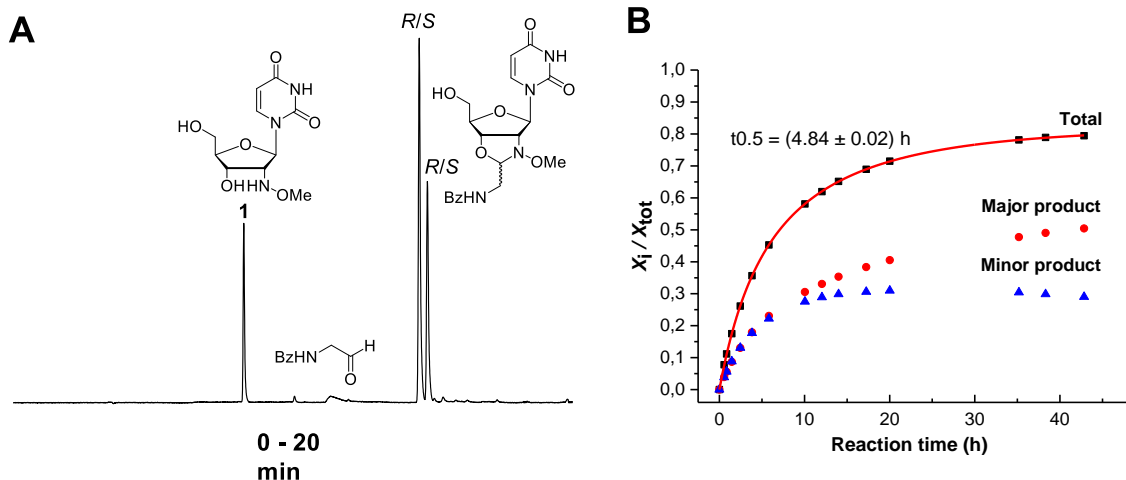
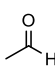
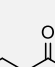
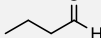
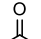
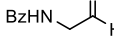
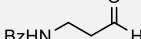
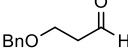


Figure 13. Selected reaction profiles for *N*-methoxyoxazolidine formation. A) RP HPLC (C18, 250 × 4.5 mm, 5 μm) profile for the reaction between **1** and *N*-Bz-Gly-H. A linear gradient (0–60% in 20 min) of MeCN over aqueous TEAA buffer (pH 7, 50 mM), a flow rate of 1.0 ml min⁻¹, and a detection wavelength of 260 nm were employed. B) Kinetic profile for *N*-methoxyoxazolidine formation between **1** and *N*-Bz-Gly-H at pH 4.

Table 1. Thermodynamic and kinetic data for *N*-methoxyoxazolidine formation between **1** and small-molecular aldehydes.

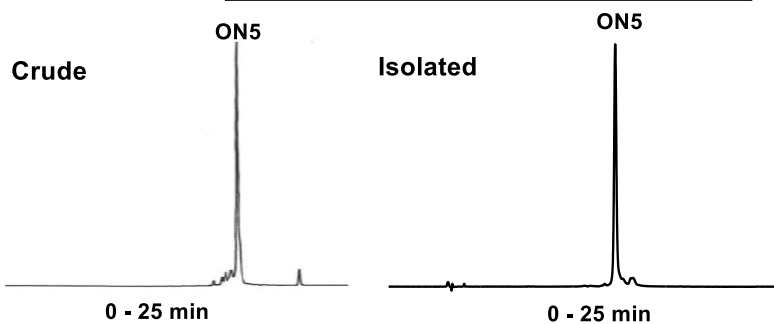
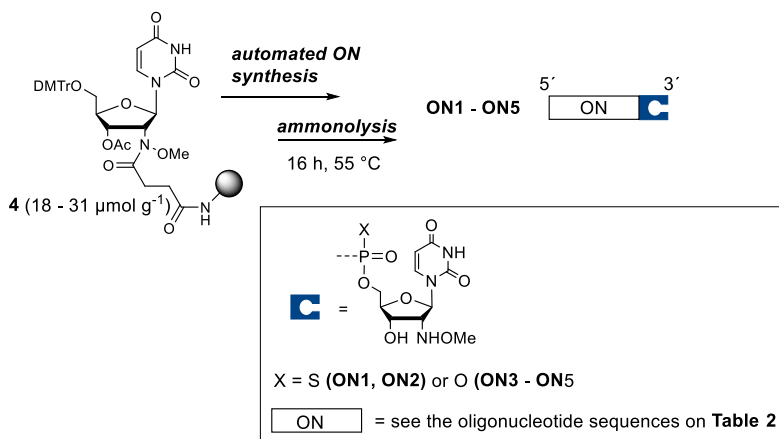
Entry	Aldehyde	pH	$t_{1/2}$ formation	$t_{1/2}$ decay	Equilibrium yield (%)	Equilibrium constant (M ⁻¹)
1		4	7.90 ± 0.27	1.54 ± 0.30 h	59	693 ± 29
2		5	25.8 ± 0.6 min	3.32 ± 0.40 h	62	856 ± 27
3		6	3.93 ± 0.09 h	43.1 ± 2.7 h	67	1211 ± 39
4		4	11.8 ± 0.6 min	1.50 ± 0.34 h	62	835 ± 49
5		5	40.1 ± 0.6 min	5.29 ± 0.58 h	54	499 ± 7
6		6	4.14 ± 0.04 h	N/A	49	379 ± 3
7		4	4.84 ± 0.02 h	16.1 ± 0.7 h	82	4958 ± 50
8		5	33.0 h ± 1.3 h	75.5 ± 16.3 h	86	9038 ± 1265
9		6	12.8 ± 0.6 d	N/A	74	2224 ± 183
10		4	29.2 ± 6.6 min	5.28 ± 0.58 h	75	2398 ± 425
11		5	N/A	28.5 ± 2.2 h	N/A	N/A
12		6	N/A	310 ± 34 h	N/A	N/A
13		4	21.6 ± 0.5 min	2.00 ± 0.14 h	64	959 ± 28
14		5	1.92 ± 0.05 h	9.98 ± 0.38 h	66	1144 ± 39
15		6	25.0 ± 0.7 h	88.2 ± 6.8 h	63	939 ± 34

3.2 Acid-labile conjugation of therapeutic oligonucleotides

Delivery of therapeutic oligonucleotides into specific cells can be improved by conjugating them with molecules that helps with targeting to cell-specific structures.^{121,129–133} The intake can also be enhanced with various tissue-penetrative conjugate groups. In this context, acid-labile linkers can be used to further improve the targeting i.e. by enhancing the endosomal escape of the oligonucleotide.^{122–124} Herein, applicability of *N*-methoxyoxazolidine as acid-labile linker was evaluated. For this, therapeutically relevant oligonucleotides modified with 3'-terminal nucleoside (U^{NOMe}-ONs, chapter 3.2.1) and different conjugate groups with aldehyde handles (chapter 0) were synthesized. These two entities were then conjugated together via *N*-methoxyoxazolidine to form conjugates (chapter 3.2.3). Finally, the hydrolysis of the conjugates, i.e., the cleavage of *N*-methoxyoxazolidine linkage was studied under slightly acidic to neutral conditions to assess if *N*-methoxyoxazolidine linkage could be used for site-specific release of therapeutic oligonucleotides (chapter 3.2.4). The hypothesis was that the conjugates should be stable under physiological pH 7.4 but cleaved under slightly acidic conditions (pH 5–6) perceived to early endosomes.

3.2.1 Synthesis of oligonucleotides bearing 3'-terminal 2'-deoxy-2'-*N*-methoxyuridine (U^{NOMe}-ONs)

Solid support **4** (cf. synthesis in **Scheme 16**) was used to synthesize oligonucleotides bearing 3'-terminal nucleoside **1** (U^{NOMe}-ONs) as shown in **Scheme 18**. Various U^{NOMe}-ONs including 2'-*O*-methyl-RNA with phosphorothioate backbones (**ON1** and **ON2**), 2'-*O*-(2-methoxyethyl)-RNAs (**ON3** and **ON4**), and DNA (**ON5**) were synthesized on solid support **4** using commercial phosphoroamidite building blocks and regular coupling conditions. After chain elongation, the U^{NOMe}-ONs were cleaved using concentrated aq. ammonia (16 h at 55 °C) and then purified by RP HPLC (**Scheme 18**). The isolated yields varied between 17–40% (**Table 2**). The yields are comparable to oligonucleotides synthesized by using fully commercial building blocks and, after obtaining support **4**, the protocol is identical to a regular automated oligonucleotide synthesis. Furthermore, the solid support **4** can be obtained in multigram scale via simple synthesis and from inexpensive materials and stored in refrigerated conditions (>2 years with no notable decomposition). These facts make the U^{NOMe}-ONs attractive for research purposes.



Scheme 18. Automated synthesis of U^{NOMe} -ONs (ON1–ON5) and a typical RP HPLC profile of crude and isolated product. Full sequences are displayed in Table 2. RP HPLC (C18, 250 × 10 mm, 5 μm) conditions were as follows. A linear gradient of MeCN (5–40% in 25 min) over aqueous TEAA (pH 7, 50 mM), a flow rate of 2.5 ml min^{-1} , and a detection wavelength of 260 nm were employed.

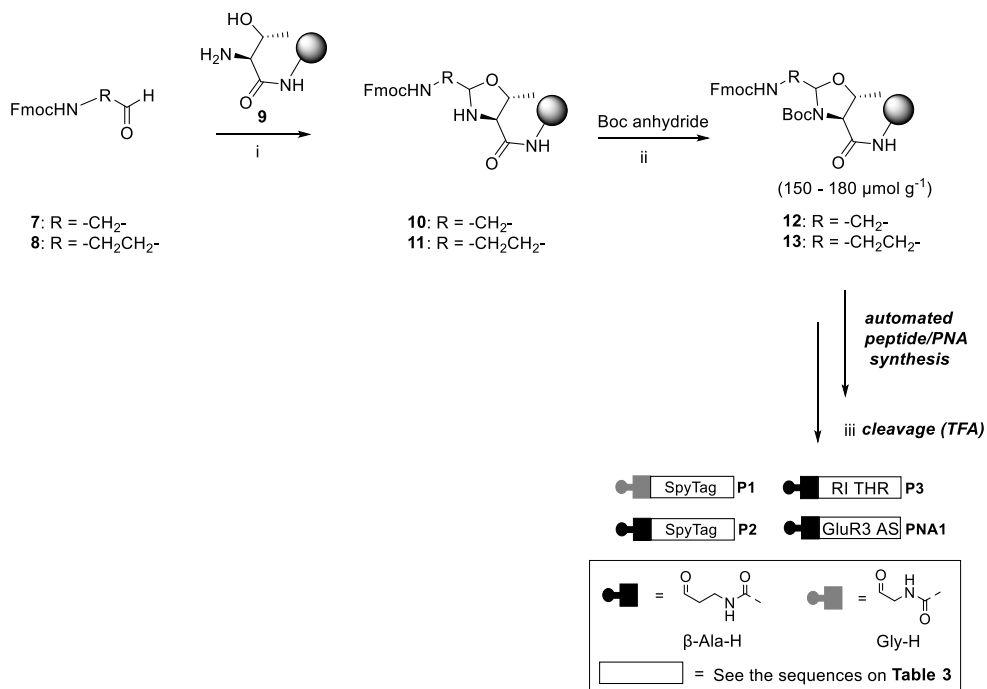
Table 2. The sequences and yields for the synthesized 3'- U^{NOMe} - ONs.

Oligonucleotide	Sequence ^a	Yield (%) ^b
ON1	CUAGUAUGAAAGAGAGACAUUGU ^{NOMe} (cf. AR-V7 ISE ¹³⁴)	33
ON2	[BCN] CUAGUAUGAAAGAGAGACAUUGU ^{NOMe} (cf. AR-V7 ISE ¹³⁴)	17
ON3	<u>UCACUUUCAUAAUGCUGGU</u> ^{NOMe} (cf. Nusinersen ¹³⁵)	32
ON4	<u>TCCATTTATTAGTCTAGGAAU</u> ^{NOMe} (cf. DGAT2 AS ¹³⁶)	29
ON5	GCGTGGTCACACGCTTU ^{NOMe} (cf. tFRA3 ¹³⁷)	40

^aExplanation for the characters: bold are 2'-O-methylribonucleotides with phosphorothioate backbones, the underlined are 2'-O-(2-methoxyethyl)ribonucleotides, and the rest are 2'-deoxyribonucleotides. Explanation for the special residues: [BCN] is terminal bi cyclooctyne (commercially available), [FAM] is terminal fluorescein (commercially available). Structure of U^{NOMe} is shown in **Scheme 18**. The integrities of the isolated oligonucleotides were verified by mass spectrometry. ^bThe yields were determined UV-spectrophotometrically at 260 nm.

3.2.2 Synthesis of peptides, a PNA, and a GalNAc cluster bearing aldehyde handles

Peptides, a PNA, and a trivalent GalNAc cluster bearing aldehyde handles were synthesized to be conjugated with therapeutic U^{NOMe}-ONs. For the synthesis of peptide and PNA aldehydes, two types of solid supports were prepared (to study the rate-difference between two linkers) by attaching either Fmoc-Gly-H (**7**) or Fmoc-β-Ala-H (**8**) to H-Rink amide ChemMatrix resin (**Scheme 19**) by a published^{44,138} protocol: The Fmoc-amino aldehyde (**7** or **8**) was dissolved in a suspension of ChemMatrix-bound threonine (**9**) in anhydrous methanol basified with DIPEA to yield *N*-H-oxazolidine (**10** or **11**). The intermediate (**10** or **11**) was treated with Boc anhydride in dry THF basified with *N*-methylmorpholine to obtain *N*-Boc-oxazolidine solid support (**12** or **13**) with loading of 150 – 180 μmol g⁻¹ depending on the batch.



Scheme 19. Preparation of peptide and PNA aldehydes. Conditions: i) H-Rink amide ChemMatrix resin elongated by Thr (**9**) 270 mg, **7** or **8** 0.65 mmol, DIPEA 0.62 equiv., MeOH, 60 °C; ii) Boc anhydride 0.62 equiv., *N*-methylmorpholine 0.62 equiv., THF, 55 °C; iii) Cleavage cocktails: TFA/anisole (1:9, V/V) for **P1**, **P2**, and **PNA1**; anisole/EDT/thioanisole/TFA (2:3:5:90, V/V) for **P3**.

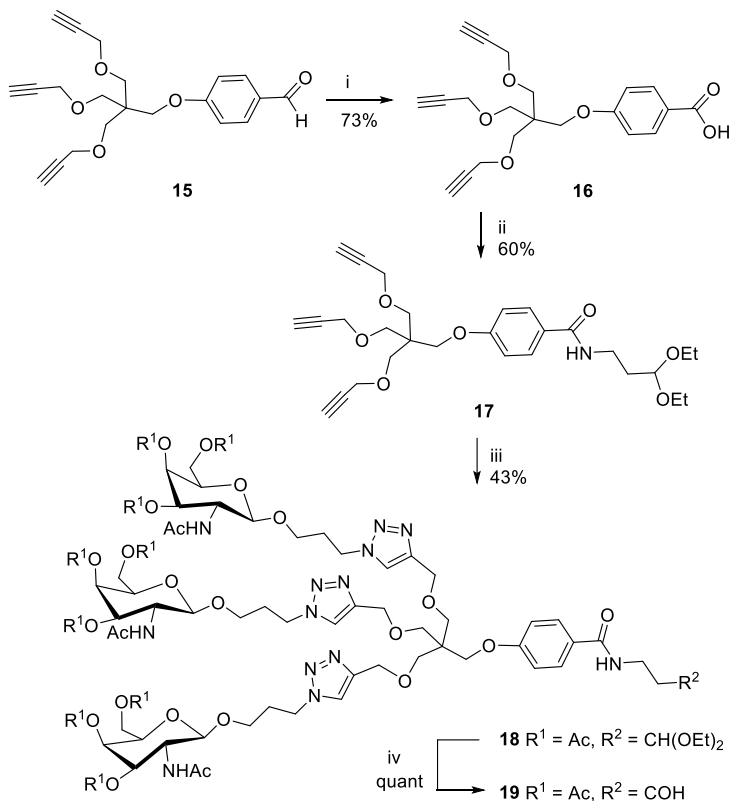
The solid support (**12** or **13**) was used in automated peptide synthesizer along with commercial Fmoc/tBu-protected building blocks and conventional coupling conditions. After chain elongation, the oligomers were cleaved from the ChemMatrix support and deprotected using TFA-based cleavage cocktails (see details in **Scheme 19**). The crude peptide and PNA aldehydes were precipitated in diethyl ether, and then purified by RP HPLC. The isolated yields for the peptide and PNA aldehydes (**P1**, **P2**, **P3**, and **PNA1**) varied between 7.1–27% (**Table 3**).

Table 3. Sequences and yields for the synthesized peptide and PNA aldehydes.

Peptide or PNA	Sequence ^a	Yield ^b (%)
P1	H ₂ N-Val-Pro-Thr-Ile-Val-Met-Val-Asp-Ala-Tyr-Lys-Pro-Thr-Lys-(AEEA) ₂ -Gly-H (cf. SpyTag ¹³⁹)	9
P2	H ₂ N-Val-Pro-Thr-Ile-Val-Met-Val-Asp-Ala-Tyr-Lys-Pro-Thr-Lys-(AEEA) ₂ -β-Ala-H (cf. SpyTag ¹³⁹)	27
P3	H ₂ N- <u>Pro-Trp-Val-Pro-Ser-Trp-Met-Pro-Pro-Arg-His</u> -β-Ala-H (cf. RI THR ¹⁴⁰)	12
PNA1	H ₂ N-GTAAGAGTGCCCT-β-Ala-H (cf. GluR3 AS ¹⁴¹)	7.1

^aThe underlined amino acids codes are D-amino acids, while the rest are L. Cursive letters are regular PNA residues. AEEA is commercially available 2-(2-(2-aminoethoxy)ethoxy)acetic acid spacer. Structure of Gly-H and β-Ala-H are shown in Scheme 19. The integrities of the isolated peptides and the PNA were verified by mass spectrometry. ^bThe yields were determined UV-spectrophotometrically: For peptides at 280 nm using the molar absorbance of Tyr and/or Thr residues and for PNA at 260 nm using the molar absorbance of corresponding nucleoside monophosphates.

The synthesis of trivalent acetyl-protected GalNAc cluster (**19**) started from pentaerythritol-based core (**15**)¹⁴² (**Scheme 20**). First, the formyl group of **15** was oxidized using the Jones reagent. The resulted acid **16** was then activated with BOP and coupled with 3-amino-1,1-diethoxypropane to obtain amide **17**. Then, using Cu(I)-catalyzed alkyne–azide cycloaddition (CuAAC), the terminal alkyne groups of **17** were decorated with 3,4,6-tri-*O*-Ac-GalNAc, resulting in **18**. Finally, the aldehyde function (β-Ala-H) was unmasked by treatment with aq. TFA to obtain the final aldehyde **19**. Noteworthy, the hydroxyl acetyl-protection groups were removed from the GalNAc units post-conjugation to reveal the biologically relevant carbohydrates.



Scheme 20. Synthesis of trivalent GalNAc cluster **19**. (i) Jones reagent, MeCN; (ii) 3-amino-1,1-diethoxypropane, DIPEA, BOP, DMF; (iii) 3-azidopropyl-2-acetamido-3,4,6-tri-O-acetyl-2-deoxy- β -D-galactopyranoside, CuI, DMF/dioxane/H₂O (3:3:1, v/v/v); (iv) TFA (0.01%, v/v) in H₂O.

3.2.3 Preparation of *N*-methoxyoxazolidine conjugates

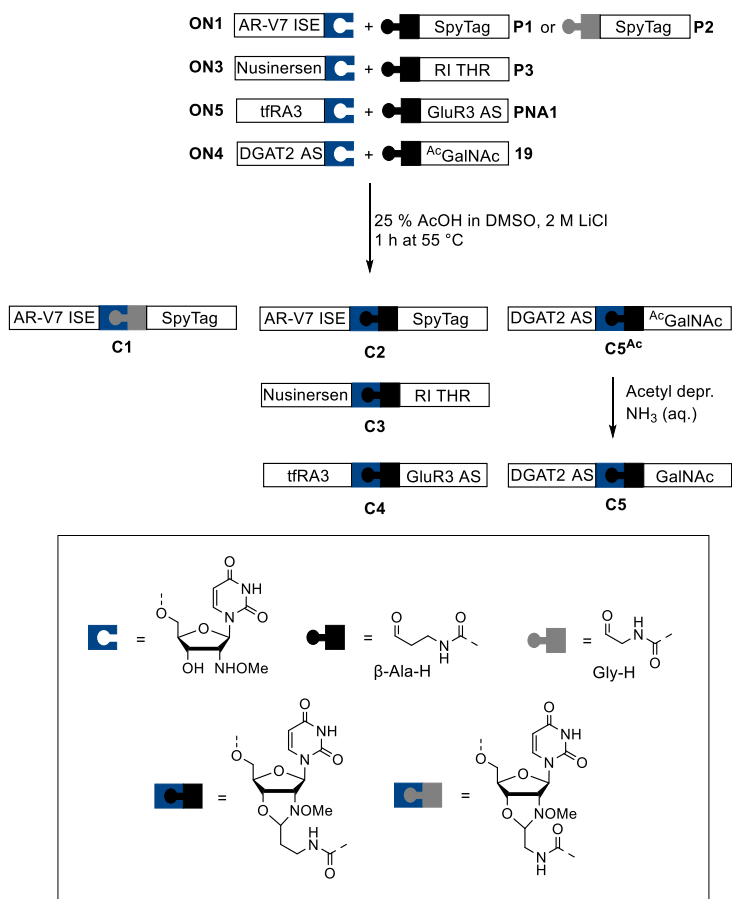
The U^{NOMe}-ONs and aldehyde-bearing conjugate groups were paired to obtain oligonucleotide conjugates. The oligonucleotide conjugates were designed to consist of a therapeutically active molecule (**ON1**, **ON3**, **ON4**, or **PNA1**) linked via *N*-methoxyoxazolidine linkage to a delivery-assisting conjugate group (**P1**, **P2**, **P3**, **ON5**, or **19**) as shown in **Scheme 21**. The rationale for each conjugate is as follows:

C1 and **C2**: AR-V7 ISE¹³⁴ is a phosphorothioate which reduces the expression of androgenic receptor splice variant 7 and is a potential treatment for castration-resistant prostate cancer. Its target is located in prostatic tumor cells. SpyTag¹³⁹ is a peptide tag that binds through irreversible isopeptide bond to a SpyCatcher protein domain. This specific binding could be utilized to attach the SpyTag-ON conjugate to a cell-targeting antibody, although, immunogenicity issues should be resolved before used in medicines. U^{NOMe} AR-V7 ISE (**ON1**) was conjugated to SpyTag via Gly-H (**C1**) or β -Ala-H (**C2**) to study the difference between these two linkers.

C3: Nusinersen¹³⁵ is approved antisense oligonucleotide for treatment of spinal muscular atrophy. Its target is located in CNS, and the current treatment is performed via intrathecal injection. Retro inverse THR peptide¹⁴⁰ binds to transferring receptor that may enhance delivery across blood brain barrier.

C4: GluR3 antisense PNA¹⁴¹ inhibits GluR3 expression and reduces glutamate excitotoxicity associated with amyotrophic lateral sclerosis (ALS). Its target is located in CNS. TfRA3¹³⁷ is a transferring receptor-binding aptamer that may have use as blood-brain barrier crossing agent.

C5: DGAT2 AS¹³⁶ reduces DGAT2 enzyme production and is potential treatment for nonalcoholic steatohepatitis currently in phase 2 clinical trials by IONIS Pharma. Its target is located in liver. GalNAc tricluster is well-known targeting ligand to increase hepatic uptake.



Scheme 21. Conjugation of therapeutic U^{NOMe}-ONs (**ON1**, **ON3**, **ON4**, **ON5**) with their respective conjugate groups (**P1**, **P2**, **P3**, **PNA1**, and **19**) for the preparation of conjugates **C1**, **C2**, **C3**, **C4**, and **C5**.

The conjugation was performed by mixing the U^{NOMe} -ON with the corresponding aldehydic conjugate group and dissolving them in minimal amount of acidic solvent mixture (25% (v/v) AcOH in DMSO, 2 M LiCl). The high concentration of the reactive species pushes the formation of the reversible *N*-methoxyoxazolidine link. Excess of aldehyde was used (2–8 equiv, see **Table 4**) for efficient employment of the U^{NOMe} -ON. The reaction mixture was heated to 55 °C for one hour, then quenched by neutralization (NaOH in H₂O/MeCN (1:1, v/v)) and purified by RP HPLC (**Figure 14**). After lyophilization, the intermediate **C5^{Ac}** was further exposed to aq. ammonia to remove the acetyl protection from the GalNAc units. The conjugates **C1–C5** were obtained in isolated yields between 19–47% and characterized using mass spectrometry (ESI-TOF) (**Table 4**). Phosphorothioate **ON1** (in conjugates **C1** and **C2**) suffered only minor amount of desulfurization (S → O) during the acidic conjugation process (**C2** shown as example in **Figure 15**). This is notable, as phosphorothioates are prone to oxidation in acidic conditions. As a conclusion, the *N*-methoxyoxazolidine conjugation method is a simple and facile method to produce oligonucleotide conjugates in high isolated yields. The crude reaction mixtures showed little to no side-product formation, underlining the biocompatibility of the reaction. Moreover, both the U^{NOMe} -ONs and peptide aldehydes (or PNA aldehydes) can be synthesized using modified solid supports in automated fashion, which makes the process simple and quick for synthesis of a given oligonucleotide–peptide conjugate.

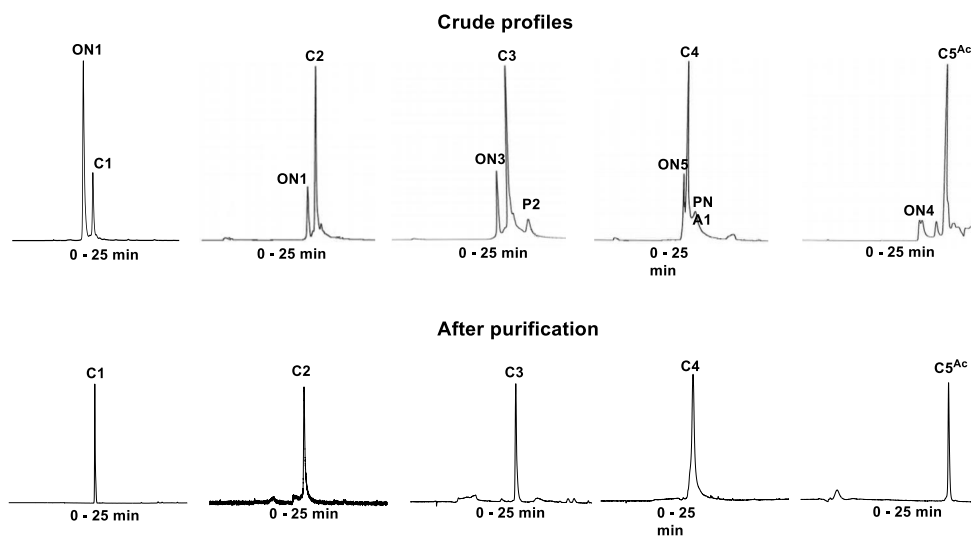
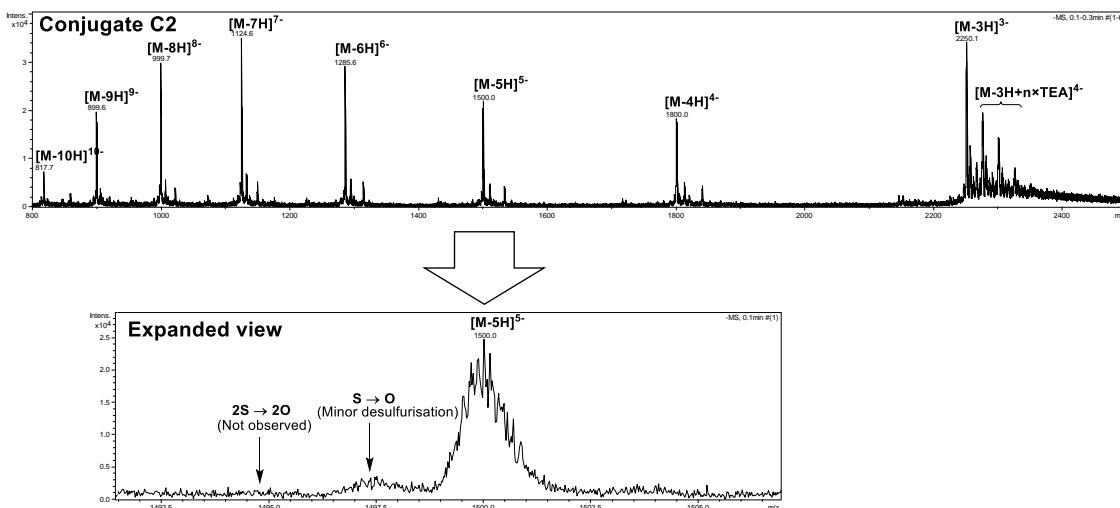


Figure 14. RP HPLC (C18, 250 × 4.6 mm, 5 μm) profiles for crude and purified mixtures of conjugates **C1–C4** and **C5^{Ac}**. A linear gradient (0–70% in 25 min) of MeCN over aqueous TEAA buffer (pH 7, 50 mM), a flow rate of 1.0 ml min⁻¹, and a detection wavelength of 260 nm were employed.

Table 4. Isolated yields for conjugates **C1–C5**.

Conjugate	Oligonucleotide	Aldehyde	Aldehyde excess (equiv.)	Isolated Yield (%) ^a	Observed Molecular Mass	Calculated Molecular Mass
C1	ON1	P1	2	41	9985.3	9985.8
C2	ON1	P2	8	25	9999.4	9999.8
C3	ON3	P3	8	19	9006.2	9006.3
C4	ON5	PNA1	2	43	8851.1	8852.7
C5	ON4	19	5	47	8860.4	8859.8

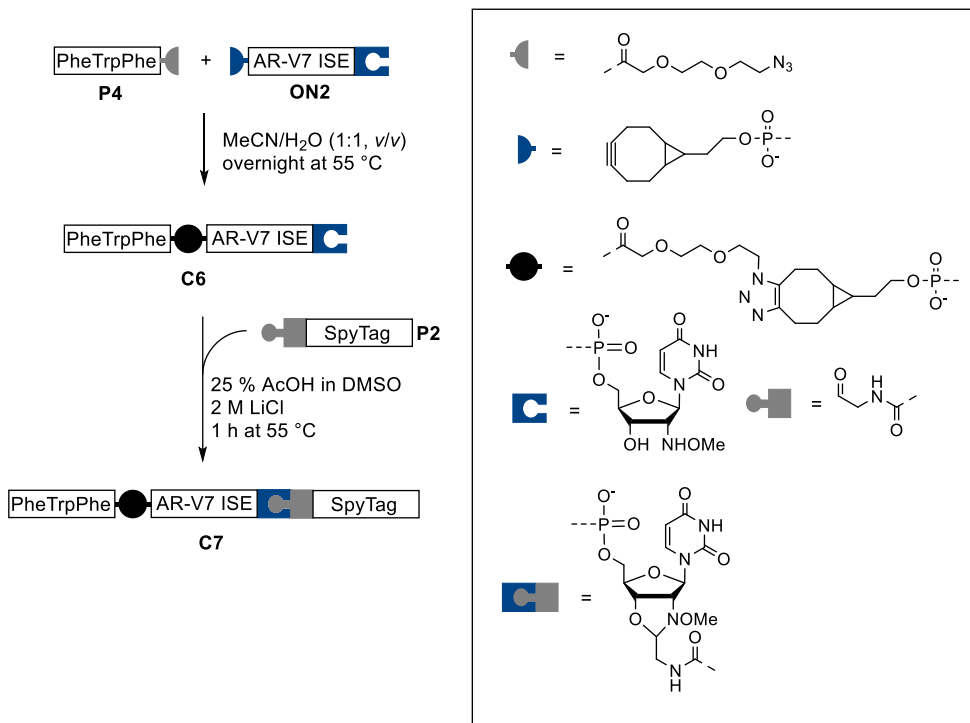
^aDetermined UV-spectrophotometrically at 260 nm using the molar absorbance of oligonucleotides and PNA.

**Figure 15.** Mass spectrum (ESI-TOF) of **C2** showing minor amount of desulfurization.

3.2.3.1 Bis-conjugation via *N*-methoxyoxazolidine and SPAAC

Bis-conjugation may be necessary for delivery of TONs across various biological barriers.^{122–124} Herein, it was examined if strain-promoted azide–alkyne cycloaddition (SPAAC) and *N*-methoxyoxazolidine could be used as orthogonal bis-conjugation strategy (**Scheme 22**). First, bis-functionalized **ON2** was coupled with azidopeptide **P4** via SPAAC resulting in triazole-linked **C6** (48% after RP HPLC, **Figure 16**). Conjugate **C6** was then coupled with Gly-H peptide aldehyde **P2** in acidic anhydrous conditions via *N*-methoxyoxazolidine formation to obtain bis-conjugate **C7** (38% after RP HPLC, **Figure 16**). The rationale for the bis-conjugate **C7** is that therapeutic AR-V7 ISE¹³⁴ (**ON2**) could be attached to various cell-targeting ligands via the SpyTag peptide¹³⁹ (**P2**), while PheTrpPhe (**P4**) is a known

endosomal escape domain ¹⁴³. Good yields of **C6** and **C7** and no cross-reactions between the linkers were observed, proving the bis-conjugation via SPAAC and *N*-methoxyoxazolidine a viable synthetic procedure.



Scheme 22. Bis-conjugation of **ON2** with **P4** (full sequence: N₃-AEEA-Phe-Trp-Phe-CONH₂, synthesized from commercially available building blocks) and **P2** via SPAAC and *N*-methoxyoxazolidine, respectively.

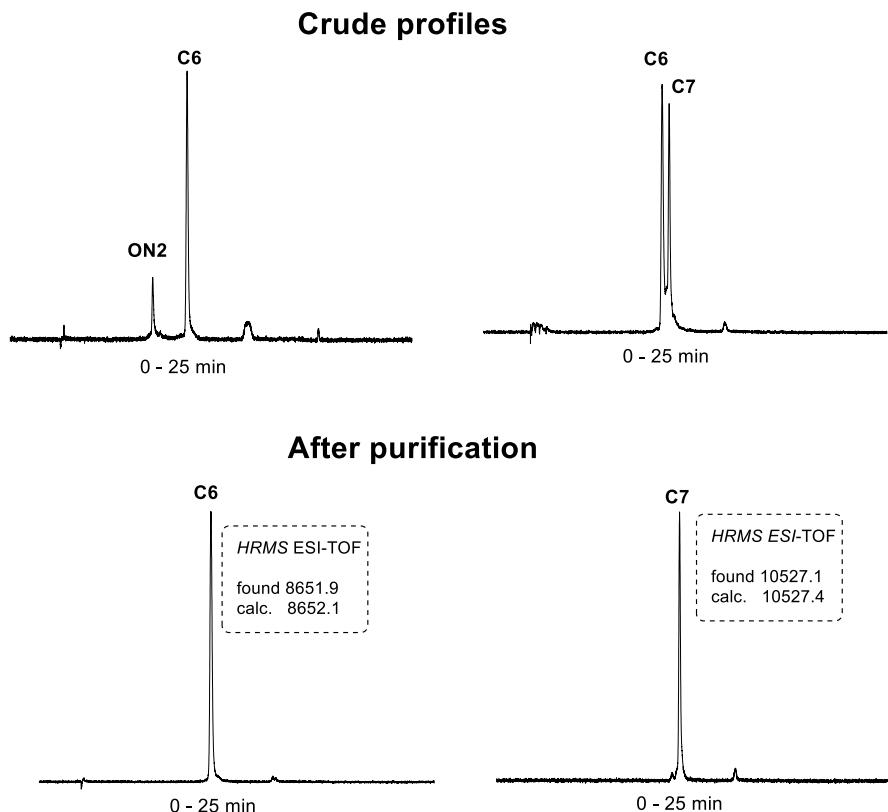
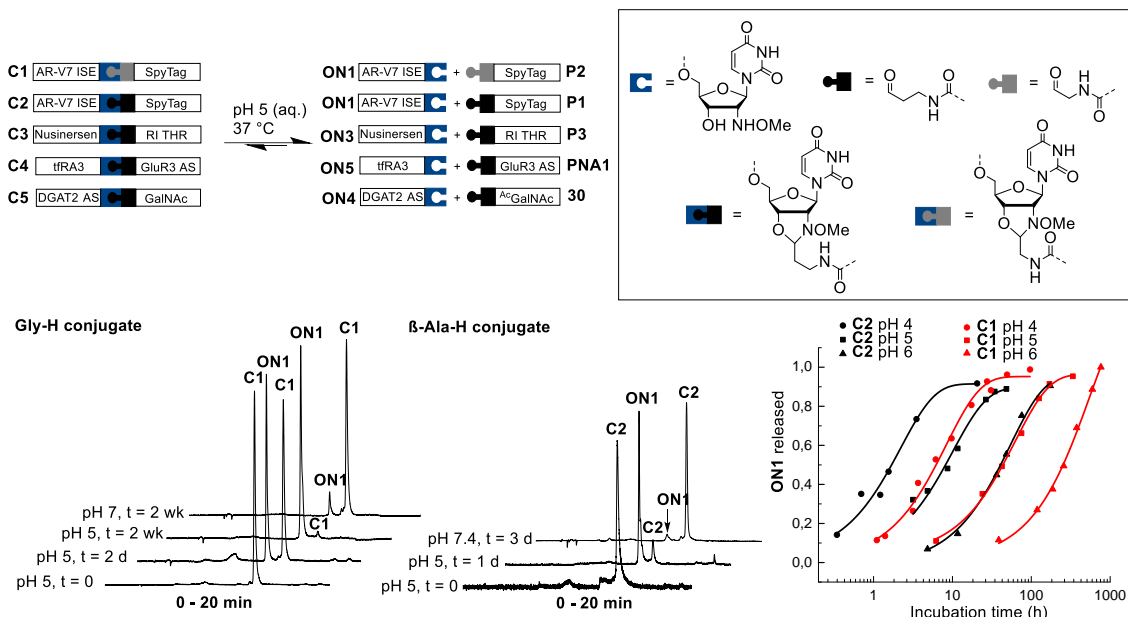


Figure 16. Crude and purified RP HPLC (C18, 250 × 4.6 mm, 5 μm) profiles of conjugates **C6** and **C7**. A linear gradient of MeCN (0–100% in 25 min) over aqueous TEAA (pH 7, 50 mM), a flow rate of 1.0 ml min⁻¹, and a detection wavelength of 260 nm were employed.

3.2.4 Hydrolysis of *N*-methoxyoxazolidine conjugates

To assess the pH-sensitivity of the *N*-methoxyoxazolidine linkage cleavage in the U^{NOMe}-conjugates, the stabilities of **C1–C5** were determined under fully aqueous conditions first at pH 5.0 and pH 7.4. Preferably, the conjugates would be stable under physiological conditions but cleaved under slightly acidic conditions perceived to early endosomes. The conjugates (**C1–C5**, 5 μM) were incubated at 37 °C and the hydrolytic release of the U^{NOME}-ON was monitored by RP HPLC (**Scheme 23**). At pH 5, the conjugates with β-Ala-H linker (**C2–C5**) were hydrolyzed at similar rates with $t_{1/2}$ between 4.41–10.2 h (**Table 5** entries 5, 7, 8, and 9), while the Gly-H-linked conjugate (**C1**) was more stable with $t_{1/2}$ of 41.7 h (**Table 5** entry 2). All the conjugates were significantly more stable at pH 7.4 with only minor hydrolysis after three days (**C1** and **C2** shown as examples in **Scheme 23**).



Scheme 23. Hydrolysis of conjugates **C1–C5** and selected RP HPLC (C18, 250 \times 4.5 mm, 5 μ m) and kinetic profiles. RP HPLC analyses were performed using a linear gradient (0–48% in 20 min) of MeCN over aqueous TEAA (pH 7, 50 mM), a flow rate of 1.0 ml min⁻¹, and detection wavelength of 260 nm.

At pH 5, conjugates **C1**, **C2**, and **C4** hydrolyzed near-quantitatively (**Table 5** entries 2, 5, and 8), which is expected under micromolar concentration (cf. *K* in **Table 1**). In contrast, conjugates **C3** and **C5** stalled at 59% and 64% of free U^{NOME}-ON at equilibrium (**Table 5** entries 7 and 9), which represent ca. 20-fold higher equilibrium constant compared to the small molecule data. Incomplete hydrolysis implies a non-covalent interaction between the oligonucleotide and the aldehydic conjugate group. Conjugates **C1** and **C2** were also examined at pH 4 and 6 for more accurate comparison of pH-profiles between Gly-H and β -Ala-H linkers. For the whole pH-range (4–6), β -Ala-H linker (**C2**) hydrolyzed roughly 4- to 6-fold faster than Gly-H linker (**C1**). This acceleration is like the rate-difference between two pH units (as visualized in **Scheme 23**).

Table 5. Hydrolysis rates for the *N*-methoxyoxazolidine Gly-H (**C1**) and β -Ala-H (**C2–C5**) conjugates (5 μ M) at pH 5.

Entry	Conjugate	pH	$t_{1/2}$ (h)	U ^{NOMe} -ON released at equilibrium (%)
1	C1	4	5.80 \pm 0.52	95 \pm 3
2	C1	5	41.7 \pm 2.3	96 \pm 2
3	C1	6	222 \pm 20	quant.
4	C2	4	1.53 \pm 0.25	92 \pm 6
5	C2	5	7.17 \pm 0.77	90 \pm 3
6	C2	6	37.3 \pm 3.3	96 \pm 4
7	C3	5	4.41 \pm 0.17	59 \pm 1
8	C4	5	10.2 \pm 0.81	94 \pm 3
9	C5	5	7.40 \pm 1.03	64 \pm 3

The hydrolysis studies of the *N*-methoxyoxazolidine conjugates showed that the kinetic stability of the conjugate is dictated by the local structure of the linker, for which small-molecular models with different aldehydes can be used as an estimate. Also, macromolecular interactions (e.g. electrostatic interactions between positively charged peptides and phosphodiester bonds) are relevant and may lead to incomplete hydrolysis of the conjugate. The release rates for β -Ala-H-linked conjugates were in the same range as a hydrazone linker ($t_{1/2}$ ca. 4.7 h at pH 4.5 according to first order kinetics) used in antibody–small molecule drug conjugates Mylotarg¹⁴⁴ and Besponsa¹⁴⁵, indicating that the *N*-methoxyoxazolidine linker can be considered as an acid-labile linker^{12–14} for therapeutic conjugates.

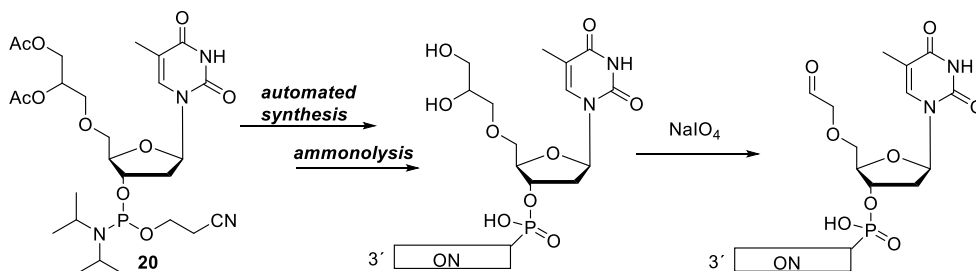
3.3 Target-directed dynamic combinatorial chemistry of oligonucleotides

Target-directed dynamic combinatorial chemistry (tdDCC) is an emerging field for finding receptors or ligands for a given molecular template.⁸ Oligonucleotides are intriguing reactants for tdDCC due to their duplex formation that allows DNA-templated synthesis, but also for their tendencies to bind with various molecules by aptameric interactions. The latter one could be utilized for ligand-triggered functionality or biosensing.^{118,146} In this chapter, *N*-methoxyoxazolidine ligation between oligonucleotides is reported. For this, U^{NOMe}-ONs were synthesized as before (cf. Chapter 3.2) and suitable oligonucleotides modified by 5'-terminal aldehyde were developed and synthesized (Chapter 0). The dynamic *N*-methoxyoxazolidine ligation was studied first using well-established model of DNA-templated ligation (Chapter 0). These studies were followed by fragment-based

synthesis of a split aptamer templated by its small-molecular substrate (Chapter 3.3.3) and similar self-assembly of split G-quadruplex sequence templated by K^+ (Chapter 3.3.4). In all these studies, the main hypothesis was that the ligation product could be obtained in highly increased yield when the template was present due to increased local concentration while the absence of template leads to dissociation of the reactive oligonucleotides.

3.3.1 Synthesis of oligonucleotides modified by 5'-terminal aldehyde

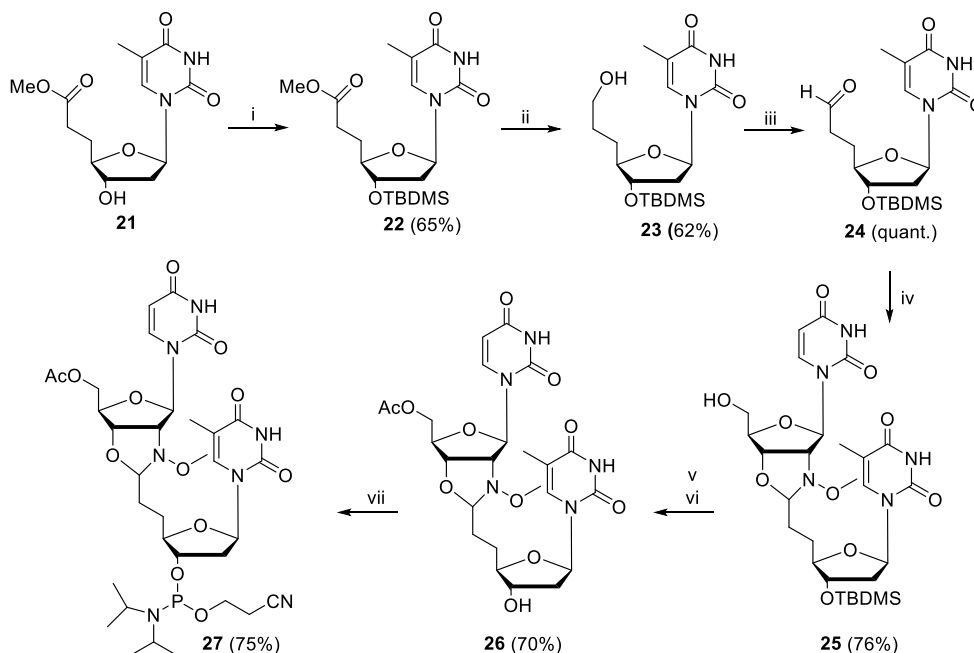
For the tdDCC oligonucleotide studies, a suitable precursor for oligonucleotides bearing 5'-aldehyde functionality was synthesized. Initially, a well-known strategy¹⁴⁷ was utilized. Here, a modified thymidine phosphoramidite with protected 5'-diol functionality (**20**) was attached to oligonucleotide 5'-terminus (**Scheme 24**). After cleavage and deprotection, the vicinal diol was oxidized to aldehyde using $NaIO_4$. This synthetic strategy was later abandoned due to difficult purification (erratic HPLC patterns and suspected instability during lyophilization). Another reason for developing a new strategy was the electronegativity of the carbonyl carbon (due to the bridging oxygen), making it a subpar group to form *N*-methoxyoxazolidines based on the small-molecular studies.



Scheme 24. Synthesis of 5'-aldehyde oligonucleotides using $NaIO_4$ oxidation of vicinal diol.

A new strategy was developed based on protected 5'-aldehyde nucleoside phosphoramidite **27**, which was synthesized following **Scheme 25**. Starting from thymidine 5'-ester analog **21**¹⁴⁸, aldehyde **24** was obtained by subsequent reduction/oxidation of the ester group. The aldehyde **24** was condensed with nucleoside **1** to obtain *N*-methoxyoxazolidine-linked dinucleoside **25**. The dinucleoside was then treated with acetic anhydride to cap the 5'-hydroxyl and subsequently desilylated to obtain **26**, which was phosphitylated to obtain phosphoramidite **27** to be used as a precursor for 5'-aldehydic oligonucleotides. The *N*-methoxyoxazolidine protection group of the aldehyde is stable to the conditions

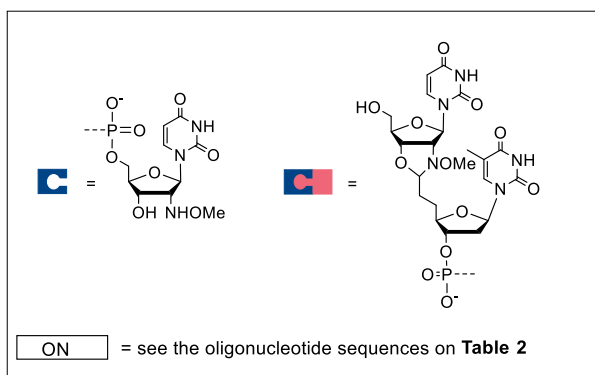
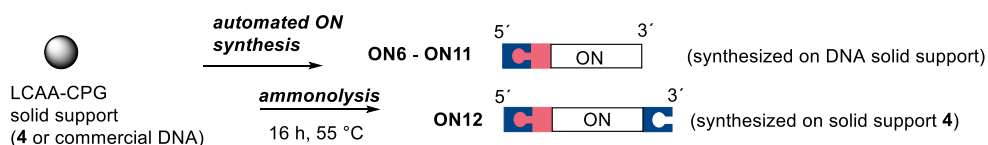
of ammonolytic cleavage and deprotection of oligonucleotides, thus, the sensitive aldehyde functionality stays protected during the isolation but can be cleaved *in situ* during tDCC oligonucleotide experiments.



Scheme 25. Synthesis of phosphoramidite 18. Conditions: i) TBDMSCl 2.1 equiv., TEA 4.9 equiv., DMAP cat., RT; ii) LiAlH₄ 1.3 equiv., THF, 0 °C; iii) IBX 1.3 equiv., DMSO 2.0 equiv., dioxane (deoxygenated using argon), 70 °C; iv) nucleoside **1** 1.0 equiv., AcOH in DMSO (1:3, v/v), 40 °C; v) acetic anhydride 2.0 equiv., DMAP cat; vi) tetrabutylammonium fluoride 3.3 equiv., THF, 55 °C; vii) *N,N*-diisopropylcyanoethylchlorophosphoramidite 1.2 equiv., DIPEA 2.4 equiv.

The 5′-aldehyde oligonucleotides (**ON6–ON11**) were prepared using commercial solid support and building blocks with a final coupling with phosphoramidite **27** (**Scheme 26**). After elongation, ammonolysis (55 °C, 16 h) followed by RP HPLC purification (**Figure 17**) was performed. The 5′-aldehyde oligonucleotides were obtained as their *N*-methoxyoxazolidine-protected form with isolated yields between 3–15% (**Table 6**). One bifunctional oligonucleotide (**ON12**) having both 3′-U^{NOMe} and 5′-aldehyde modifications was prepared on solid support **4** with final coupling with phosphoramidite **27**. The bifunctional oligonucleotide **ON12** was obtained in its *N*-methoxyoxazolidine-protected form in 5% yield after RP HPLC (**Figure 17**). The *N*-methoxyoxazolidine protection group of **ON6–ON12** can be cleaved in acidic conditions to unmask the 5′-aldehyde functionality. Unmasking the aldehyde results in wide and erratic RP HPLC patterns (cf. step i in

Scheme 28), presumably due to (intramolecular) aldehyde–acetal equilibria, which frustrates the RP HPLC isolation. In contrast, *N*-methoxyoxazolidine-protected aldehydes resolved well from the truncated sequences due to comparatively lipophilic *N*-methoxyoxazolidine bond (cf. **Figure 17**). Thus, the deprotection of the aldehyde was always performed *in situ*. While the purity of the obtained 5′-aldehyde oligonucleotides was excellent, the crude products showed major amounts of truncated sequences and the yields were low to modest. Optimization of the coupling conditions such as using more excess of the modified phosphoramidite or longer coupling times could be considered to increase the yield. Also, partial hydrolysis of *N*-methoxyoxazolidine protecting group during the ammonolysis is plausible. The synthetic methods were not optimized due to low amounts of oligonucleotides required for the tdDDC studies.



Scheme 26. Automated synthesis of protected 5′-aldehyde ONs (**ON6–ON11**), and protected 5′-aldehyde U^{NOMe}-ON (**ON12**). Full sequences are displayed in Table 6.

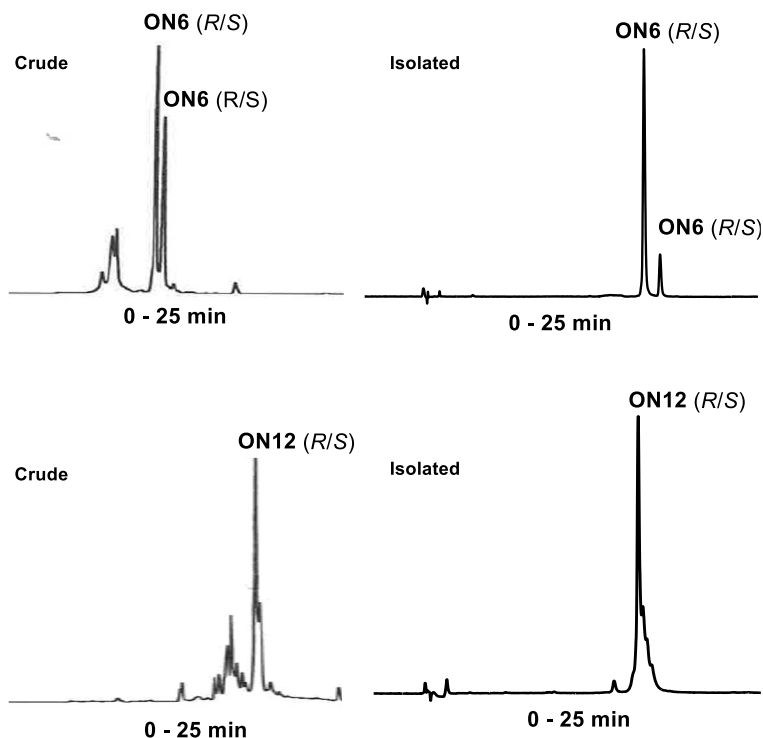


Figure 17. Typical RP HPLC (C18, 250 × 10 mm, 5 μm) profiles for the 5'-aldehyde-modified oligonucleotides including 5'-aldehyde oligonucleotide (top) and bifunctional oligonucleotide (bottom). A linear gradient of MeCN (5–40% in 25min) over aqueous TEAA (pH 7, 50 mM), a flow rate of 2.5 ml min⁻¹, and a detection wavelength of 260 nm were employed. The (*R/S*) stands for the *N*-methoxyoxazolidine stereoisomers originating from phosphoramidite **27**.

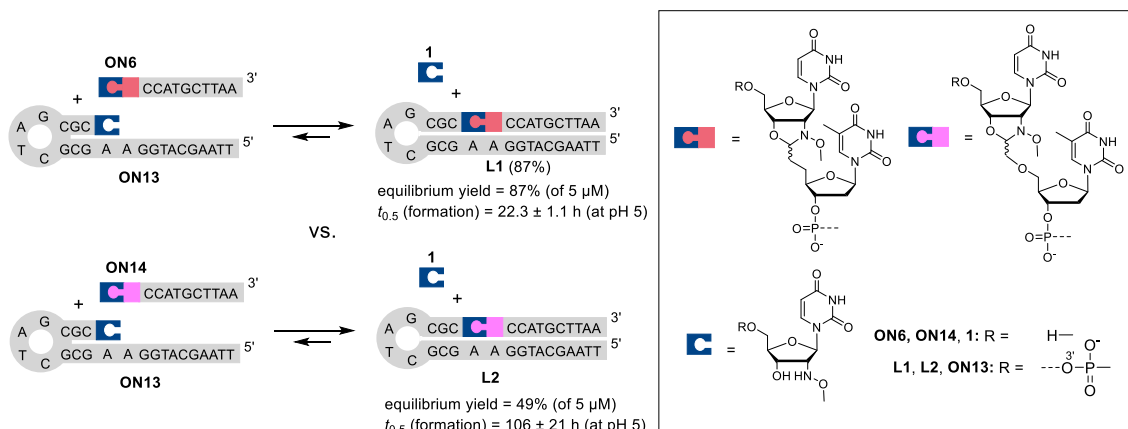
Table 6. The sequences and yields for the synthesized 3'-U^{NOMe}- and 5'-aldehydic ONs.

Oligonucleotide	Sequence ^a	Yield (%) ^b
ON6	T ^{AldPr} CCATGCTTAA	15
ON7	T ^{AldPr} GTTCTTCAATGAAGTGGGACGACA	13
ON8	T ^{AldPr} AGTGGGACGACA	12
ON9	T ^{AldPr} AGGGTTAGGGTTAGGGTT	3
ON10	T ^{AldPr} AGGGTTAGGGTT	3
ON11	T ^{AldPr} AGGGTT	6
ON12	T ^{AldPr} GTTCTTCAATGAU ^{NOMe}	5

^aExplanation for the characters: bold are 2'-*O*-methylribonucleotides with phosphorothioate backbones, underlined, underlined are 2'-*O*-(2-methoxyethyl)ribonucleotides, and the rest are 2'-deoxyribonucleotides. U^{NOMe} and T^{AldPr} are shown in **Scheme 26**. The integrities of the isolated oligonucleotides were verified by mass spectrometry. ^bThe yields were determined UV-spectrophotometrically at 260 nm.

3.3.2 N-methoxyoxazolidine formation on DNA hairpin template

DNA-templated ligation is a well-established method to increase ligation efficiency.^{1,2} It is applied in DNA-templated synthesis to manufacture diverse range of molecules ranging from small-molecules in pharmaceutical screening to more experimental DNA-encoded synthetic polymers.⁶⁸ Herein, the DNA-templated *N*-methoxyoxazolidine ligation was studied using a model reaction between complementary U^{NOMe}-ON (**ON13**) and protected 5'-aldehyde oligonucleotide (**ON6**) that formed hairpin **L1** (**Scheme 27**). A similar model has been studied previously for maleimide-thiol-ligation¹⁴⁹ and neoglycosylation¹⁵⁰. The simple model is easy to monitor, and the duplex preorganization of the overhang region makes it an efficient template.¹¹²

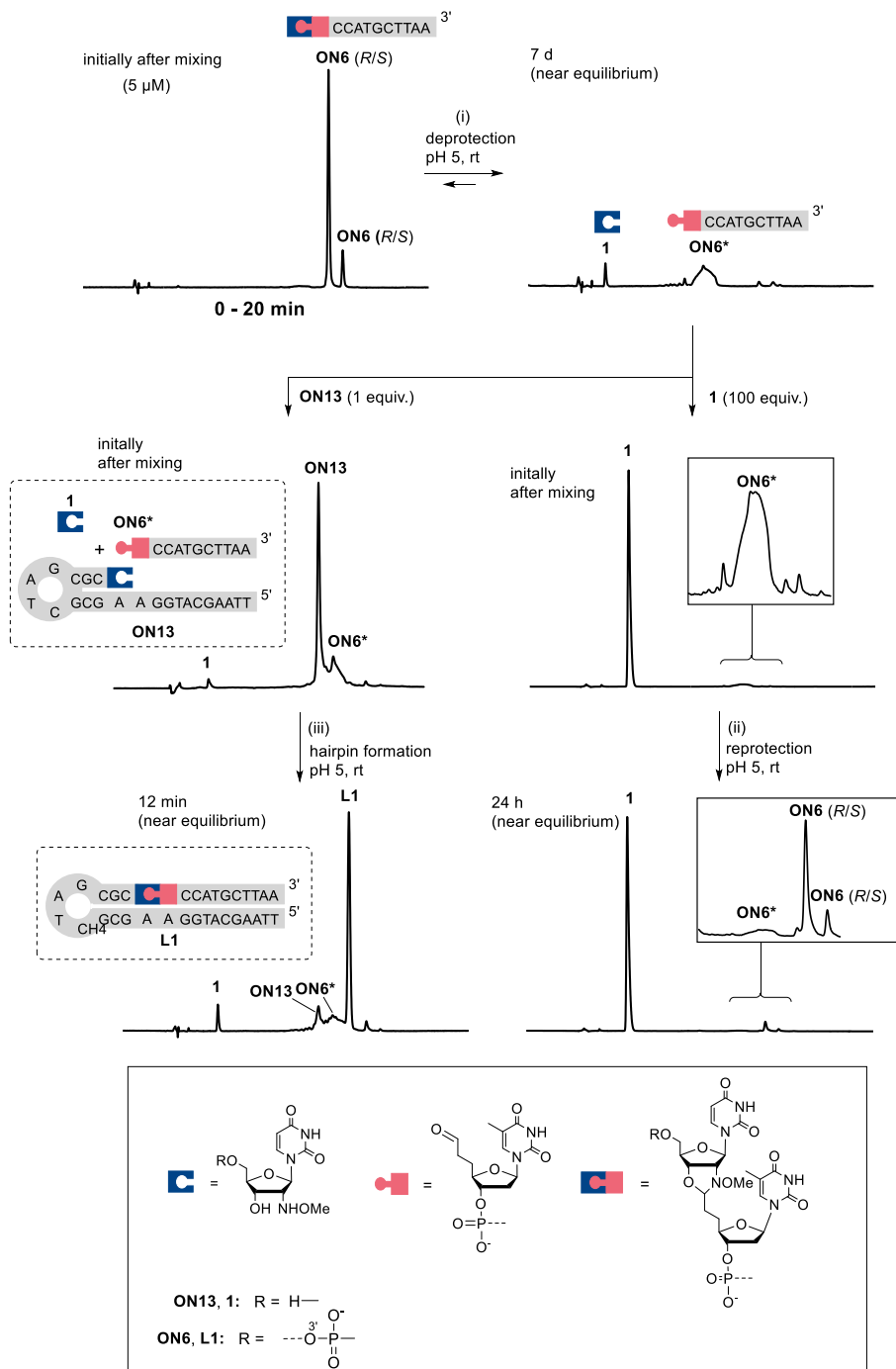


Scheme 27. Comparison of two aldehyde structures in DNA-templated *N,O*-transacetalization. **ON14** was synthesized by the previously published procedure¹⁴⁷ of NaIO₄-oxidation of vicinal diol (cf. chapter 3.3.1) and then protected using excess of **1** followed by RP HPLC isolation.

To begin with, a baseline examination was done by studying the dynamic deprotection of the 5'-aldehyde oligonucleotides, i.e., hydrolysis of *N*-methoxyoxazolidine. The 5'-aldehyde deprotection rate was determined by incubating **ON6** (5 μ M) in pH-adjusted water at room temperature. The deprotection was monitored using RP HPLC (**Scheme 28 i**) and the kinetic data was fitted to the reversible bimolecular integrated rate law. Near complete deprotection with >96% free aldehyde (**ON6***) at equilibrium formed at a rate proportional to the acidity of the reaction solution ($t_{1/2}$ = 8.56 h – 70 d between pH 4–7, **Table 7**). If excess of protection group **1** (500 μ M, 100 equiv.) was added into the deprotected mixture, the equilibrium shifted back to ca. 32% of **ON6** (K = 944 M⁻¹, $t_{1/2}$ = 1.85 h – 70.2 d

between pH 4–7, **Scheme 28** ii), which matches well with the small molecule data (cf. **Table 1**). These experiments showed the non-templated ligation rate for the modified oligonucleotide **ON6**.

Instead, if **ON6** was deprotected as before and then complementary **ON13** (5 μM , 1 equiv.) was added into the deprotected mixture, the hairpin **L1** was formed in average yield of 80% (**Scheme 28**, iii). If the templated ligation is treated as intermolecular reaction, the yield means over 4000-fold stabilization (K value of $4 \times 10^6 \text{M}^{-1}$) of *N*-methoxyoxazolidine compared to the non-templated reaction. The rate of *N*-methoxyoxazolidine formation was highly improved ($t_{1/2} = 3.42 \text{ min} - 27.9 \text{ h}$ between pH 5–10) but was unexpectedly slow at pH 4 ($t_{1/2} = 29.4 \text{ min}$) and no product was formed at pH 11. Shutdown of the reaction at extreme pHs was consistent with melting points (T_m) of the preligated duplex, which was measured using full DNA analogs of **ON13** and **ON6** (Table 7).



Scheme 28. RP HPLC (C18, 250 \times 4.6 mm, 5 μ m) for (i) deprotection of **ON6**; (ii) re-protection of **ON6*** after addition of **1**; (iii) **L1** formation after addition of **ON13**. The analyses were run with a linear gradient of MeCN (5–20% in 25 min) over aqueous TEAA buffer (pH 7.0, 50 mM). A detection wavelength of 260 nm was employed.

Table 7. Thermodynamic and kinetic data for *N*-methoxyoxazolidine formation between **ON6** and **1** or **ON13** at RT.

pH ^a	T_m (°C) Starting material ^b	$t_{1/2}$ ON6 deprotection ^c	$t_{1/2}$ ON6* reprotection ^d	$t_{1/2}$ L1 hairpin formation ^e	$t_{1/2}$ <i>N,O</i> - transacetalization ^f
4	not found	8.57 ± 0.14 h (96 ± 2 %) ^g	1.85 ± 0.04 h (33 ± 1 %) ^g	29.4 ± 0.6 min (76 ± 1 %) ^g	7.69 ± 0.45 h (76 ± 1 %) ^g
5	22.1 ± 0.1	30.3 ± 0.5 h (96 ± 1 %) ^g	5.00 ± 0.15 h (30 ± 1 %) ^g	3.42 ± 1.30 min (94 ± 19 %) ^g	22.3 ± 1.1 h (87 ± 1 %) ^g
6	26.3 ± 0.1	188 ± 6 h (97 ± 3 %) ^g	30.1 ± 0.7 h (34 ± 1 %) ^g	5.70 ± 0.58 min (83 ± 5 %) ^g	228 ± 38 h (95 ± 6 %) ^g
7	31.5 ± 0.1	70.2 ± 9.9 d (15.9 ± 9.4 %) ^g	235 ± 12 h (29 ± 1 %) ^g	29.6 ± 0.7 min (79 ± 1 %) ^g	N/A
8	30.8 ± 0.1	N/A	N/A	3.05 ± 0.07 h (79 ± 1 %) ^g	N/A
9	27.6 ± 0.1	N/A	N/A	13.7 ± 0.3 h (75 ± 2 %) ^g	N/A
10	23.1 ± 0.1	N/A	N/A	27.9 ± 1.3 h (78 ± 2 %) ^g	N/A
11	not found	N/A	N/A	N/A	N/A

N/A: Reactions were not monitored due to their slowness (< 4% of product after one month). ^aBuffers ($c = l = 0.1$ M, l adjusted using NaCl): Acetic acid (pH 4, 5) MES (pH 6), HEPES (pH 7, 8), CHES (pH 9, 10), CAPS (pH 11). ^b T_m obtained using non-modified DNA analogues of **ON6** and **ON13**. ^c**ON6** (5 μ M). ^d**ON6*** (5 μ M) + **1** (500 μ M). ^e**ON6*** (5 μ M) + **ON13** (5 μ M) + **1** (5 μ M). ^f**ON6** (5 μ M) + **ON13** (5 μ M). ^gThe equilibrium yield.

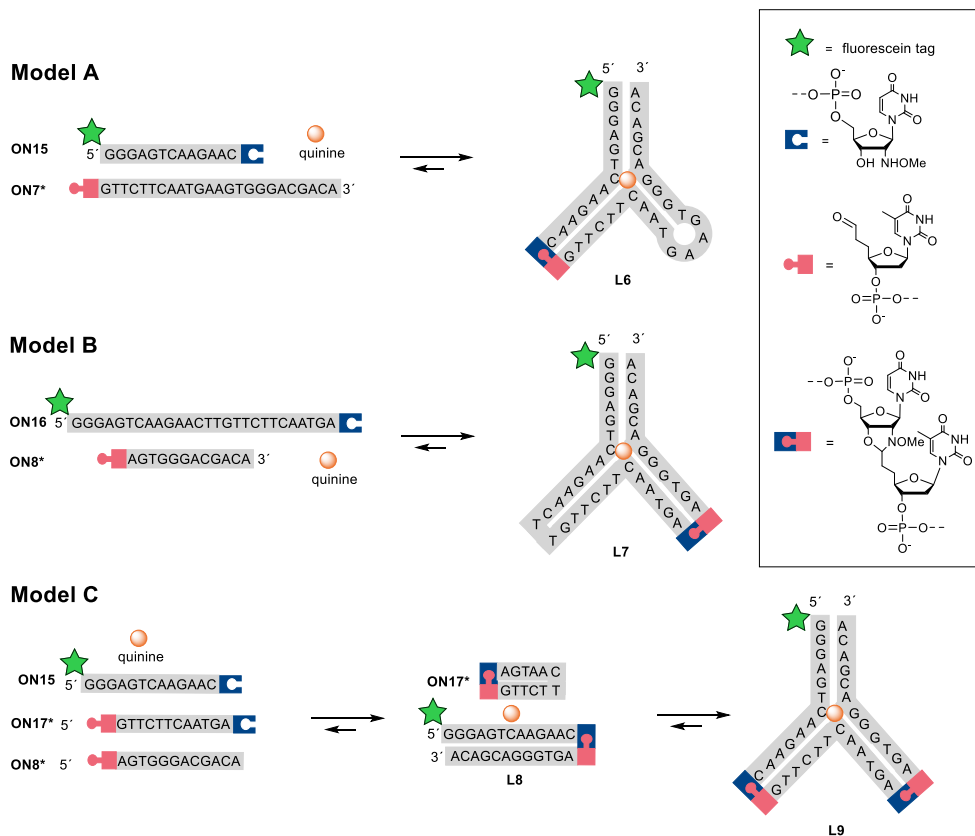
DNA-templated *N,O*-transacetalization was studied by mixing **ON13** (5 μ M) directly with **ON6** (5 μ M) without preliminary deprotection step. As expected, the yield of **L1** remained, but the rate of formation ($t_{1/2}$ of 7.69 h – 9.5 d between pH 4–6) was now limited by the deprotection step. To examine how aldehyde structure affects the DNA-templated ligation, **ON13** (5 μ M) was mixed with **ON14** (5 μ M) to form hairpin **L2** (**Scheme 27**). Now, the hairpin **L2** was formed in lower yield (49% vs. 80%) and slower ($t_{1/2} = 106$ h vs. 22.3 h at pH 5) than **L1**. The slower rate is coherent with the small molecule data (cf. **Table 1**), where EWGs on the aldehyde leads to deceleration. The lower yield may indicate that the *N*-methoxyoxazolidine linkage in **L2** fits worse in the stem-region of the hairpin than the linkage in **L1**. Indeed, slightly higher melting temperature was obtained for **L1** (74.0 ± 0.3 °C) than **L2** (72.4 ± 0.1 °C), but both were less stable than a non-modified DNA hairpin ($T_m = 79.3 \pm 0.1$ °C).

The results show that the DNA-template increased equilibrium constant of *N*-methoxyoxazolidines by ca. 4000-fold that, under micromolar concentration, results in yield increase from nearly zero to quantitative. The DNA-templated *N*-methoxyoxazolidine ligation proceeded optimally at pH 5 with $t_{0.5}$ of 3.4 min under 5 μ M nominal concentration of the reactive species. The catalytic effect of the template allowed the ligation to proceed remarkably well up to pH 10, while the reaction practically shuts down at pH 8 without the template. The rate and yield, reversibility of the reaction and pH-dependency make the formation of *N*-methoxyoxazolidines a useful reaction for DNA-encoded polymer synthesis.

3.3.3 Quinine-templated aptamer assembly

Aptamers are oligonucleotides with high binding affinity to specific substrates. Aptamer can be split into two or more fragments while still maintaining these recognition characteristics. These so-called split aptamers have been utilized as biosensors.^{15,151} The split aptamer assembly can be stabilized using a covalent ligation between the split fragments, which enables highly sensitive detection architectures.^{146,152,153} Herein, it was evaluated if *N*-methoxyoxazolidine could be used as a linker for ligation of aptamer fragments into full aptamer templated by its substrate.

Three models were examined (**Scheme 29**), which are all based on cocaine-binding aptamer (CBA).^{154,155} Model **A** is similar to a model that has previously been studied in noncovalent¹⁵⁶ and irreversible covalent^{152,153,157} aptamer assembly, while model **B** has alternative splitting site. Model **C** is made of two splitting sites and may be thought as a combination of models **A** and **B**. In theory, formation of model **C** is the most difficult, as there is less concomitant binding between the starting materials and there are multiple plausible non-desired ligation products, both intra- and intermolecular. In all models, quinine was used as the template for the aptamer assembly (it has been shown that CBA binds to quinine with comparable affinity to cocaine)^{155,158}.



Scheme 29. Quinine-induced dynamic aptamer assembly models **A**, **B**, and **C**.

The quinine-dependency of the ligation was studied first using models **A** and **B**. To begin with, the corresponding oligonucleotides (**ON15** with **ON7** and **ON16** with **ON8**) were mixed with variable amount of quinine (0, 1, 10, 100, or 1000 μM) and incubated overnight in aqueous solution (pH 5) at 55 $^{\circ}\text{C}$ for complete deprotection of the aldehydes (**ON7*** and **ON8***). At this point, no ligation product was found in any models, indicating complete denaturation. The reaction mixtures were allowed to cool to room temperature and monitored by denaturing PAGE (**Figure 18**) and mass spectrometry (**Table 8**). After incubating one hour at room temperature, model **A** showed 1.6–72% yield of aptamer **L6** in the presence of 0–1000 μM quinine (**Figure 18**). The assembly stalled to 18–89% equilibrium yield of **L6** after one day, which persisted after one month of incubation. After one month in room temperature, the reaction mixtures of model **A** were reheated to 55 $^{\circ}\text{C}$ for one day and then cooled back to room temperature. The ligation product **L6** was disassembled completely by the heating step and reassembled with similar yields to the first assembly. For model **A**, a control reaction was studied, in which **ON15** or **ON7** was replaced with a non-

modified DNA. As expected, no aptamer assembly was observed. In contrast to model **A**, model **B** showed only 0–22% **L7** after one day and stalled to equilibrium of 0–36% after one week in the presence of 0–1000 μM quinine (**Figure 18**).

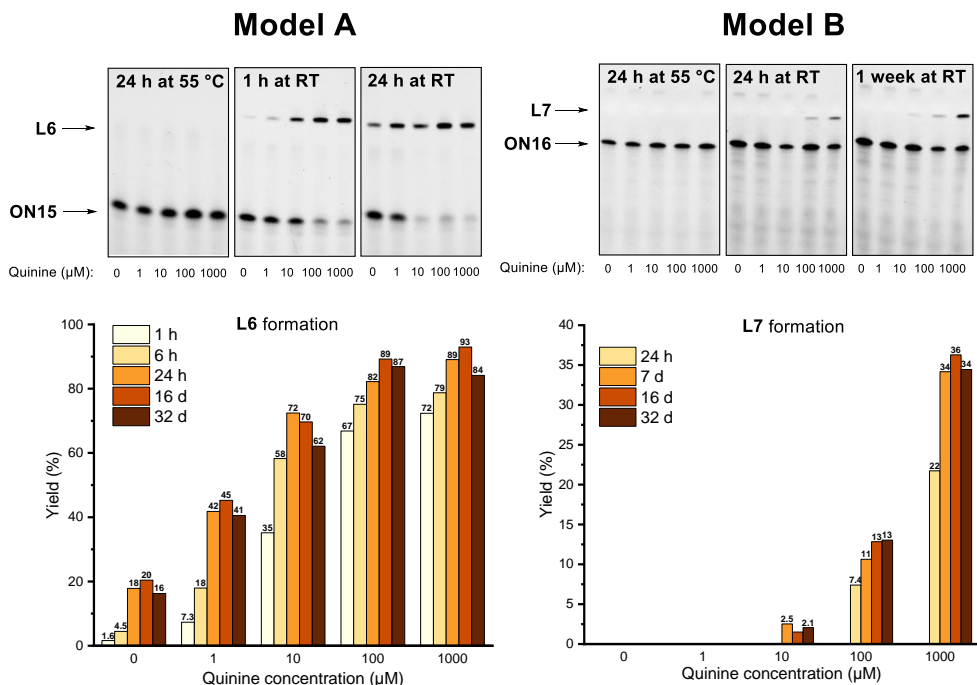


Figure 18. Aptamer formation in models **A** and **B** as quantified by denaturing PAGE. Reaction conditions: **A**: **ON15** + **ON7** + quinine (0–1000 μM); **B**: **ON16** + **ON8** quinine (0–1000 μM). The initial concentration of each oligonucleotide was 1 μM . Water was used as the solvent (pH 5, 50 mM acetic acid/sodium acetate).

Table 8. Mass spectrometric measurements for the split aptamer formation models **A**, **B**, and **C**.

Ligation product	Observed molecular weight	Calculated molecular weight
L6	12634.5	12634.5
L7	13242.0	13244.9
L8	8936.7	8937.1
L9	13218.1	13219.9

Model **C** was studied by mixing the oligonucleotides (**ON15**, **ON8**, and **ON17**) with quinine (100 μM) and incubated in aqueous solution (pH 5) overnight at 55 $^{\circ}\text{C}$ and then cooled to room temperature. After one day at room temperature, 72% of truncated product **L8** and 5.7% of the desired aptamer **L9** were formed (**Figure 19**, lane 6). After one month, the yield of **L9** rose to 32% with slight improvement to

37% in a duplicate reaction with added MgCl_2 (50 mM) (cf. lanes 6 and 7 in **Figure 19**). In parallel with the main reactions, multiple exclusion experiments were run, in which one of the oligonucleotides or quinine was excluded from the mixture. No **L9** was found even after one month if quinine was excluded from the mixture (**Figure 19**, lane 1). Without quinine, the yield of **L8** also dropped (from 72% to 21% after one day, cf. lanes 6 and 3 in **Figure 19**). This does not necessarily mean that **L8** is a functional aptamer itself, as removal of **ON17** also reduced the yield of **L8** (**Figure 19**, lane 5).

Model C

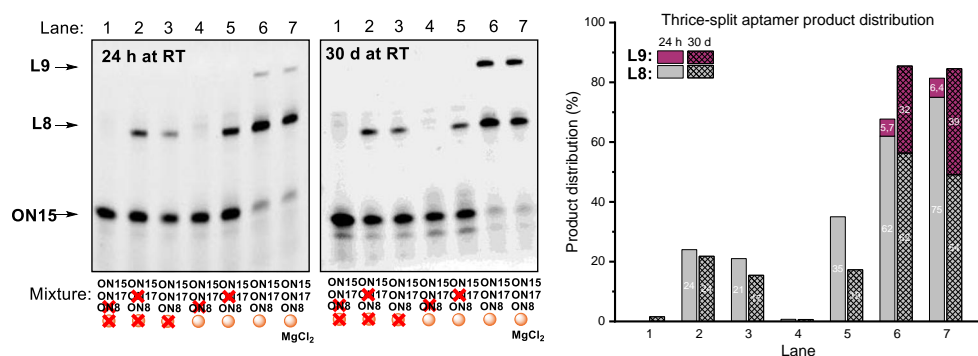
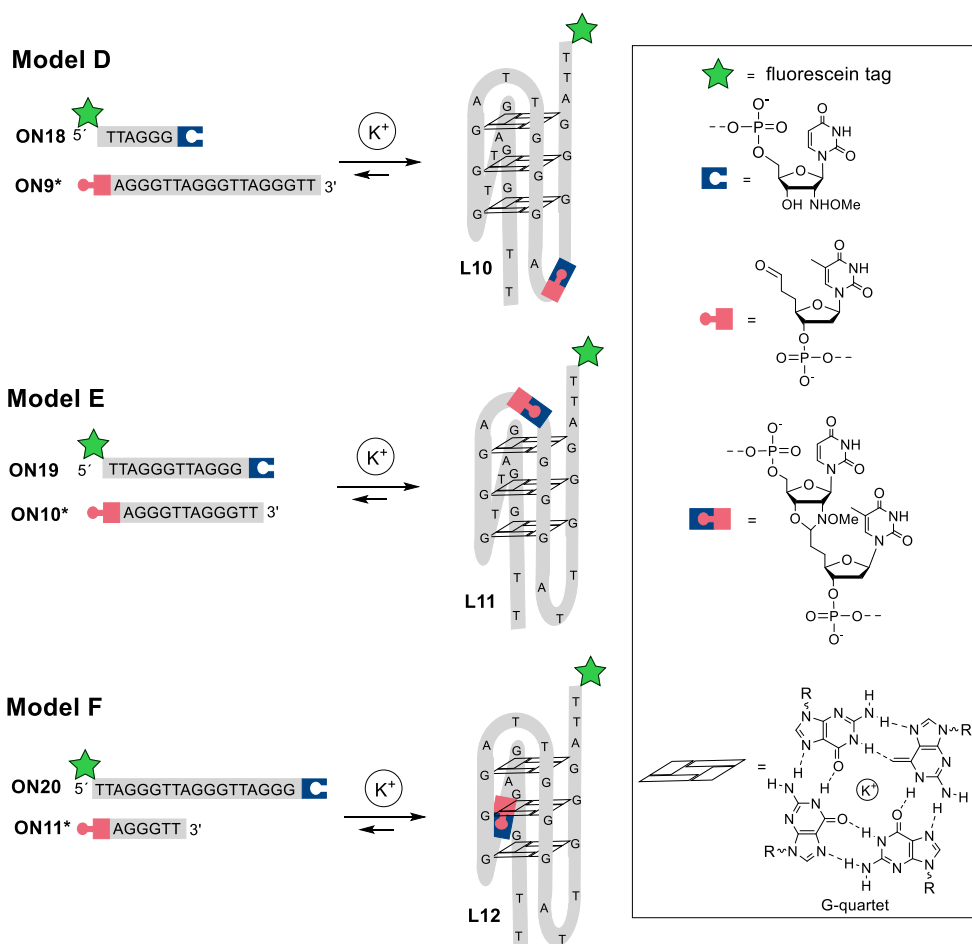


Figure 19. Aptamer formation in model **C** as quantified by denaturing PAGE. Reaction conditions: **ON15** + **ON17** + **ON8** + quinine (100 μM) and various exclusions as shown in the figure. The initial concentration of each oligonucleotide was 5 μM . Water was used as the solvent (pH 5, 50 mM acetic acid/sodium acetate)

The results show that *N*-methoxyoxazolidine ligation can be templated by a small-molecule, if a suitable split-aptamer sequence is used. The most efficient model **A** could discriminate between 0 and 1 μM of quinine with ca. 2-fold more ligation product with quinine. Most notably, this was observed at the equilibrium. The ligation products could be cleaved by heating and then synthesized again by allowing the mixture to cool back to room temperature. These fully reversible processes may find use as reusable biosensors.^{15,151} Moreover, it was shown in model **C** that the aptamer could be synthesized from three sequence, again, only in the presence of the quinine template. Multi-component assembly reduces the background ligation; thus, it may be used to enhance the template-specificity of the ligation. Furthermore, it may be found as tool for finding new aptamers by tdDCC experiments. Dynamically forming aptamers may also be useful in targeted drug delivery as small-molecule carriers¹⁵⁹ that unload the cargo due to acidic conditions perceived to tumours.

3.3.4 Potassium-induced G-quadruplex assembly

Oligonucleotides with high guanine-content can fold into G-quadruplexes, which are tertiary structures made of stacked G-quartets (cf. **Scheme 30**). G-quadruplex formation is sensitive to temperature, and specifically, they are stabilized by Na^+ and K^+ , but not by Li^+ .¹⁶⁰ Herein, it was examined how a human telomer repeat sequence (wTel26)¹⁶¹, known to fold into G-quadruplex, acts as a template for the *N*-methoxyoxazolidine formation, and how K^+ -ion concentration contributes to the ligation efficiency. In addition to potential sandwich biosensor reliability,^{15,146,151,152} dynamically formed G-quadruplexes may be applied e.g. as small molecule drug scaffolds in targeted drug-delivery.¹⁶²



Scheme 30. Potassium induced *N*-methoxyoxazolidine ligation based on G-quadruplex formation. The tertiary structures of ligation products (**L10–L12**) represented here is G-quadruplex (type 2 hybrid) similar to the parent DNA wTel26¹⁶¹.

Three split models (**D**, **E**, **F**) were designed by splitting wTel26 fragment from three sites between thymidine residues and replacing those thymidines with 3'-U^{NOMe} and 5'-T^{AldPr} (**Scheme 30**). The K⁺-dependency of the G-quadruplex-ligation was studied by mixing the corresponding oligonucleotides (**ON18** with **ON9**, **ON19** with **ON10**, and **ON20** with **ON11**; 1 μM each) in aqueous solution (pH 5) with variable amount of KCl (0, 0.1, 1, 10, or 100 mM). The mixtures were incubated overnight at 45 °C to ensure complete deprotection of the aldehyde oligonucleotides. No ligation products were found by denaturing PAGE analysis after overnight heating. The reaction mixtures were then placed at room temperature and further monitored. After one hour in room temperature, the desired ligation product (confirmed by mass spectrometry, **Table 9**) was found in all models with 100 mM K⁺ (**Figure 20**). After four days of incubation, a near equilibrium state was reached with notable differences between the models: 65%, 40%, and 30% of the corresponding ligation product, **L10**, **L11**, or **L12**, was formed in models **D**, **E**, and **F** in the presence of 100 mM K⁺. The ligation yield was highly dependent on the concentration of K⁺, and no product formation was observed with 0 mM K⁺. A minimum of 1 mM was required to obtain a considerable amount of the product (although traces of product can be seen in models **D** and **E** with 0.1 mM K⁺). Based on the K⁺-dependent yield, *N*-methoxyoxazolidine was formed due to formation of G-quadruplex that increases the local concentration of the reactive heads. In other words, K⁺ acted as a template that induced G-quadruplex-mediated ligation of oligonucleotides.

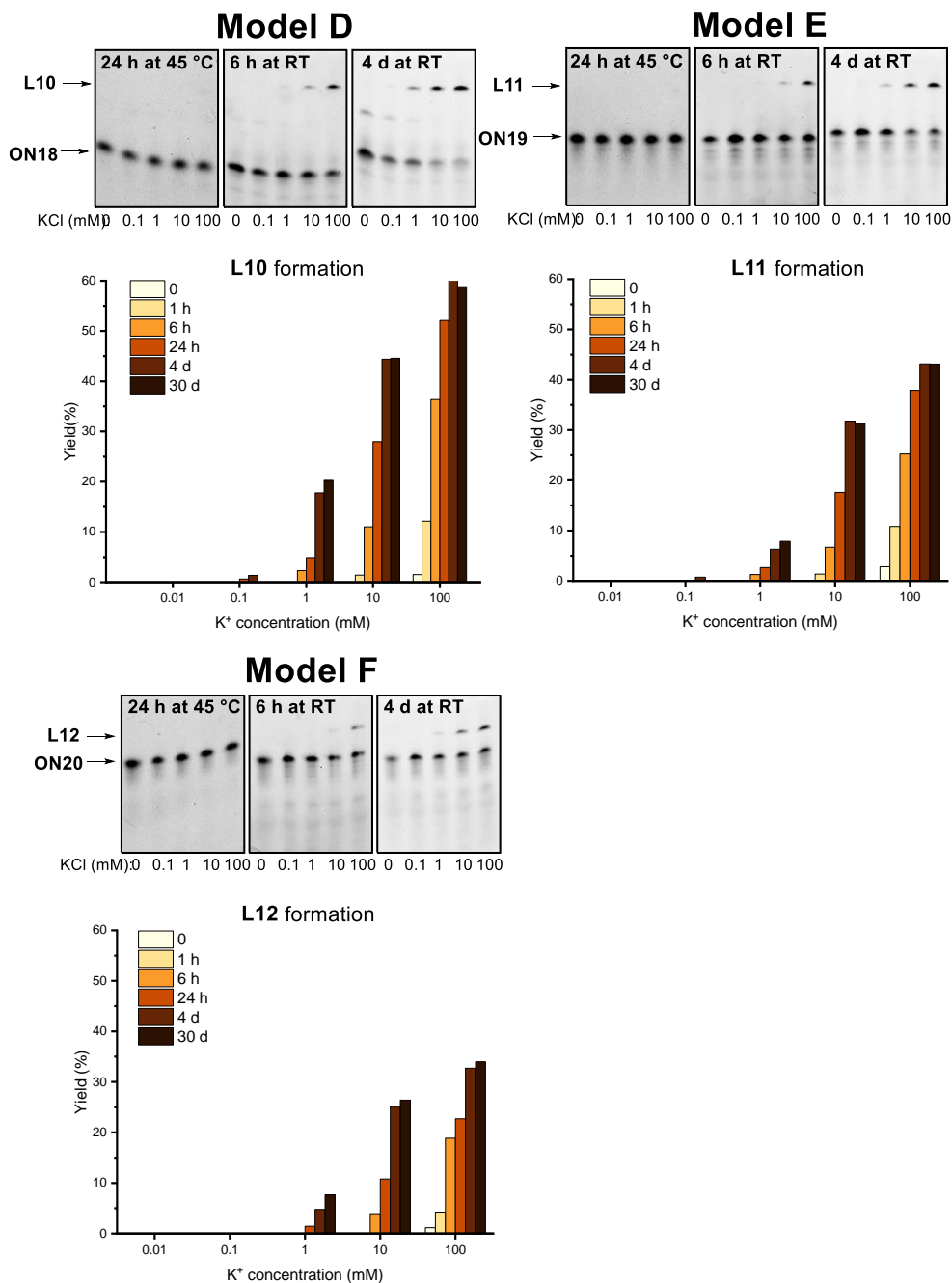


Figure 20. G-quadruplex ligation yields in models D, E, and F. Reaction conditions: **D:** ON18 + ON9; **E:** ON19 + ON10; **F:** ON20 + ON11. The initial concentration of each oligonucleotide was 5 μ M. Water was used as the solvent (pH 5, 50 mM acetic acid/lithium acetate).

Table 9. Mass spectrometric measurements for the G-quadruplex ligation models **D**, **E**, and **F**.

Ligation product	Observed molecular weight	Calculated molecular weight
L10	8697.7	8697.8
L11	8696.6	8697.8
L12	8696.6	8697.8

4 Summary

The dynamic formation of *N*-methoxyoxazolidines was studied. Using the model reaction between nucleoside **1** and various aldehydes, it was found out that the formation and hydrolysis rates were faithfully faster at lower pH in range 4–7. At room temperature and pH 7 the hydrolysis rate was negligible, thus, RP HPLC purification and long-term storage of the *N*-methoxyoxazolidines in water solution can be done. Instead, stereoisomeric purity was not always achievable due to rapid *R/S*-isomerization in solution. Effect of aldehyde structure on *N*-methoxyoxazolidine formation was studied. EWGs on aliphatic aldehydes stabilized *N*-methoxyoxazolidines both kinetically and thermodynamically. Generally, *N*-methoxyoxazolidine formation seems to be specific towards non-hindered aliphatic aldehydes. Aromatic aldehydes (benzaldehyde and *p*-methoxybenzaldehyde) and ketones (acetone) were less prone to react, although not studied in detail. The effect of aldehyde structure on thermodynamic stabilities of *N*-methoxyoxazolidines are coherent with the general trends of acetals.²¹ The pH-rate profiles of *N*-methoxyoxazolidines resemble those of hydrazones, but the selectivity is slightly different as hydrazines prefer to react with aromatic over aliphatic aldehydes.⁶⁵ Also, the specificity of *N*-methoxyoxazolidine formation may be considered higher compared to hydrazones, which are efficiently formed both from aldehydes and ketones.

Efficient method for synthesizing oligonucleotides elongated by nucleoside **1** ($\text{U}^{\text{NOMe}}\text{-ONs}$) via solid support **4** was developed. High yields of $\text{U}^{\text{NOMe}}\text{-ONs}$ up to 40% after isolation by RP HPLC were obtained following the paradigmatic automated synthesis protocol. $\text{U}^{\text{NOMe}}\text{-ONs}$ were efficiently conjugated to various aldehyde-bearing molecules via *N*-methoxyoxazolidine linkage. The conjugation was performed under slightly acidic anhydrous conditions. The conditions were mild enough even for acid-sensitive phosphorothioates with only minor amount of desulfurization ($\text{S}\rightarrow\text{O}$) occurring during the conjugation. The conjugates were relatively stable at pH 7.4 but hydrolysed under acidic conditions (pH 4–6), releasing the $\text{U}^{\text{NOMe}}\text{-ONs}$ from the aldehyde groups. The facile preparation, biocompatibility, and pH-dependent cleavage makes *N*-methoxyoxazolidine conjugation a viable strategy for studying acid-labile drug delivery systems.

N-methoxyoxazolidine formation in various templated synthesis models were studied. For this, a method for synthesizing 5'-aldehydic oligonucleotides using phosphoramidite **27** was developed. *N*-methoxyoxazolidine was used as a protecting group for the sensitive aldehyde functionality, that was deprotected *in situ* during the templated ligation experiments. The 5'-aldehyde oligonucleotides were ligated with U^{NOMe}-ONs in the presence of various templates (DNA, small-molecule, metal ion). A complementary DNA-sequence was used as a template to produce near quantitative ligation yield under micromolar concentration, exceeding non-templated equilibrium constant by 4000-fold. Split aptamers and G-quadruplex fragments were ligated together by quinine and K⁺ ions (respectively). The equilibrium yields of these dynamic covalent assemblies were predictable and dependent on the template concentration. All the templated ligation products were sufficiently stable under neutral conditions for isolation and mass spectrometric analysis.

Dynamic assembly of split aptamers and DNAzymes have found applications as biosensors.^{15,151} The split aptamer detection can be based on non-covalent¹⁵⁶ joining of the fragments or on covalent ligation^{146,152,153}. Certain applications, such as continuous intracellular monitoring, benefit from dynamicity of the non-covalent approach. However, this may not be achievable for a given functional oligonucleotide, as splitting can lose the activity due to destabilization. Dynamic ligation may bring the best of the two approaches, stabilizing the functional assembly enough in the presence of the target, while allowing denaturation when the target is not present anymore. Such dynamic DNAzymes have been explored using boronate ester ligation.^{117,118} The results of this thesis suggest that *N*-methoxyoxazolidine could similarly be used for stabilization of target-induced functional assembly. Plausibly, the specific application in this context could be acidic biological compartments, in which dynamic stabilization may be highly essential due to weak hybridization of oligonucleotides. Furthermore, the pH-dependent stability of *N*-methoxyoxazolidines could make it a tool for DCL for discovering various target-specific oligomers exceeding the attributes of natural ones, such as peptide-oligonucleotide chimeras¹⁶³ or aptamers/DNAzymes with non-natural modifications¹⁶⁴. The studies herein showed that *N*-methoxyoxazolidine is well suitable for DNA-templated synthesis and dynamic combinatorial systems based on oligonucleotides.

5 Materials and Methods

5.1 General

The synthesis and characterization of the compounds (small-molecules, oligonucleotides, peptides, PNAs) are described in the original publications. The compounds were characterized by ^1H NMR, ^{13}C NMR, ^{31}P NMR, and mass spectrometry when applicable.

5.2 Thermodynamic and kinetic experiments

For RP HPLC monitoring of the thermodynamic and kinetic experiments, samples were taken from the reaction mixtures at adequate intervals, quenched by adjusting the pH to 7–8 (if not mentioned otherwise) with excess of buffer solution, and analysed promptly. Reactant ratios were conducted by comparing the relative peak areas of the reactants at 260 nm after correcting the different absorption coefficients (details in the original publications). For denaturing PAGE monitoring, samples (5 μl) were premixed with NovexTM TBE–Urea 2x sample buffer, applied to gel wells, and the loaded gels were run at 200 V and 45 mA for 45–60 min. The PAGE runs were performed using precast TBE–Urea gel (15% acrylamide, TBE, 7 M urea), which was fixed into a vertical electrophoresis chamber and the chamber was filled with the running buffer (90 mM Tris, 90 mM borate, and 2 mM EDTA, pH 8.3). The completed gels were imaged by the fluorescence label in **ON15**, **ON16**, **ON18**, **ON19**, or **ON20**. The relative fluorescence signal intensities were quantified by processing the images into 2D density profiles and integrating the resulted peaks using ImageJ software.

5.2.1 *N*-methoxyoxazolidine formation between **1** and small-molecular aldehydes

The compounds were purchased as reagent-grade (acetaldehyde, butyraldehyde, 3-benzyloxy propionaldehyde) or synthesized (**1**, *N*-Bz-Gly-H, *N*-Bz- β -Ala-H) and were quantified by weighing (purchased ones), UV-spectrophotometrically (**1**), or by ^1H NMR (*N*-Bz-Gly-H, *N*-Bz- β -Ala-H). In a typical *N*-methoxyoxazolidine

formation experiment, an aqueous solution (ca. 100 μ l, pH 4, 5, or 6) of aldehyde (5 mM) was incubated for 30 min in RT before addition of **1** (5 mM). The reaction mixture was incubated at RT in a capped micro vial and were monitored by RP HPLC (cf. conditions in **Figure 13**). The *N*-methoxyoxazolidine concentration over time was obtained by fitting the data points to the reversible bimolecular integrated rate equation (details in the supporting information of the original publication I). From the resulting graph, equilibrium constants were directly obtained, and half-lives were determined as the first half-life. The *N*-methoxyoxazolidine hydrolysis was studied like the formation by isolating the major isomer and redissolving (5 mM) it in water.

5.2.2 Hydrolysis of conjugates **C1–C5**

In a typical deconjugation experiment, an isolated conjugate (10 μ M) was incubated in water (330 μ l, adjusted to pH 5.0 or 7.4 by 100 mM acetic acid or phosphate buffer) at 37 °C and monitored by RP HPLC (cf. conditions in **Scheme 23**). The data points were fitted to the integrated 1st order reaction rate law from which the amount of free oligonucleotide over time and deconjugation half-life was obtained directly (cf. graphs in **Scheme 23**).

5.2.3 Target-directed dynamic combinatorial chemistry

5.2.3.1 Self-assembly of a DNA-hairpin

N,O-transacetalization: **ON13** (750 pmol, 5 μ M) and **ON6** (750 pmol, 5 μ M) were dissolved in water (150 μ l) with pH adjusted (cf. **Table 7**) by 0.1 M buffers. The reaction was monitored by RP HPLC (cf. conditions in **Scheme 28**). The data points were fitted to an exponential decay function (details in the original publication IV), from which the equilibrium yield and half-life for the formation of **L1** were obtained directly (**Table 7**).

Aldehyde deprotection: **ON6** (750 pmol, 5 μ M) was dissolved in water (150 μ l) with pH adjusted (cf. **Table 7**) by 0.1 M buffers. The reaction was monitored by RP HPLC (cf. conditions in **Scheme 28**). The data points were fitted to a reversible bimolecular integrated rate law (details in the original publication IV), from which the equilibrium constant was obtained directly, and the half-life was determined as the first half-life (**Table 7**).

Aldehyde reprotection: **ON6** (825 pmol, 5.5 μ M) was dissolved in water (150 μ l) adjusted to pH 5 using trace amount of acetic acid and then incubated overnight at 37°C after which RP HPLC analysis indicated that **ON6** was fully deprotected into **ON6***. Then, the mixture was allowed to cool to room temperature and the pH was

adjusted (cf. **Table 7**) by addition of 1.0 M buffer (15 μ l). To the solution was added nucleoside **1** (3.94 μ l of stock solution for final concentration of 500 μ M). The reaction was monitored by RP HPLC (cf. conditions in **Scheme 28**). The data points were fitted to the reversible bimolecular integrated rate law (details in the original publication IV), from which the equilibrium constant was obtained directly, and the half-life was determined as the first half-life (**Table 7**).

DNA-templated N-methoxyoxazolidine formation: **ON6** (825 pmol, 5.5 μ M) was dissolved in water (150 μ l) adjusted to pH 5 using trace amount of acetic acid. The solution was incubated overnight at 37 $^{\circ}$ C after which RP HPLC analysis indicated that **ON6** was fully deprotected into **ON6***. Then, the mixture was allowed to cool to room temperature and the pH was adjusted (cf. **Table 7**) by addition of 1.0 M buffer (15 μ l). To the solution was added **ON13** (825 pmol, 5 μ M). The reaction was monitored (the samples were quenched to pH 11) by RP HPLC (cf. conditions in **Scheme 28**). The data points were fitted to reversible bimolecular integrated rate law (details in the original publication IV), from which the equilibrium constant was obtained directly, and the half-life was determined as the first half-life.

5.2.3.2 Quinine- and potassium-templated aptamer and G-quadruplex assembly

A typical quinine or potassium templated aptamer or G-quadruplex assembly experiment was carried out as follows: *N*-methoxyoxazolidine-protected 5'-aldehyde ON(s) (**ON7**, **ON8**, **ON17**, **ON9**, **ON10**, **ON11**) were incubated with U^{NOMe} ONs (**ON15**, **ON16**, **ON18**, **ON19**, **ON20**) (cf. the corresponding oligonucleotides and concentrations of models **A–F** in **Scheme 29** and **Scheme 30**) overnight in water solution (pH 5, 50 mM acetic acid buffer, and the corresponding amount of quinine or KCl) at 45–55 $^{\circ}$ C and then placed in RT. The reactions were monitored by denaturing PAGE. Noteworthy, the heating step (pH 5, 45 $^{\circ}$ C, overnight) was confirmed by RP HPLC to completely deprotect the *N*-methoxyoxazolidine-protected aldehydes by incubating them alone in the said conditions (data not shown).

Acknowledgements

This thesis is based on experimental work performed in the Laboratory of Organic Chemistry and Chemical Biology at the Department of Chemistry, University of Turku during the years 2019–2023. The financial support from the University of Turku Graduate School: Doctoral Programme in Exact Sciences (Exactus) and Finnish Cultural Foundation are gratefully acknowledged. I wish to acknowledge Prof. Sabine Müller and Prof. Michael Smietana for pre-examination of my thesis. Thank you for the thought-provoking comments. I wish to thank Dr. Lajos Kovács for accepting to act as my opponent.

Most greatly, I want to thank Prof. Pasi Virta, my research director, for guiding me through all these years. From your seemingly endless bag of ideas, you gave me the most interesting subject to study with all the support to grow as a researcher. I am ultimately grateful for all the knowledge you have shared during this thrilling journey. I also want to thank my supervisor Dr. Heidi Korhonen for the methodological lessons in laboratory work. You were always the person I felt comfortable talking to even about the tiniest problems I had. I also want to thank Prof. Tuomas Lönnberg for always being open for discussion about oligonucleotides whenever I have rushed into your room.

I want to thank the whole Bioorganic Chemistry Group, the past and the present members, with whom I have worked during my doctoral research: Dr. Asmo Aro-Heinilä, Dr. Antti Äärelä, Dr. Dattatraya Ukale, Hanni Haapsaari, Heidi Kähkölä, Dr. Tharun Kotamagari, Tommi Österlund, Toni Laine, Verner Saari, Dr. Vijay Gulumkar, Dr. Ville Tähtinen, Dr. Lange Saleh, Dr. Madhuri Hande, Mark Afari, Dr. Mikko Ora, Dr. Satu Mikkola, Dr. Sajal Maity, Mika Sulkanen, and Dr. Petja Rosenqvist. Thank you for all the collaboration, altruistic help, and inspirational discussions throughout the years. Special thanks for all the entertainment provided by the old coffee group personnel Antti, Asmo, Petja, and Ville. Whether it was about research, cursing on the instruments, or monitoring birds at the yard, you made the crumbly Arcanum feel like home. Furthermore, thank you Antti and Petja for crawling with me in the trenches, i.e., sharing a room in office and lab.

I want to thank Mauri Nauma and Kari Loikas for all the troubleshooting and exorcism they provided for the cursed instruments during the years. I also want to

thank Kirsi Laaksonen and Tiina Buss for the dynamic supply of chemicals and equipment. Thank you Dr. Alex Dickens, Dr. Jani Rahkila, and Dr. Denys Mavrynsky at the Instrument Center/CCMA for your assistance in MS and NMR measurements.

Finally, I want to thank all my friends for all the out-of-laboratory activities. Huge thanks to my parents Jukka and Minna and for my big brother Panu for always being there, supporting me in everything, and sharing your wisdom. Thank you Minja for sharing a home and life with me. Thank you for all the joy, care, and balance you bring with you. Thank you for your patience during my near-meltdown experiences during this thesis. Thank you Vesku, my furry friend, for keeping my feet warm during the late stages of editing.

September 2024

Aap! Alce

List of References

- (1) Li, X.; Liu, D. R. *Angew. Chem. Int. Ed.* **2004**, *43*, 4848–4870.
- (2) O'Reilly, R. K.; Turberfield, A. J.; Wilks, T. R. *Acc Chem Res* **2017**, *50*, 2496–2509.
- (3) Ma, P.; Xu, H.; Li, J.; Lu, F.; Ma, F.; Wang, S.; Xiong, H.; Wang, W.; Buratto, D.; Zonta, F.; Wang, N.; Liu, K.; Hua, T.; Liu, Z.-J.; Yang, G.; Lerner, R. A. *Angew. Chem.* **2019**, *131*, 9355–9362.
- (4) Castañón, J.; Román, J. P.; Jessop, T. C.; de Blas, J.; Haro, R. *SLAS Discov.* **2018**, *23*, 387–396.
- (5) Cougnon, F. B. L.; Sanders, J. K. M. *Acc Chem Res* **2012**, *45*, 2211–2221.
- (6) Frei, P.; Pang, L.; Silbermann, M.; Eriş, D.; Mühlethaler, T.; Schwardt, O.; Ernst, B. *Chem. - Eur. J.* **2017**, *23*, 11570–11577.
- (7) Durai, C. R. S.; Harding, M. M.; Durai, C. R. S.; Harding, M. M. *Aust J Chem* **2011**, *64*, 671–680.
- (8) Frei, P.; Hevey, R.; Ernst, B. *Chem. Eur. J.* **2019**, *25*, 60–73.
- (9) Ashkenasy, G.; Hermans, T. M.; Otto, S.; Taylor, A. F. *Chem Soc Rev* **2017**, *46*, 2543–2554.
- (10) Reddavid, F. V.; Lin, W.; Lehnert, S.; Zhang, Y. *Angew. Chem. Int. Ed.* **2015**, *54*, 7924–7928.
- (11) Moulin, E.; Cormos, G.; Giuseppone, N. *Chem Soc Rev* **2012**, *41*, 1031–1049.
- (12) Bargh, J. D.; Isidro-Llobet, A.; Parker, J. S.; Spring, D. R. *Chem Soc Rev* **2019**, *48*, 4361–4374.
- (13) Sheyi, R.; de la Torre, B. G.; Albericio, F. *Pharmaceutics* **2022**, *14*, 396.
- (14) Su, Z.; Xiao, D.; Xie, F.; Liu, L.; Wang, Y.; Fan, S.; Zhou, X.; Li, S. *Acta Pharm Sin B* **2021**, *11*, 3889–3907.
- (15) Debais, M.; Lelievre, A.; Smietana, M.; Müller, S. *Nucleic Acids Res* **2020**, *48*, 3400–3422.
- (16) Brochu, A. B. W.; Craig, S. L.; Reichert, W. M. *J Biomed Mater Res A* **2011**, *96*, 492.
- (17) Rahman, M. W.; Shefa, N. R. *Polym. Adv.* **2021**, *2021*, 7848088.
- (18) Meyer, V.; Janny, A. *Berichte der deutschen chemischen Gesellschaft* **1882**, *15*, 1164–1167.
- (19) Satchell, D. P. N.; Satchell, R. S. *Chem. Soc. Rev.* **1990**, *19*, 55–81.
- (20) Johnson, J. B.; Mani, J. S.; Broszczak, D.; Prasad, S. S.; Ekanayake, C. P.; Strappe, P.; Valeris, P.; Naiker, M. *Phytother. Res.* **2021**, *35*, 3484–3508.
- (21) Dong, J.-L.; Yu, L.-S.-H.; Xie, J.-W. *ACS Omega* **2018**, *3*, 4974–4985.
- (22) Cordes, E. H.; Bull, H. G. *Chem. Rev.* **1974**, *74*, 581–603.
- (23) Liu, B.; Thayumanavan, S. *J. Am. Chem. Soc.* **2017**, *139*, 2306–2317.
- (24) Pluth, M. D.; Bergman, R. G.; Raymond, K. N. *Angew. Chem.* **2007**, *119*, 8741–8743.
- (25) Dean, K. E. S.; Kirby, A. J. *J. Chem. Soc., Perkin trans. II* **2002**, *2*, 428–432.
- (26) Cui, L.; Cohen, J. L.; Chu, C. K.; Wich, P. R.; Kierstead, P. H.; Fréchet, J. M. J. *J. Am. Chem. Soc.* **2012**, *134*, 15840–15848.
- (27) Shinde, P. D.; Borate, H. B.; Wakharkar, R. D. *ARKIVOC* **2004**, *2004*, 110–117.
- (28) Burghardt, T. E. *J. Sulphur Chem.* **2005**, *26*, 411–427.
- (29) Sawatzky, E.; Drakopoulos, A.; Rölz, M.; Sottriffer, C.; Engels, B.; Decker, M. *Beilstein J. Org. Chem.* **2016**, *12*, 2280–2292.
- (30) Hine, J.; Narducco, K. W. *J. Am. Chem. Soc.* **1973**, *95*, 3362–3368.
- (31) Fife, T. H.; Pellino, A. M. *J Am Chem Soc* **1980**, *102*, 3062–3071.
- (32) Fife, T. H.; Hutchins, J. E. C. *J Am Chem Soc* **1976**, *98*, 2536–2543.

- (33) Fife, T. H.; Hutchins, J. E. C.; Pellino, A. M. *J. Am. Chem. Soc.* **1978**, *100*, 6455–6462.
- (34) Fife, T. H.; Hagopian, L. *J. Am. Chem. Soc.* **1968**, *90*, 1007–1014.
- (35) Johansen, M.; Bundgaard, H. *J. Pharm. Sci.* **1983**, *72*, 1294–1298.
- (36) Fife, T. H.; Hutchins, J. E. C. *J. Org. Chem.* **1980**, *45*, 2099–2104.
- (37) Bourne, S. A.; Fitz, L. D.; Kashyap, R. P.; Krawiec, M.; Walker, R. B.; Watson, W. H.; Williams, L. M. *J. Chem. Crystallogr.* **1997**, *27*, 35–44.
- (38) Canle, M.; Lawley, A.; McManus, E. C.; O’Ferrall, R. A. M. *Pure Appl. Chem.* **1996**, *68*, 813–818.
- (39) Bundgaard, H.; Johansen, M. *Int. J. Pharm.* **1982**, *10*, 165–175.
- (40) Ede, N. J.; Bray, A. M. *Tetrahedron Lett.* **1997**, *38*, 7119–7122.
- (41) Agami, C.; Couty, F. *European J Org Chem* **2004**, *2004*, 677–685.
- (42) Diness, F.; Meldal, M. *European J Org Chem* **2015**, *2015*, 1433–1436.
- (43) Sélambarom, J.; Monge, S.; Carré, F.; Roque, J. P.; Pavia, A. A. *Tetrahedron* **2002**, *58*, 9559–9566.
- (44) Ede, N. J.; Bray, A. M. *Tetrahedron Lett.* **1997**, *38*, 7119–7122.
- (45) Halli, J.; Hofman, K.; Beisel, T.; Manolikakes, G. *EurJOC* **2015**, *2015*, 4624–4627.
- (46) Morales-Monarca, G. H.; Gnecco, D.; Terán, J. L. *EurJOC* **2022**, *2022*, e202200267.
- (47) Sahiba, N.; Sethiya, A.; Soni, J.; Agarwal, D. K.; Agarwal, S. *Top Curr Chem (Cham)* **2020**, *378*, 34.
- (48) Bermejo-Velasco, D.; Nawale, G. N.; Oommen, O. P.; Hilborn, J.; Varghese, O. P. *ChemComm* **2018**, *54*, 12507–12510.
- (49) Fife, T. H.; Natarajan, R.; Shen, C. C.; Bembi, R. *J Am Chem Soc* **1991**, *113*, 3071–3079.
- (50) Saiz, C.; Wipf, P.; Manta, E.; Mahler, G. *Org Lett* **2009**, *11*, 3170.
- (51) Casi, G.; Huguenin-Dezot, N.; Zuberbühler, K.; Scheuermann, J.; Neri, D. *J Am Chem Soc* **2012**, *134*, 5887–5892.
- (52) Pratt, E. F.; Kamlet, M. J. *J. Org. Chem.* **1961**, *26*, 4029–4031.
- (53) Hine, J.; Via, F. A. *J Am Chem Soc* **1972**, *94*, 190–194.
- (54) Hie, J.; Yeh, C. Y. *J Am Chem Soc* **1967**, *89*, 2669–2676.
- (55) Wolfenden, R.; Jencks, W. P. **1961**, *54*.
- (56) Anderson, B. M.; Jencks, W. P. *J Am Chem Soc* **1960**, *82*, 1773–1777.
- (57) Hine, J.; Via, F. A. *J Am Chem Soc* **1972**, *94*, 190–194.
- (58) Godoy-Alcántar, C.; Yatsimirsky, A. K.; Lehn, J. M. *J Phys Org Chem* **2005**, *18*, 979–985.
- (59) Cordes, E. H.; Jencks, W. P. *J. Am. Chem. Soc.* **1962**, *84*, 832–837.
- (60) Hine, J.; Craig, J. C.; Underwood, J. G.; Via, F. A. *J Am Chem Soc* **1970**, *92*, 5194–5199.
- (61) Cordes, E. H.; Jencks, W. P. *J Am Chem Soc* **1963**, *85*, 2843–2848.
- (62) Kalia, J.; Raines, R. T. *Angew. Chem. Int. Ed.* **2008**, *47*, 7523–7526.
- (63) Wiberg, K. B.; Glased, R. *J. Am. Chem. Soc* **1992**, *114*, 841–850.
- (64) Kulchat, S.; Chaur, M. N.; Lehn, J. M. *Chem. - Eur. J.* **2017**, *23*, 11108–11118.
- (65) Kölmel, D. K.; Kool, E. T. *Chem Rev* **2017**, *117*, 10358–10376.
- (66) Doronina, S. O.; Toki, B. E.; Torgov, M. Y.; Mendelsohn, B. A.; Cerveny, C. G.; Chace, D. F.; DeBlanc, R. L.; Gearing, R. P.; Bovee, T. D.; Siegall, C. B.; Francisco, J. A.; Wahl, A. F.; Meyer, D. L.; Senter, P. D. *Nat. Biotechnol* **2003**, *21*, 778–784.
- (67) Furka, Á. *Drug Discov Today* **2022**, *27*, 103308.
- (68) Goodnow, R. A.; Dumelin, C. E.; Keefe, A. D. *Nat. Rev. Drug Discov* **2016**, *16*, 131–147.
- (69) *CC BY-SA 3.0 DEED*.
- (70) Manociluca. *Wikipedia: DNA-encoded chemical library*.
- (71) Li, J.; Nowak, P.; Otto, S. *J Am Chem Soc* **2013**, *135*, 9222–9239.
- (72) Corbett, P. T.; Leclaire, J.; Vial, L.; West, K. R.; Wietor, J. L.; Sanders, J. K. M.; Otto, S. *Chem Rev* **2006**, *106*, 3652–3711.
- (73) Herrmann, A. *Chem Soc Rev* **2014**, *43*, 1899–1933.
- (74) Otto, S.; Kubik, S. *J Am Chem Soc* **2003**, *125*, 7804–7805.

- (75) Rodriguez-Docampo, Z.; Eugenieva-Ilieva, E.; Reyheller, C.; Belenguer, A. M.; Kubik, S.; Otto, S. *ChemComm* **2011**, *47*, 9798–9800.
- (76) Rauschenberg, M.; Bomke, S.; Karst, U.; Jan Ravoo, B.; Rauschenberg, M.; Ravoo, B. J.; Bomke, S.; Karst, U.; Humpf, H. U. *Angew. Chem. Int. Ed.* **2010**, *49*, 7340–7345.
- (77) Leclaire, J.; Husson, G.; Devaux, N.; Delorme, V.; Charles, L.; Ziarelli, F.; Desbols, P.; Chaumonnot, A.; Jacquin, M.; Fotiadu, F.; Buono, G. *J Am Chem Soc* **2010**, *132*, 3582–3593.
- (78) Chung, M. K.; Severin, K.; Lee, S. J.; Waters, M. L.; Gagné, M. R. *Chem Sci* **2011**, *2*, 744–747.
- (79) Klein, J. M.; Saggiomo, V.; Reck, L.; Lüning, U.; Sanders, J. K. M. *Org Biomol Chem* **2012**, *10*, 60–66.
- (80) Lam, R. T. S.; Belenguer, A.; Roberts, S. L.; Naumann, C.; Jarrosson, T.; Otto, S.; Sanders, J. K. M. *Science* **2005**, *308*, 667–669.
- (81) Bugaut, A.; Toulmé, J. J.; Rayner, B. *Org Biomol Chem* **2006**, *4*, 4082–4088.
- (82) Kanlidere, Z.; Jochim, O.; Cal, M.; Diederichsen, U. *Beilstein Journal of Organic Chemistry* **2016**, *12*, 2136–2144.
- (83) Hartman, A. M.; Gierse, R. M.; Hirsch, A. K. H. *Eur JOC* **2019**, *2019*, 3581–3590.
- (84) Maraković, N.; Šinko, G. *Acta Chim Slov* **2017**, *64*, 15–39.
- (85) Mondal, M.; Hirsch, A. K. H. *Chem Soc Rev* **2015**, *44*, 2455–2488.
- (86) Miller, B. L. *Top Curr Chem* **2012**, *322*, 107–138.
- (87) Matsumoto, M.; Estes, D.; Nicholas, K. M. *Eur J Inorg Chem* **2010**, *2010*, 1847–1852.
- (88) Gasparini, G.; Prins, L. J.; Scrimin, P. *Angew. Chem. Int. Ed.* **2008**, *47*, 2475–2479.
- (89) Brisig, B.; Sanders, J. K. M.; Otto, S. *Angew. Chem.* **2003**, *115*, 1308–1311.
- (90) Poulsen, S. A.; Bornaghi, L. F. *Bioorg. Med. Chem.* **2006**, *14*, 3275–3284.
- (91) Nguyen, R.; Huc, I. *ChemComm* **2003**, *8*, 942–943.
- (92) Sindelar, M.; Wanner, K. T. *ChemMedChem* **2012**, *7*, 1678–1690.
- (93) Mondal, M.; Radeva, N.; Kçster, H.; Park, A.; Potamitis, C.; Zervou, M.; Klebe, G.; Hirsch, A. K.; Mondal, M.; Hirsch, A. K.; Radeva, N.; Kçster, H.; Park, A.; Klebe, G.; Potamitis, C.; Zervou, M. *Angew. Chem. Int. Ed.* **2014**, *53*, 3259–3263.
- (94) Huc, I.; Lehn, J. M. *Proc Natl Acad Sci U S A* **1997**, *94*, 2106–2110.
- (95) Fang, Z.; He, W.; Li, X.; Li, Z.; Chen, B.; Ouyang, P.; Guo, K. *Bioorg. Med. Chem. Lett.* **2013**, *23*, 5174–5177.
- (96) Demetriades, M.; Leung, I. K. H.; Chowdhury, R.; Chan, M. C.; McDonough, M. A.; Yeoh, K. K.; Tian, Y.-M.; Claridge, T. D. W.; Ratcliffe, P. J.; Woon, E. C. Y.; Schofield, C. J. *Angew. Chem.* **2012**, *124*, 6776–6779.
- (97) Leung, I. K. H.; Brown, T.; Schofield, C. J.; Claridge, T. D. W. *Med. Chem. Comm.* **2011**, *2*, 390–395.
- (98) Shi, B.; Greaney, M. F. *ChemComm* **2005**, *4*, 886–888.
- (99) Ludlow, R. F.; Otto, S. *J. Am. Chem. Soc.* **2008**, *130*, 12218–12219.
- (100) Erlanson, D. A.; Braisted, A. C.; Raphael, D. R.; Randal, M.; Stroud, R. M.; Gordon, E. M.; Wells, J. A. *PNAS* **2000**, *97*, 9367–9372.
- (101) Wessjohann, L. A.; Rivera, D. G.; León, F. *Org Lett* **2007**, *9*, 4733–4736.
- (102) Dumartin, M.; Septavaux, J.; Donnier-Maréchal, M.; Jeamet, E.; Dumont, E.; Perret, F.; Vial, L.; Leclaire, J. *Chem Sci* **2020**, *11*, 8151–8156.
- (103) Kool, E. T.; Park, D. H.; Crisalli, P. *J Am Chem Soc* **2013**, *135*, 17663–17666.
- (104) Netto, G. J.; Tawil, A. N.; Newman, J. T.; Savino, D. A. *Bayl. Univ. Med. Cent. Proc.* **1990**, *3*, 45–52.
- (105) Berg, M. D.; Brandl, C. J. *RNA Biol* **2021**, *18*, 316.
- (106) Petruska, J.; Goodman, M. F. *J. Biol. Chem.* **1995**, *270*, 746–750.
- (107) Bae, J. H.; Fang, J. Z.; Zhang, D. Y. *Nucleic Acids Res* **2020**, *48*, e89–e89.
- (108) Owczarzy, R.; Moreira, B. G.; You, Y.; Behlke, M. A.; Wälder, J. A. *Biochemistry* **2008**, *47*, 5336–5353.
- (109) Zhang, J.; Lang, H. P.; Yoshikawa, G.; Gerber, C. *Langmuir* **2012**, *28*, 6494–6501.

- (110) Xu, M.; Dai, T.; Wang, Y.; Yang, G. *RSC Adv* **2022**, *12*, 23356.
- (111) Khandelwal, G.; Bhyravabhotla, J. *PLoS One* **2010**, *5*, 12433.
- (112) Dorr, M.; M.G. Loffler, P.; Monnard, P.-A. *Curr Org Synth* **2013**, *9*, 735–763.
- (113) Rosenbaum, D. M.; Liu, D. R. *J Am Chem Soc* **2003**, *125*, 13924–13925.
- (114) Kleiner, R. E.; Brudno, Y.; Birnbaum, M. E.; Liu, D. R. *J Am Chem Soc* **2008**, *130*, 4646–4659.
- (115) Barbeyron, R.; Vasseur, J. J.; Smietana, M. *Chem Sci* **2015**, *6*, 542.
- (116) Barbeyron, R.; Martin, A. R.; Vasseur, J. J.; Smietana, M. *RSC Adv* **2015**, *5*, 105587–105591.
- (117) Debais, M.; Lelievre, A.; Vasseur, J. J.; Müller, S.; Smietana, M. *Chem. - Eur. J.* **2021**, *27*, 1138–1144.
- (118) Lelièvre-Büttner, A.; Schnarr, T.; Debais, M.; Smietana, M.; Müller, S. *Chem. Eur. J.* **2023**, *29*, e202300196.
- (119) Khongorzul, P.; Ling, C. J.; Khan, F. U.; Ihsan, A. U.; Zhang, J. *Mol. Cancer* **2020**, *18*, 3–19.
- (120) Benizri, S.; Gissot, A.; Martin, A.; Vialet, B.; Grinstaff, M. W.; Barthelemy, P. B. *Bioconjugate Chem.* **2019**, *30*, 366–383.
- (121) Roberts, T. C.; Langer, R.; Wood, M. J. A. *Nat. Rev. Drug Discov.* **2020**, *19*, 673–694.
- (122) Rozema, D. B.; Lewis, D. L.; Wakefield, D. H.; Wong, S. C.; Klein, J. J.; Roesch, P. L.; Bertin, S. L.; Reppen, T. W.; Chu, Q.; Blokhin, A. V.; Hagstrom, J. E.; Wolff, J. A. *Proc Natl Acad Sci U S A* **2007**, *104*, 12982–12987.
- (123) Parmar, R. G.; Poslusney, M.; Busuek, M.; Williams, J. M.; Garbaccio, R.; Leander, K.; Walsh, E.; Howell, B.; Sepp-Lorenzino, L.; Riley, S.; Patel, M.; Kemp, E.; Latham, A.; Leone, A.; Soli, E.; Burke, R. S.; Carr, B.; Colletti, S. L.; Wang, W. *Bioconjugate Chem* **2014**, *25*, 896–906.
- (124) Xiang, B.; Jia, X. L.; Qi, J. L.; Yang, L. P.; Sun, W. H.; Yan, X.; Yang, S. K.; Cao, D. Y.; Du, Q.; Qi, X. R. *Int. J. Nanomed.* **2017**, *12*, 2385–2405.
- (125) McClorey, G.; Banerjee, S. *Biomedicines* **2018**, *6*.
- (126) Boisguérin, P.; Deshayes, S.; Gait, M. J.; O'Donovan, L.; Godfrey, C.; Betts, C. A.; Wood, M. J. A.; Lebleu, B. *Adv. Drug Deliv. Rev.* **2015**, *87*, 67.
- (127) Ogawa, A.; Tanaka, M.; Sasaki, T.; Matsuda, A. *J. Med. Chem.* **1998**, *41*, 5094–5107.
- (128) Wallin, J.; Lönnberg, T. *Eur. J. Org. Chem.* **2022**, *2022*, e202200538.
- (129) Ämmälä, C.; Drury, W. J.; Knerr, L.; Ahlstedt, I.; Stillemark-Billton, P.; Wennberg-Huldt, C.; Andersson, E. M.; Valeur, E.; Jansson-Löfmark, R.; Janzén, D.; Sundström, L.; Meuller, J.; Claesson, J.; Andersson, P.; Johansson, C.; Lee, R. G.; Prakash, T. P.; Seth, P. P.; Monia, B. P.; Andersson, S. *Sci Adv* **2018**, *4*, 3386–3403.
- (130) Prakash, T. P.; Graham, M. J.; Yu, J.; Carty, R.; Low, A.; Chappell, A.; Schmidt, K.; Zhao, C.; Aghajan, M.; Murray, H. F.; Riney, S.; Booten, S. L.; Murray, S. F.; Gaus, H.; Crosby, J.; Lima, W. F.; Guo, S.; Monia, B. P.; Swayze, E. E.; Seth, P. P. *Nucleic Acids Res* **2014**, *42*, 8796–8807.
- (131) Gandioso, A.; Massaguer, A.; Villegas, N.; Salvans, C.; Sánchez, D.; Brun-Heath, I.; Marchán, V.; Orozco, M.; Terrazas, M. *ChemComm* **2017**, *53*, 2870–2873.
- (132) McNamara, J. O.; Andrechek, E. R.; Wang, Y.; Viles, K. D.; Rempel, R. E.; Gilboa, E.; Sullenger, B. A.; Giangrande, P. H. *Nat. Biotechnol.* **2006**, *24*, 1005–1015.
- (133) Tai, W. *Molecules* **2019**, *24*, 2211.
- (134) Luna Velez, M. V.; Verhaegh, G. W.; Smit, F.; Sedelaar, J. P. M.; Schalken, J. A. *Oncogene* **2019**, *38*, 3696–3709.
- (135) Neil, E. E.; Bisaccia, E. K. *J. Pediatr. Pharmacol. Ther.* **2019**, *24*, 194.
- (136) Cheol, S. C.; Savage, D. B.; Kulkarni, A.; Xing, X. Y.; Liu, Z. X.; Morino, K.; Kim, S.; Distefano, A.; Samuel, V. T.; Neschen, S.; Zhang, D.; Wang, A.; Zhang, X. M.; Kahn, M.; Cline, G. W.; Pandey, S. K.; Geisler, J. G.; Bhanot, S.; Monia, B. P.; Shulman, G. I. *JBC* **2007**, *282*, 22678–22688.
- (137) MacDonald, J.; Houghton, P.; Xiang, D.; Duan, W.; Shigdar, S. *Nucleic Acid Ther.* **2016**, *26*, 348–354.
- (138) Ede, N. J.; Eagle, S. N.; Wickham, G.; Bray, A. M.; Warne, B.; Shoemaker, K.; Rosenberg, S. J. *Pept. Sci.* **2000**, *6*, 11–18.

- (139) Zakeri, B.; Fierer, J. O.; Celik, E.; Chittock, E. C.; Schwarz-Linek, U.; Moy, V. T.; Howarth, M. *PNAS* **2012**, *109*, E690–E697.
- (140) Arranz-Gibert, P.; Ciudad, S.; Seco, J.; García, J.; Giral, E.; Teixidó, M. *Sci. Rep.* **2018**, *8*, 6446.
- (141) Rembach, A.; Turner, B. J.; Bruce, S.; Cheah, I. K.; Scott, R. L.; Lopes, E. C.; Zagami, C. J.; Beart, P. M.; Cheung, N. S.; Langford, S. J.; Cheema, S. S. *J. Neurosci. Rep.* **2004**, *77*, 573–582.
- (142) Szekely, T.; Roy, O.; Dériaud, E.; Job, A.; Lo-Man, R.; Leclerc, C.; Taillefumier, C. *J Med Chem* **2018**, *61*, 9568–9582.
- (143) Lönn, P.; Kacsinta, A. D.; Cui, X. S.; Hamil, A. S.; Kaulich, M.; Gogoi, K.; Dowdy, S. F. *Sci. Rep.* **2016**, *6*, 1–9.
- (144) Hamann, P. R.; Hinman, L. M.; Hollander, I.; Beyer, C. F.; Lindh, D.; Holcomb, R.; Hallett, W.; Tsou, H. R.; Upešlacis, J.; Shochat, D.; Mountain, A.; Flowers, D. A.; Bernstein, I. *Bioconjugate Chem* **2001**, *13*, 47–58.
- (145) DiJoseph, J. F.; Armellino, D. C.; Boghaert, E. R.; Khandke, K.; Dougher, M. M.; Sridharan, L.; Kunz, A.; Hamann, P. R.; Gorovits, B.; Udata, C.; Moran, J. K.; Popplewell, A. G.; Stephens, S.; Frost, P.; Damle, N. K. *Blood* **2004**, *103*, 1807–1814.
- (146) Smietana, M.; Müller, S. *Chempluschem* **2024**, *89*, e202300613.
- (147) Miduturu, C. V.; Silverman, S. K. *J. Org. Chem.* **2006**, *71*, 5774–5777.
- (148) Ito, Y.; Kimura, A.; Osawa, T.; Hari, Y. *J. Org. Chem.* **2018**, *83*, 36.
- (149) Gartner, Z. J.; Liu, D. R. *J Am Chem Soc* **2001**, *123*, 6961–6963.
- (150) Korhonen, H.; Virta, P. *Org. Lett.* **2018**, *20*, 1496–1499.
- (151) Chen, A.; Yan, M.; Yang, S. *Trends Anal. Chem.* **2016**, *80*, 581–593.
- (152) Sharma, A. K.; Heemstra, J. M. *J Am Chem Soc* **2011**, *133*, 12426–12429.
- (153) Sharma, A. K.; Kent, A. D.; Heemstra, J. M. *Anal Chem* **2012**, *84*, 6104–6109.
- (154) Neves, M. A. D.; Reinstein, O.; Johnson, P. E. *Biochemistry* **2010**, *49*, 8478–8487.
- (155) Shoara, A. A.; Slavkovic, S.; Donaldson, L. W.; Johnson, P. E. *Can J Chem* **2017**, *95*, 1253–1260.
- (156) Stojanovic, M. N.; De Prada, P.; Landry, D. W. *J Am Chem Soc* **2000**, *122*, 11547–11548.
- (157) Spiropoulos, N. G.; Heemstra, J. M. *Artif DNA PNA XNA* **2012**, *3*, 123.
- (158) Pei, R.; Shen, A.; Olah, M. J.; Stefanovic, D.; Worgall, T.; Stojanovic, M. N. *ChemComm* **2009**, *14*, 3193–3195.
- (159) Wei, Z.; Zhou, Y.; Wang, R.; Wang, J.; Chen, Z. *Pharmaceutics* **2022**, *14*, 2561.
- (160) You, J.; Li, H.; Lu, X. M.; Li, W.; Wang, P. Y.; Dou, S. X.; Xi, X. G. *Biosci.* **2017**, *37*, 20170771.
- (161) Lin, C.; Yang, D. *Methods. Mol. Biol.* **2017**, *1587*, 171–196.
- (162) Wang, K.; You, M.; Chen, Y.; Han, D.; Zhu, Z.; Huang, J.; Williams, K.; Yang, C. J.; Tan, W. *Angew. Chem. Int. Ed.* **2011**, *50*, 6098–6101.
- (163) Stephanopoulos, N. *Bioconjug Chem* **2019**, *30*, 1915–1922.
- (164) Odeh, F.; Nsairat, H.; Alshaer, W.; Ismail, M. A.; Esawi, E.; Qaqish, B.; Bawab, A. Al; Ismail, S. I. *Molecules* **2020**, *25*.



**TURUN
YLIOPISTO**
UNIVERSITY
OF TURKU

ISBN 978-951-29-9794-7 (PRINT)
ISBN 978-951-29-9795-4 (PDF)
ISSN 0082-7002 (Print)
ISSN 2343-3175 (Online)